COMPARISON OF MODULATION AND DETECTION TECHNIQUES FOR CDMA CELLULAR SYSTEM

by

Michael Xiaolong Li

B.Eng. Tsinghua University, 1990, Beijing, China

A THESIS SUBMITTED IN PARTIAL FULFILLMENT
OF THE REQUIREMENTS FOR THE DEGREE OF
MASTER OF APPLIED SCIENCE

in the School
of
Engineering Science

SIMON FRASER UNIVERSITY
June, 1996

APPROVAL

Name: Michael Xiaolong Li

Degree: Master of Applied Science

Title of thesis : Comparison of Modulation and Detection Techniques for CDMA Cellular System

Examining Committee: Dr. Kamal Gupta
Associate Professor, Engineeering Science, SFU
Chairman

Dr. Paul Ho
Associate Professor, Engineering Science, SFU
Senior Supervisor

Dr. Jacques Vaisey
Assistant Professor, Engineering Science, SFU
Supervisor

Dr. Steve Hardy
Professor, Engineering Science, SFU
Examiner

Date Approved: June 28, 1996

PARTIAL COPYRIGHT LICENSE

I hereby grant to Simon Fraser University the right to lend my thesis, project or extended essay (the title of which is shown below) to users of the Simon Fraser University Library, and to make partial or single copies only for such users or in response to a request from the library of any other university, or other educational institution, on its own behalf or for one of its usrs. I further agree that permission for multiple copying of this work for scholarly purposes may be granted by me or the Dean of Graduate Studies. It is understood that copying or publication of this work for financial gain shall not be allowed without my written permission.

Title of Thesis/Project/Extended Essay

"Comparison of Modulation and Detection Techniques for CDMA Cellular System"

Author:

(signature)

(name)

June 24, 1996
(date)

ABSTRACT

Direct Sequence Code Division Multiple Access is a modulation and multiple access technique currently being implemented in cellular mobile radio communication. Different coding, spreading and detection techniques are being investigated to improve the performance of cellular mobile systems. The channel in CDMA cellular mobile communication exhibits frequency-selective Rayleigh fading, where the RAKE receiver plays an important role in the system. In addition, the appearance of self-interference is a major concern in CDMA cellular mobile systems. Pilot Symbol Assisted Modulation can improve the performance of coherent detection without complex signal processing. This thesis studies the error performance of PSAM and differential detection of MPSK signals in a 3-ray frequency-selective Rayleigh fading channel with additive white Gaussian noise and self-interference. We investigate the effects of rate $1/2$ and $1/3$ convolutional codes with different constraint lengths in BPSK modulation, where different channel conditions are considered. We find the trade off between rate $1/2$ code with larger processing gain and rate $1/3$ code with smaller processing gain while the transmission bandwith is fixed. While keeping the information throughput unchanged, we compared the performance of rate $1/2$ PSAM QPSK and rate $1/3$ PSAM 8PSK modulation. Various constraint length convolutional code and channel conditions are also considered. It is found that rate $1/2$ QPSK performs better than rate $1/3$ 8PSK modulation, and at lower fading rate ($f_D T < 0.05$), PSAM can improve the performance better than differential detection by 2dB. We also perform the uplink error performance simulation on a combined orthogonal/convolutional coding scheme for cellular CDMA. Closed loop power control and RAKE receiver are implemented, and the results are also compared with PSAM.

ACKNOWLEDGEMENTS

I would like to thank my supervisor Dr. Paul Ho for suggesting the subject of the thesis and supervising me helpfully and patiently throughout the course of the research.

Financial support from National Science and Engineering Research Committee (NSERC) of Canada and SFU Graduate Fellowship Committee is gratefully acknowledged.

Finally, special thanks to my wife, parents and sister for their support and encouragement during the past three years.

Contents

List of Figures

List of Tables

ABBREVIATIONS

AWGN	Additive white Gaussian noise
BPSK	Binary phase shift keying
CDMA	Code division multiple access
CSI	Channel State information
dB	Decibel
DPSK	Differential phase shift keying
DS	Direct sequence
FDMA	Frequence division multiple access
FEC	forward error correction or forward error correcting codes
FH	Frequency hopping
FM	Frequency modulation
Hz	Hertz
IEEE	Institute of Electrical and Electronic Engineers
iid	independent and identically distributed
kHz	kiloHertz
MHz	megaHertz
MPSK	M-ary phase shift keying
PSAM	Pilot symbol assisted modulation
PSK	Phase shift keying
RPpoles	Poles on the right-half of the complex s-plane
SIR	Signal to interference ratio
TDMA	Time division multiple access
UHF	Ultra high frequency

VARIABLES AND FUNCTIONS

c	Speed of light
f_c	Carrier frequency
f_D	Maximum Doppler frequency
$f_D T$	Normalized maximum Doppler frequency or fade rate
$g(t)$	Channel fading process
g_k	A sample of the fading process
$n_w(t)$	Channel AWGN
$s(t)$	Baseband transmitted signal
s_k	Transmitted symbol in the interval $kT \leq t \leq (k+1)T$
$r(t)$	Baseband received signal
t	Time
E_b	Bit energy
$\frac{E_b}{N_0}$	Received bit signal to noise ratio
E_s	Symbol energy
$\frac{E_s}{N_0}$	Received symbol signal to noise ratio
$E\{\bullet\}$	Statistical average
$J_0\{\bullet\}$	Bessel function of order zero
P_b	Bit error probability
$R_g(\tau)$	Autocorrelation function of the fading process
T	Symbol interval
σ^2	Variance
$\phi_D(s)$	Characteristic function

Chapter 1

Introduction

The ultimate objective of communications is to enable anybody to communicate instantly with anybody else from anywhere on the earth. This objective can be achieved only by mobile communications in conjunction with highspeed backbone wireline networks. For this reason, mobile communication has received worldwide attention. With the development of digital technologies and movement towards digitalization of the world, mobile communication will be inevitably integrated into the digital telecommunications network and a variety of effective services will be provided.

Developing from the early maritime use for disaster and safety communications, mobile radio communication has developed very rapidly in the past decades [1]. The technology of cellular systems has enabled the reuse of channels, thus helping achieve efficient spectrum utilization for a large number of users. For example, the 900-MHz band has emerged as a major mobile radio frontier for land mobile communication, especially in North America. Many advanced technologies have been developed to

facilitate implementation of the new 900-MHz band mobile radio communication systems with reasonable cost. The US analog cellular system uses FDMA (frequency division multiple access) and divides the allocated spectrum into 30 kHz bandwidth channels; narrowband FM modulation is employed, resulting in a modulation efficiency of 1 call per 30 kHZ of spectrum. The TIA (Telecommunication Industry Association) proposed EIA/TLA/IS-54-B digital cellular standard uses 30 kHz FDMA channels, which are subdivided into six time slots for TDMA (time division multiple access) transmission. The frequency spectrum has become a limited resource since the spectrum for mobile communication has already been allocated. Due to the severe congestion of the mobile communication spectrum in some geographical areas, people are seeking a communication technique that offers the potential for utilizing the spectrum more effectively.

Spread spectrum communication systems, developed during the mid-1950's, have been widely studied and used for specialized applications, such as military antijamming tactical communications [1]. The use of spread spectrum naturally means that each transmitter utilizes a large amount of spectrum; however, this will be compensated by the interference reduction capability inherent in the use of spread-spectrum techniques, so that a considerable number of users might share the same spectral band. If done properly, some benefits can be achieved simultaneously, such as antijamming, antiinterference, low probability of intercept, etc. A definition of spread spectrum in [2] adequately reflects the characteristics of this technique. "Spread spectrum is a means of transmission in which the signal occupies a bandwidth in excess of the minimum necessary to send the information; the band spread is accomplished

by means of a code which is independent of the data, and a synchronized reception with the code at the receiver is used for despreading and subsequent data recovery." There are several methods to spread the spectrum: Direct Sequence (DS) modulation, in which a fast pseudorandomly generated sequence causes phase transitions in the carrier containing data; Frequency Hopping (FH), which the carrier is caused to shift frequency in a pseudo-random way; and time hopping, wherein bursts of signal are initiated at pseudo-random times. Hybrid combinations of these techniques are frequently used. In this thesis, we refer the term spread spectrum as DS.

Although current applications for spread spectrum continue to be mainly for military communications, there is a growing interest in the use of this technique for mobile radio networks. The new applications of spread-spectrum communications have characteristics that are quite different from those in the past [3, 4, 5, 8]. When intentional jamming does not exist, it is possible for us to consider ways of improving the receiver design to make the system more efficient and more practical for commercial applications. Of the many potential uses for spread-spectrum communications in civilian applications, direct sequence code division multiple access (DS/CDMA) appears to be the most popular modulation and multiple access technique being implemented in cellular mobile radio communications. Multipath is often a fundamental limitation to system performance in mobile communication; however, spread spectrum is a well-known technique to combat multipath.

Applying CDMA to mobile communication to increase the system capacity as well as to reduce the interference are major concerns. Different kinds of coding schemes,

modulation/detection techniques and spectrum spreading related methods are suggested and tested in many works of research. The subject of this thesis is to analyse, evaluate and compare the error performance of different coding, modulation and detection techniques in mobile communication systems using CDMA technique.

In the following sections, we will discuss the literature review and give a brief description of our contribution and thesis outline.

1.1 Background and Literature Review

In the past decade, mobile communication has become a very popular subject in communication engineering. Since the analog cellular system started to face its capacity limitation [9], the promotion of developing digital cellular systems for increasing capacity has been carried out. In digital systems, there are three basic multiple access schemes: frequency division multiple access (FDMA), time division multiple access (TDMA) and code division multiple access (CDMA). Theoretically it does not matter whether the spectrum is divided into frequencies, time slots or codes. The capacity provided from these three multiple access schemes is the same.

In 1985, Viterbi [6] - [8] made a straightforward comparison of the capacity of CDMA to that of conventional TDMA and FDMA for satellite applications, and suggested a reasonable edge in capacity for the latter two more conventional techniques. This edge was shown to be illusory [10] when it was realized that the capacity of CDMA system was only interference limited, not like those of FDMA and TDMA, which are primarily bandwidth limited. It is also shown in [10, 11] that voice activity

and spatial isolation are needed to improve CDMA capacity to that of FDMA and TDMA under similar assumptions for a mobile satellite application. Therefore, any reduction in interference converts directly and linearly into an increase in capacity. In [9], Lee depicts the advantage of having CDMA in cellular systems to increase the capacity. Pickholtz, et al [12] suggest spread spectrum CDMA can also be used to share the spectrum with existing narrow-band mobile users to increase the system capacity of mobile communications. Recent research in [13] finds that CDMA scheme can reuse the same (entire) spectrum for all cells in a cellular system, thereby increasing capacity by a large percentage of the normal frequency reuse factor in FDMA and TDMA.

There are, of course, some disadvantages of CDMA. The most obvious one is the problem of interference. It is caused by the non-orthogonality among the spreading sequences for different users. With the presence of data, the partial auto-correlation of the spreading sequence could also cause self-interference. This is not like FDMA or TDMA, wherein the orthogonality of the received signals can be (approximately) preserved by frequency guardbands or time slots. Associated with this is the near-far problem, that is, signals closer to the receiver of interest are received with smaller attenuation than are signals located further away. This means that power control must be used. However, this still does not gurantee that interference from neighboring cells might not arrive with untolerable power levels, especially if the waveforms in different cells are undergoing independent fading. It is seen that while the use of spread spectrum techniques offers some unique opportunities to cellular system capacity, there are issues to be concerned about as well.

As mentioned above, digital cellular systems in North America are mainly working in the ultra high frequency (UHF) band. Much work has already been done to characterize UHF mobile radio channels. The results show that the digital cellular channel exhibits the frequency-selective fading behavior. Summarizing the research and measurements in recent years, the Telecommunication Industry Association (TIA) characterizes the digital cellular channel as a frequency-selective Rayleigh fading channel.

People have designed a number of digital modulation schemes as well as detection techniques to improve bandwidth efficiency and system performance. Phase Shift Keying (PSK) is one major category of modulation techniques adopted in mobile communication system. The coherent demodulation of digital signals is known to be optimal in a linear static Gaussian channel because it can achieve a specific bit-error-rate (BER) with the least power requirement [14]. However, in a mobile environment, the channel's Rayleigh fading degrades the BER and frequently introduces an irreducible error floor. Under certain circumstances, coherent detection is even inferior to noncoherent or differential detection [15]. To improve the performance of coherent demodulation, fade compensation techniques are introduced. Pilot Symbol Assisted Modulation (PSAM) and pilot-tone aided coherent detection seem to be among the promising techniques to combat Rayleigh fading channels [16]-[20].

Pilot-tone aided coherent demodulation is an efficient method to improve the performance of coherent demodulation in fast Rayleigh fading channels. The tone provides the receiver with an explicit amplitude and phase reference for detection and thereby suppresses the error floor. However, the question of where in the spectrum to locate the tone is a difficult one, and the tone insertion often requires complex signal processing to create a spectral null at the carrier frequency. Moreover, pilot-tone insertion increases the peak factor of the modulated carrier and in order to have efficient operation of the transmitter power amplifiers, a small peak factor is more desirable.

Recently, PSAM has been introduced to improve the performance of the coherent demodulation in fast fading channels [16, 17, 18]. The system has to insert a known symbol periodically into the transmitted information stream, so that the channel state information (CSI) can be estimated at the receiver. Like pilot tone modulation, PSAM suppresses the error floor with no change to the transmitted pulse shape. Processing at the transmitter and receiver is also simpler than processing at the pilot-tone scheme. The advantage of the PSAM techniques is that it neither requires complex signal processing nor increases the peak factor of the modulated carrier. However, due to the redundancy introduced, the effective transmitting bandwidth will be reduced while it provides better error performance. Studies of PSAM [17, 18] were based on simulation and experimental implementations and they did not provide the performance analysis needed before their results can be generalized. Later, Cavers [16] presented the PSAM on a solid analytical basis which was missing from previous work. He also gave out the closed form expressions for the BER for BPSK and QPSK. The results in [16] showed that optimized PSAM outperforms differential detection.

In the analysis of the error performance of digital communication system, the calculation of the pairwise error probability is a major concern. A method of solution was suggested by Cavers and Ho [21]. This involves solving the residues of a function of the two-sided Laplace transform of the decision variable. Although frequency-selective fading complicates the calculation of the residues, we use this method to calculate the error bound in our work.

In a mobile communication system, we can use PSAM in the forward link so as to provide a coherent reference to mobile stations. On the reverse link, noncoherent reception was widely studied in [22] - [26]. M-ary orthogonal modulation is a spectrum efficient modulation scheme well suited for this application [22]. Although differential phase shift keying (DPSK) does not require phase coherence, orthogonal modulation for $M \geq 8$ is known to perform better than DPSK [14], at least in the additive white Gaussian noise (AWGN) channel. A combined orthogonal/convolutional coding scheme, which is adequate for noncoherent reception over the reverse link, is suggested in [13]. A balanced quadriphase modulation is used in their scheme, as indicated in [27]. It performs equally against multiple-access interference as well as the classical quadriphase modulation, but the former performs better against tone interference. In our thesis, we considered a simplified combined orthogonal/convolutional coding scheme to simulate the error performance over the uplink. As suggested in [13] and [26], 64-ary Walsh symbols are used to provide 64-orthogonal waveforms.

Multipath fading, which severely degrades the average error performance, is a

major concern in mobile communications. In order to achieve highly reliable digital data transmission without excessively increasing transmitter power, people adopt a diversity reception technique, which is one of the most effective techniques for this purpose. It requires a number of signal transmission paths named diversity branches, all of which carry the same information but have uncorrelated multipath fadings and a circuit to combine the received signals. There are several diversity techniques such as space diversity, angle diversity, frequency diversity, etc. Time and frequency diversity are the most popular ones. The use of wideband signals can be treated as another method to get frequency diversity. In cellular CDMA, when the transmission bandwidth is several times wider than the channel coherence bandwidth, the RAKE receiver is widely used to get the diversity advantage [3] [28].

In CDMA, a unique binary spreading sequence is assigned to each user, and all users share the same frequency spectrum. Then the total amount of interference power received at a receiver is determined by all the other simultaneous users if the sequences are not orthogonal. The auto-correlation and cross-correlation among those sequences contribute to the self-interference (multipath interference) and multiple access interference (MAI). The interference degrades the performance of the system. In addition, the near-far problem results from those transmitters near a receiver that generate overwhelming interference for those far from the receiver which experience large transmission attenuation [22]. The maximum number of users supportable in a CDMA system will be limited by multipath and near-far effects. To combat near-far effects and fading, feedback power control is an effective method used so that base stations receive the same power from each portable [29]-[31].

1.2 Motivation and Contribution

In this thesis, we studied the performance of Pilot Symbol Assisted Modulation in CDMA cellular system in the presence of multipath interference. The exact expression for the pairwise error event probability is presented. We also derived an upper bound for PSAM when used with convolutional coding. The performance of codes with different rates and modulation schemes are also analysed. While the information rate and spreaded bandwith are fixed, we found the trade off between coding rate and processing gain.

We simulated the error performance for data transmission with non-coherent orthogonal/convolutional coding in a cellular CDMA system. The RAKE receiver and power control schemes are implemented in our simulation. Results are presented with different system parameters and channel conditions. The power control technique reduces the BER effectively. We also found at slower fading, the error performances of smaller and larger interleaving sizes are similar. At faster fading, the larger the interleaving size is, the better performance it achieves. Simulation results without power control are also compared with PSAM with same convolutional coding scheme. It is found that PSAM outperforms non-coherent detection.

1.3 Thesis Outline

In Chapter 2, some terminologies and concepts about cellular CDMA are stated. This includes topics such as Rayleigh fading channel, Spread Spectrum, and RAKE receiver. The Gaussian assumption for interference modelling in the CDMA environment is also presented.

In Chapter 3, we will analyse the performance of pilot symbol assisted modulation in CDMA cellular system in the presence of multipath interference. The trade off between coding rate and processing gain will be studied. An upper bound for PSAM with convolutional coding will be also derived. The error performance comparison of rate 1/2 QPSK and rate 1/3 8PSK modulation techniques will be presented.

In Chapter 4, the simulation results of an uplink non-coherent detector in a CDMA cellular system will be illustrated. The effects of power control and system parameters selection will be discussed. Simulation results of non-coherent detection without power control are compared with Pilot Symbol Assisted Modulation that has similar coding schemes.

Finally, we will present conclusions of this study and some further research topics in Chapter 5.

Chapter 2

Cellular Code Division Multiple Access

In Section 2.1, we will discuss some terminologies commonly used in mobile communications. Section 2.2 introduces the frequency-selective Rayleigh fading channel model. Section 2.3 describes the spread spectrum techniques. Some major issues related to cellular CDMA are discussed in Section 2.4, such as power control and the RAKE receiver. Section 2.5 presents the modelling of interferences in cellular CDMA.

2.1 Some Common Terminologies in Mobile Communication

Mobile communication in an urban area usually involves an elevated fixed land-base station and mobile units travelling through the area. The unique characteristics of mobile communication come from the properties of the channel, which is a time-varying medium. Moreover, the time variations appear to be unpredictable to the

user of the channel. Due to the moving receiver/transmitter, reflection, refraction and scattering of radio waves by buildings and other man-made obstacles, if we transmit an ideal pulse over such a time-varying multipath channel, we will receive a series of pulses with different amplitude and time delays. If we repeat this experiment, we will get different results each time (refer to Figure 2.1). The changes in the relative path lengths by amounts in the order of the radio carrier wavelength will change the relative phases among the several received signals. This phase shift has a dramatic affect on the received signal quality than on the change of amplitudes of the received signal. For example, the received multipath signals may add either constructively or destructively. The result of amplitude variations in the received signal, due to the time-varying multipath characteristics of the channel, is called **multipath fading**. The envelope and phase of the channel impulse response are characterized as Rayleigh distributed and uniformly distributed between $(-\pi, \pi)$, respectively. Therefore, the transmitting channel is called **Rayleigh fading** channel, which can be expressed as follows [15]

$$\begin{cases} p(r) = \frac{r}{\sigma^2} \exp(-\frac{r^2}{2\sigma^2}) & r \geq 0 \\ p(\theta) = \frac{1}{2\pi} & -\pi \leq \theta \leq \pi \end{cases} \tag{2.1}$$

where r and θ are the envelope and phase of channel's impulse response.

Because of time variation, limited bandwidth and multipath effects, the channel exhibits time and frequency-selective behavior. The time-selective channel introduces a **Doppler effect**. Due to the relative motion between the transmitter and the receiver, there are additional frequency components contributed to the power spectrum of the transmitted signals so that the spectrum is broadened. The Doppler frequency

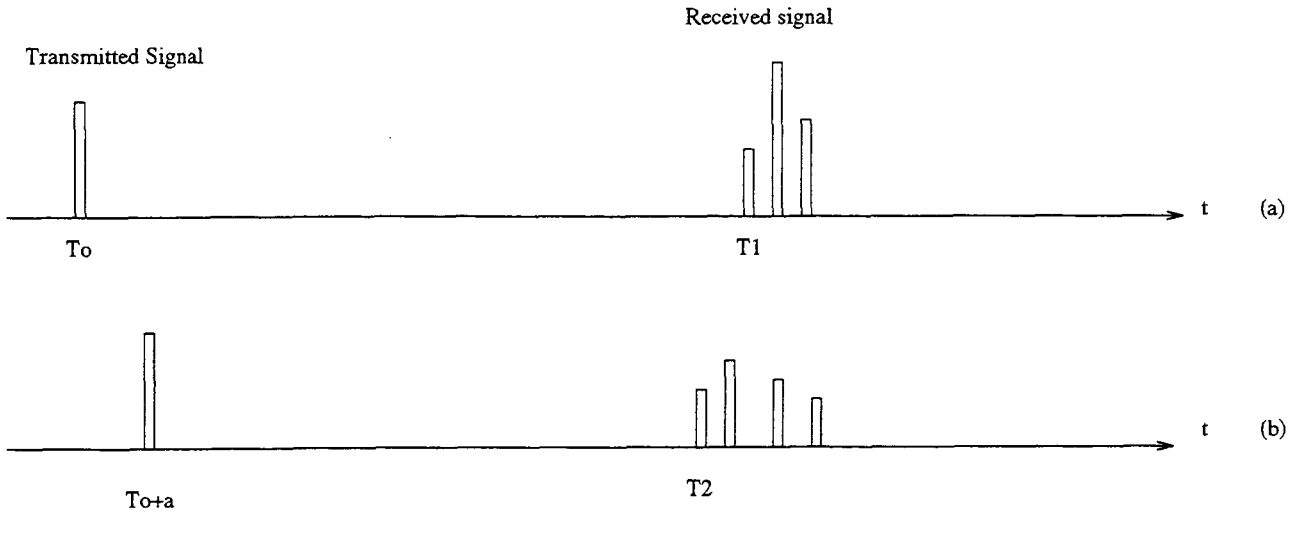

Figure 2.1: Examples of the responses of a time-varying multipath channel to a very narrow pulse.

is given as

$$f_D = \frac{f_c v}{c} \tag{2.2}$$

where v is the speed of the vehicle, f_c is the carrier frequency and c is the speed of light, which is 300,000km/s. For example, the maximum Doppler frequency is approximately 13.4 Hz if a car travels at the speed of 10 km per hour with a 900 MHz carrier frequency. The **coherence time** of the channel is defined as the reciprocal of the Doppler frequency.

The coherence bandwith of the channel is defined as the closest spacing between two frequencies with a correlation of 0.5 or higher and is inversely proportional to the rms time spread of the channel impulse response [32]. Typical coherence bandwidths range from 100 kHz to 1 MHz. Thus, a narrowband transmission is subjected to **flat Rayleigh fading** or **frequency non-selective Rayleigh fading**, i.e., there is no spectral distortion of the signal. On the other hand, a spread-spectrum transmission would encounter different fades in different portions of its spectrum. This phenomenon is called **frequency-slective Rayleigh fading**; i.e., the different frequency components of the transmitted signals are subject to different fading effects. In this thesis, the emphasis will be on the frequency-selective Rayleigh fading channel.

2.2 Baseband Representation of Fading Channel

Due to the multipath feature and the limited bandwidth of digital cellular channel, the baseband transmitted signal $s(t)$ suffers frequency-selective distortion. Generally, the impulse response $c(\tau; t)$ of the digital cellular channel is considered to be a wide-sense

stationary zero-mean complex Gaussian random process. There is also the additive white Gaussian noise (AWGN) introduced. This means the baseband received signal is

$$r(t) = \int_{-\infty}^{\infty} c(\tau; t)s(t-\tau)d\tau + n_w(t) \tag{2.3}$$

where $c(\tau; t)$ is the time-varying impulse response of the channel and $n_w(t)$ is the channel's noise. In [14], Proakis indicates that in most transmission media, the attenuation and phase shift of the channels associated with path delay τ_1 is uncorrelated with those associated with path delay τ_2. Thus, the autocorrelation function of $c(\tau; t)$ becomes

$$\phi_c(\tau_1, \tau_2; \lambda_1 - \lambda_2) = \frac{1}{2}E[c^*(\tau_1; \lambda_1)c(\tau_2; \lambda_2)] = J_0[2\pi f_D(\lambda_1 - \lambda_2)]G(\tau_1)\delta(\tau_1 - \tau_2) \tag{2.4}$$

where $J_0(\bullet)$ is the zero*th* order Bessel function of the first kind, $E(\bullet)$ represents statistical average, and f_D is the maximum Doppler frequency as mentioned before. The normalized Doppler frequency is more commonly used, which is defined as $f_D T$, where T is the pulse duration and $\frac{1}{T}$ is the pulse rate. In this thesis, we consider $f_D T$ from 0.05 to 0.0002. In the case of the flat fading channel, the delay power profile is simply

$$G(\tau) = \sigma_g^2 \delta(\tau) \tag{2.5}$$

where σ_g^2 is the variance of the flat fading process.

The mathematical model for a frequency-selective Rayleigh fading channel used in this thesis is the tapped delay line model shown in Figure 2.2. The transmitted signal $s(t)$ arrives at the receiver through three rays. There is flat fading in each ray, but

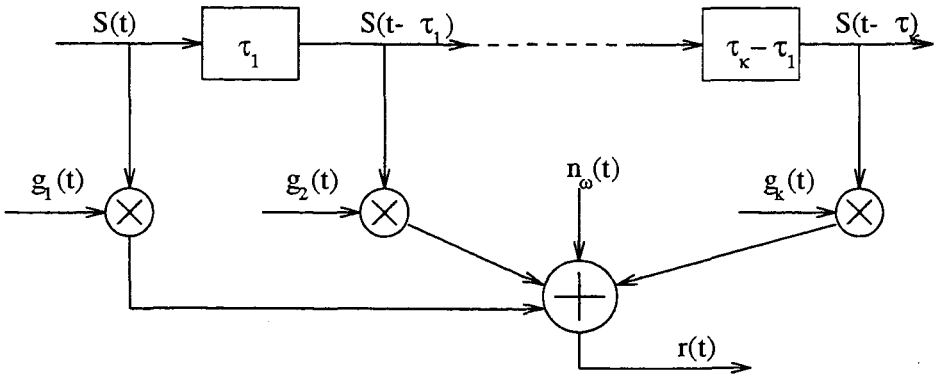

Figure 2.2: Tapped delay line frequency-selective Rayleigh fading channel model.

the combination of the three flat fading processes represents the frequency-selective fading process. Mathematically the recived signal $r(t)$ can be written as

$$r(t) = g_1(t)s(t) + g_2(t)s(t-\tau_1) + g_3(t)s(t-\tau_2) + n_w(t) \tag{2.6}$$

where the process $n_w(t)$ is additive white Gaussian noise (AWGN) in the channel and it has a two-sided power spectral density of N_0. On the other hand, $g_1(t)$, $g_2(t)$ and $g_3(t)$ are also zero mean complex Gaussian processes, but each of them represents the effect of a flat fading process. Their autocorrelation functions are

$$\phi_{g1}(\lambda) = \frac{1}{2}E[g_1(t)g_1^*(t-\lambda)] = \sigma_{g_1}^2 J_0(2\pi f_D \lambda) \tag{2.7}$$

$$\phi_{g2}(\lambda) = \frac{1}{2}E[g_2(t)g_2^*(t-\lambda)] = \sigma_{g_2}^2 J_0(2\pi f_D \lambda) \tag{2.8}$$

and

$$\phi_{g3}(\lambda) = \frac{1}{2}E[g_3(t)g_3^*(t-\lambda)] = \sigma_{g_3}^2 J_0(2\pi f_D \lambda) \tag{2.9}$$

where λ in these equations is the delay variable; $\sigma_{g_1}^2$, $\sigma_{g_2}^2$ and $\sigma_{g_3}^2$ are variances of the three fading processes. In addition, we define the power split ratio between the three rays as

$$\Gamma_1 = \frac{\sigma_{g_2}^2}{\sigma_{g_1}^2} \tag{2.10}$$

$$\Gamma_2 = \frac{\sigma_{g_3}^2}{\sigma_{g_1}^2} \tag{2.11}$$

2.3 Spread Spectrum

Spread spectrum is a technique for effeciently using the spectrum by allowing additional users to use the same bandwidth as other existing users. The idea behind spread spectrum is to transform a signal $s(t)$ with bandwidth B_s into a noise-like signal with much larger bandwidth B_{ss}. This is illustrated in Figure 2.3; the ratio B_{ss}/B_s is called the processing gain and is usually denoted by G. If G equals 30dB, then this means the power of the radiated spread spectrum signal is spread over 1000 times the original bandwidth. Its power spectral density is correspondingly reduced by the same amount. It is this feature that gives the spread spectrum signal the characteristic of being "noise-like". It also gives spread spectrum the advantages such as anti-interference and multiple user random access communications with selective addressing capability.

There are the two most popular signal spreading schemes: direct sequence (DS) and frequency hopping (FH). In DS, each information bit is symbolized by a large number of coded bits called chips. For example, assume an information bit rate of $R = 10kb/s$ and a corresponding transmission bandwidth $B_s = 10kHz$. If each bit of the 10 kb/s data stream is coded into 100 chips, then the chip rate is 1 M chips/s, which needs a DS bandwidth of $B_{ss} = 1$MHz. The processing gain (G) is

$$G = 10 \log \frac{B_{ss}}{B_s} = 20dB \tag{2.12}$$

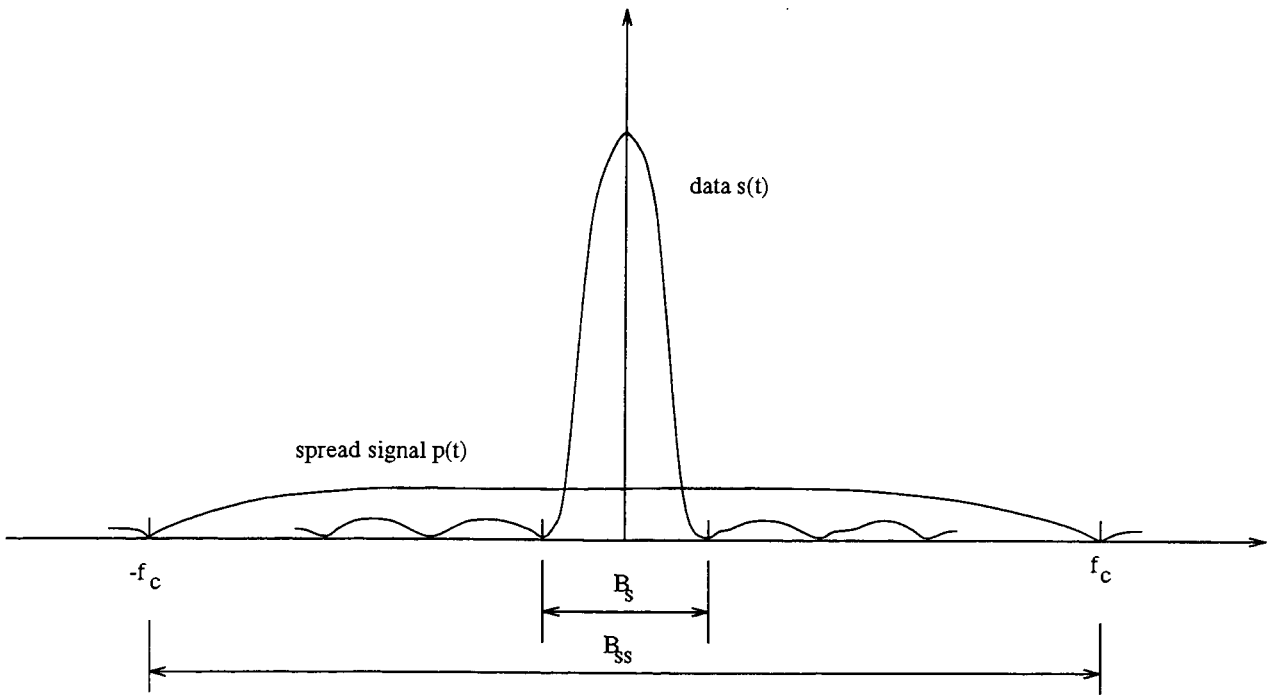

Figure 2.3: Power spectrum of data and of spread signal.

In FH, the receiver would equip N frequency channels for an active call to hop over those N frequencies with a determined hopping pattern. For example, if the information channel bandwidth is 10 kHz and there are $N = 100$ channels to hop, the FH bandwidth B_{ss} will be 1 MHz. Since the original spectrum is spread from 10 kHz (no hopping) to 1 MHz (frequency hopping), the processing gain is again

$$G = 10 \log N = 20dB \tag{2.13}$$

The total number of hopping frequency channels are also called chips. FH can be done slowly (one hop per many symbols) or fast (many hops per symbol).

Spread spectrum modulation can be used for reducing intentional interference. When people started to consider using it to increase the relative capacity of a CDMA

system compared to FDMA or TDMA, they found that DS is an effective way to serve this purpose. We will concentrate our work on DS in this thesis and we will introduce some of the relevant concepts in DS spread spectrum in the following sections.

2.3.1 Direct Sequence

Figure 2.4(a) is a simple block diagram to illustrate the basic DS technique and Figure 2.4(b) shows the waveforms involved in generating a direct sequence signal. The spreading is accomplished by multiplying the modulated information-bearing signal by a binary ± 1 baseband code sequence waveform $PN_i(t)$. The code sequence waveform may be thought of as being pseudo randomly generated so that each binary chip can change every T_c seconds. Thus, the signal for the ith transmitter is

$$s_i(t) = PN_i(t)A \cdot d_i(t)\cos(\omega_0 t + \phi_i) \tag{2.14}$$

where $d_i(t)$ is the data modulation (assumed to be ± 1 for BPSK signaling), A is the amplitude of the BPSK waveform and ϕ_i is a random phase. From equation (2.14), it is clear that a receiver with access to $PN_i(t)$ and who is also synchronized to the spread spectrum transmitter, can receive the data signal $d_i(t)$ by a simple correlation. In the interval $[0, T]$, if the data symbol is $d_i(k)$, which can take on values ± 1, the received signal after de-spreading will be

$$\begin{aligned} \frac{2}{T}\int_0^T PN_i(t)\cos(\omega_0 t + \phi_i)s_i(t)dt &= \qquad (2.15) \\ \frac{2}{T}\int_0^T PN_i(t)\cos(\omega_0 t + \phi_i)PN_i(t)\cos(\omega_0 t + \phi_i)Ad_i(k) &= Ad_i(k) = \pm A \end{aligned}$$

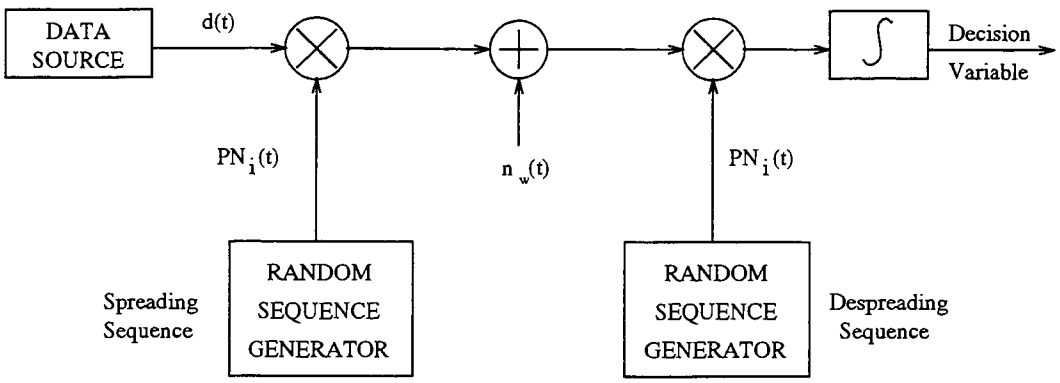

(a)

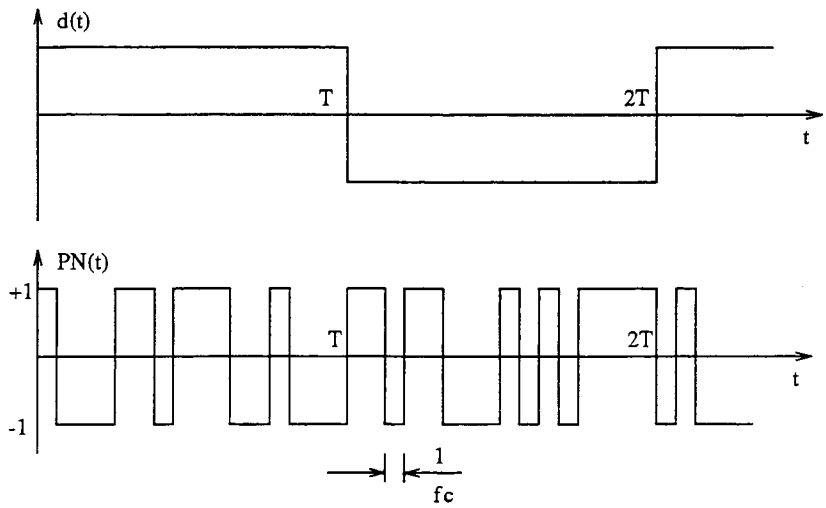

(b)

Figure 2.4: (a) Direct-sequence spread spectrum system for transmitting a single binary digit (baseband). (b) Data bit and chipping sequence.

2.3.2 Pseudo-Noise Sequence

For spreading, people usually use pseudo-random or pseudo-noise (PN) sequences. These sequences have many of the random properties of a fair-coin-toss experiment. These properties include the following:

1. In a long sequence, about 1/2 the chips will be $+1$ and 1/2 will be -1;
2. A run of length r chips of the same sign will occur about $2^{-r}l$ times in a sequence of l chips;
3. The autocorrelation of the sequence $PN_i(t)$ will be very small except in the vicinity of $\tau = 0$;
4. The cross correlation of any two sequences $PN_i(t)$ and $PN_j(t+\tau)$ will be small.

An important class of sequences called maximal length linear feedback shift register (MLLFSR) sequences are well known to have properties 1), 2), and 3). The autocorrelation function

$$R_i(\tau) = \frac{1}{T_p}\int_0^{T_p} PN_i(t)PN_i(t+\tau)dt \tag{2.16}$$

is given as

$$R_i(\tau) = \begin{cases} 1 - \frac{\tau}{T_p}(1+\frac{T_c}{T_p}), & 0 \leq |\tau| \leq T_c \\ -\frac{T_c}{T_p}, & T_c \leq |\tau| \leq (N-1)T_c \\ \tau - \frac{T_p - T_c}{T_c}(1+\frac{T_p}{T_c}) - \frac{T_p}{T_c}, & (N-1)T_c \leq |\tau| \leq NT_c \end{cases} \tag{2.17}$$

where T_p is the period of the sequence and $R_i(\tau)$ is also periodic with period T_p. The correlation property is quite significant in a mobile communications system. For

example, if $T = T_p$ and $G = T/T_c = 128$, then equation (2.16) tells us that a signal due to multipath, arriving τ seconds after the first signal, is attenuated by $R_i(\tau)$. In particular, if $T_c \leq \tau \leq T - T_c$, then the power of the multipath signal is reduced by $(T_c/T)^2 = (1/128)^2$, or about 42dB. Figure 2.5 shows the autocorrelation function and the power spectral density of PN sequence. When the period L of the PN sequence is very large, the spectral lines get closer together. For practical purposes, the spectrum may be viewed as being continuous and similar to that of a purely random binary waveform as shown in Figure 2.3.

One point about the anti-multipath capability of DS needs to be clarified. Equation (2.16) refers to a full correlation (a correlation over the complete period of the spreading sequence). In reality, data are usually present on the signal, and data transitions typically occur 50% of the time. With the presence of data, assumed to take on values ± 1, and after correlation with the local PN sequence, the received signal is

$$\pm \frac{1}{T_p} \int_0^{\tau} PN_i(t) PN_i(t+\tau) dt \pm \frac{1}{T_p} \int_{\tau}^{T_p} PN_i(t) PN_i(t+\tau) dt \qquad (2.18)$$

where the independent $\pm$ signs on the two terms of equation (2.18) correspond to the fact that they are due to different data symbols. When either both signs are plus or minus, equation (2.16) applies and, as in the example presented above, the attenuation would indeed be 42 dB. However, when the two signs differ, equation (2.18) applies, indicating that we now have the sum of two partial correlations rather than one total correlation. In particular, if $\tau = 32T_c$ (i.e., the multipath is delayed by about one quarter of the symbol duration), then for one specific maximal length shift register sequence, the attenuation of the multipath can be shown to be reduced

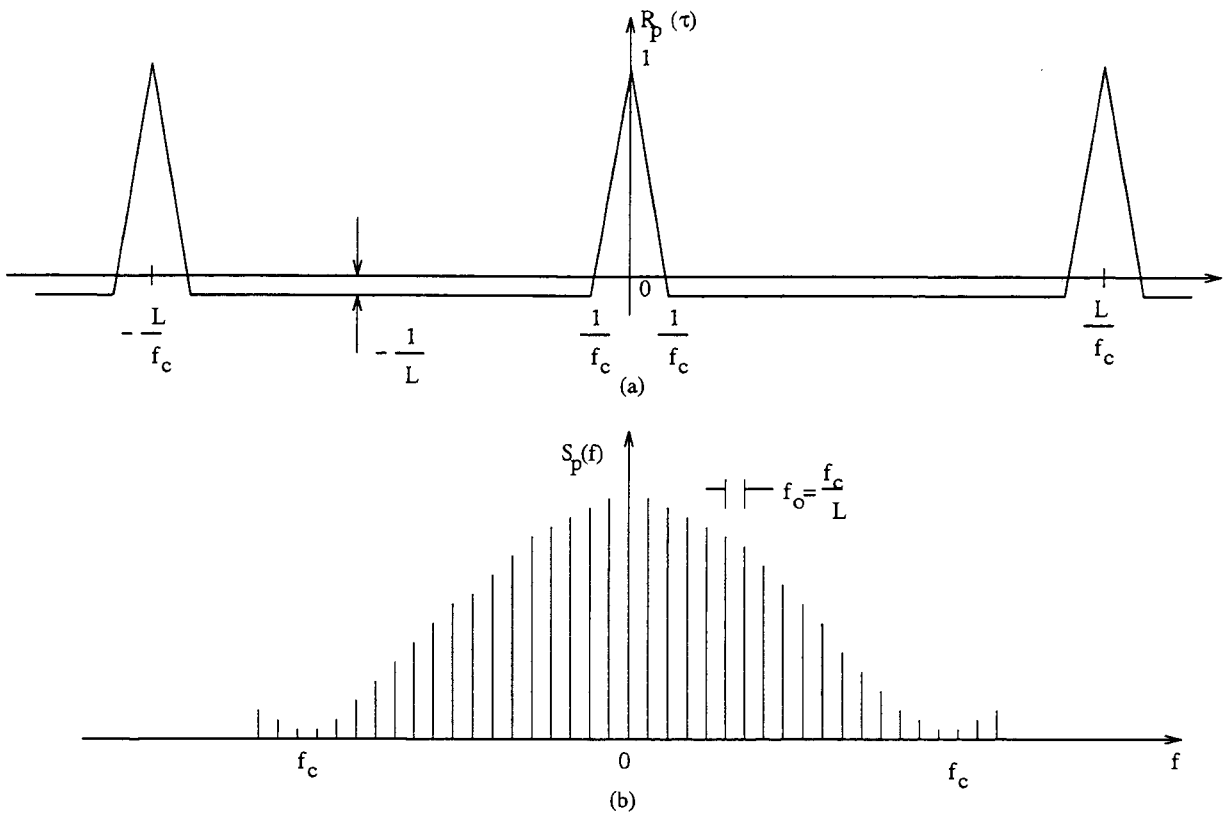

Figure 2.5: Autocorrelation function $R_p(\tau)$ and power spectral density of MLLFSR sequence waveform $p(t)$. (a) Autocorrelation function of $p(t)$. (b) Power spectral density of $p(t)$

from 48dB to 12 dB.

2.4 Major Issues within Cellular CDMA

There are three multiple access schemes that can be used to share resources in mobile communication system: FDMA, TDMA and CDMA. FDMA serves the calls with different frequency channels; TDMA serves the calls with different time slots; and CDMA serves the calls with different code sequences. The illustration of the differences among these three multiple access schemes are shown in Figure 2.6. In DS CDMA, each user's signal is modulated by a different orthogonal pseudo-random binary sequence that spreads the spectrum of the waveform. A large number of CDMA signals share the same frequency spectrum. The signals are separated in the receivers by using a correlator which accepts only signal energy from the selected binary sequence and despreads its spectrum. The other users' signals, whose codes do not match, are not despread in bandwidth and as a result, contribute only to the noise and represent a multiple access interference (MAI) generated by the system.

The reason that the spread spectrum is used for cellular communication is that CDMA can allow many users to access the channel simultaneously. The distinction between CDMA and either TDMA or FDMA is that the former provides, in addition to the basic multiple accessing capability, the other attributes such as privacy, no network synchronization, multipath tolerance, etc. These later attributes are either not available with the use of the narrow-band waveforms which are employed

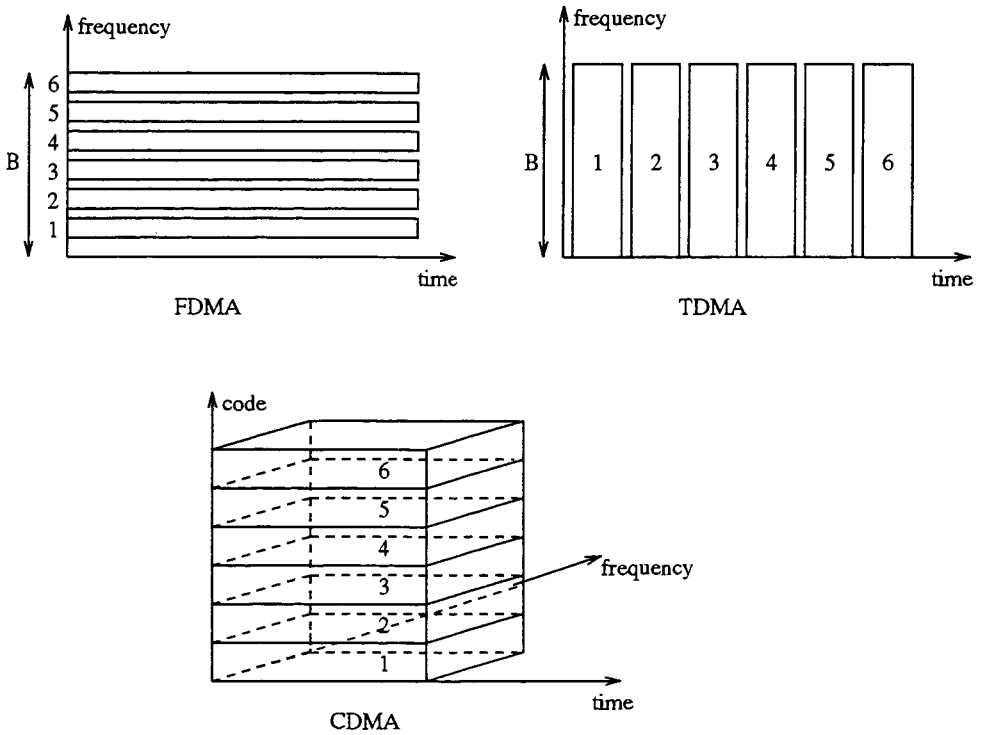

Figure 2.6: Illustration of different multiple access systems.

with TDMA or FDMA, or are much more difficult to achieve. For example, one can typically implement a narrowband digital communication link that is tolerant to multipath interference by including in the receiver an adaptive equalizer. However, this increases the complexity of the receiver, and may affect the ability to perform a smooth handover. Indeed, since the equalizer must continually adapt to an ever changing channel, it is a high-risk component of a TDMA system. Furthermore, as pointed out by some researchers, the performance of CDMA system degrades "gracefully". In FDMA and TDMA, each frequency channel or each time slot is assigned to one call. If all channels or time slots are in use, no other calls can share the same channel or time slot during the call period. On the other hand, CDMA can squeeze additional code sequences in the same radio channel, i.e., add the extra users, which the other two multiple access schemes cannot. However, adding additional code sequences, of course, will raise the noise level, and hence, the error rate.

2.4.1 Near-Far Problem

There are a number of disadvantages associated with cellular CDMA. The two most obvious ones are the problem of "self-jamming", i.e., the interferences, and the related problem of the "near-far" effect. The interferences arise from the fact that in an asynchronous CDMA network, the spreading sequences of the different users are not orthogonal, and hence in the despreading of a given user's waveform, non-zero contributions to that user's test statistics arise from the transmissions of the other users in the network. This is also as distinct from either TDMA or FDMA, with their reasonable time or frequency guardbands, orthogonality of the received signals

can be preserved. As for the "near-far" effect, since all the users are typically geographically separated, a receiver trying to detect the kth signal might be much closer physically to the ith transmitter rather than the kth transmitter. Therefore, if each user transmits with equal power, the signal from the ith transmitter will arrive at the receiver with a larger power than that of the kth signal. While the powers are additive, the close-in transmitter has a $(d_u/d_d)^r$ advantage in power, where d_u is the distance to the undesired transmitter, d_d is the distance to the desired transmitter, and r is the propagation exponent. This particular problem is often a severe problem with DS CDMA and must be dealt with properly for the potential of CDMA to be reached.

According to our discussion in Section 2.3.2, both the cross-correlation and the partial-correlation functions of the PN sequences are the key parameters in a DS CDMA system. The design and optimization of code sets with good partial-correlation properties can be found in many references [34]-[40]. To solve the near-far effect and achieve high capacity, quality, and other benefits, power control techniques should be considered in the cells of interest as described in the following sections.

2.4.2 Power Control

It is desirable to maximize the capacity of the CDMA system in terms of the number of simultaneous users that can be handled in a given system bandwidth. The system's capacity is maximized if the transmitting power of each mobile station is controlled so that its signal arrives at the cell site with the minimum required signal-to-interference ratio. If a mobile station's signal arrives at the cell site (uplink) with too low a value of

received power, the bit error rate is too high to permit high quality communications. If the received power is too high, the performance of this mobile station is acceptable. However, interference to all the other mobile station transmitters that are sharing the channels would be increased, and may result in unacceptable performance to other users unless the capacity is reduced. Cell site transmitter power control (downlink) is also need. In certain locations, the link from the cell site transmitter to the mobile station is disadvantaged, and the power being transmitted to this mobile station needs to be increased to make the quality acceptable. While the mobile station is located where the signal-to-interference ratio is good, the cell site transmitter should transmit the desired signal using a lower power to reduce interference to other signals being transmitted by the system.

In this thesis, we will concentrate on the uplink closed loop power control. The objective of uplink power control process is to produce a nominally-received signal power from each mobile station transmitter operating within the cell at the cell site receiver. Regardless of a mobile station's position or propagation loss, each mobile station's signal will be received at the cell at the same level. If all the mobile stations' transmitters within a cell site's area of coverage are controlled, then the total signal power received at the cell site from all mobile stations is equal to the nominallly-received power multiplied by the number of mobile stations.

In early studies, uplink power control relied on the accurate measurement of absolute signal strength at every base station. In reality, this seems to be impractical because it would require a system-wide calibration of all base-station receivers to

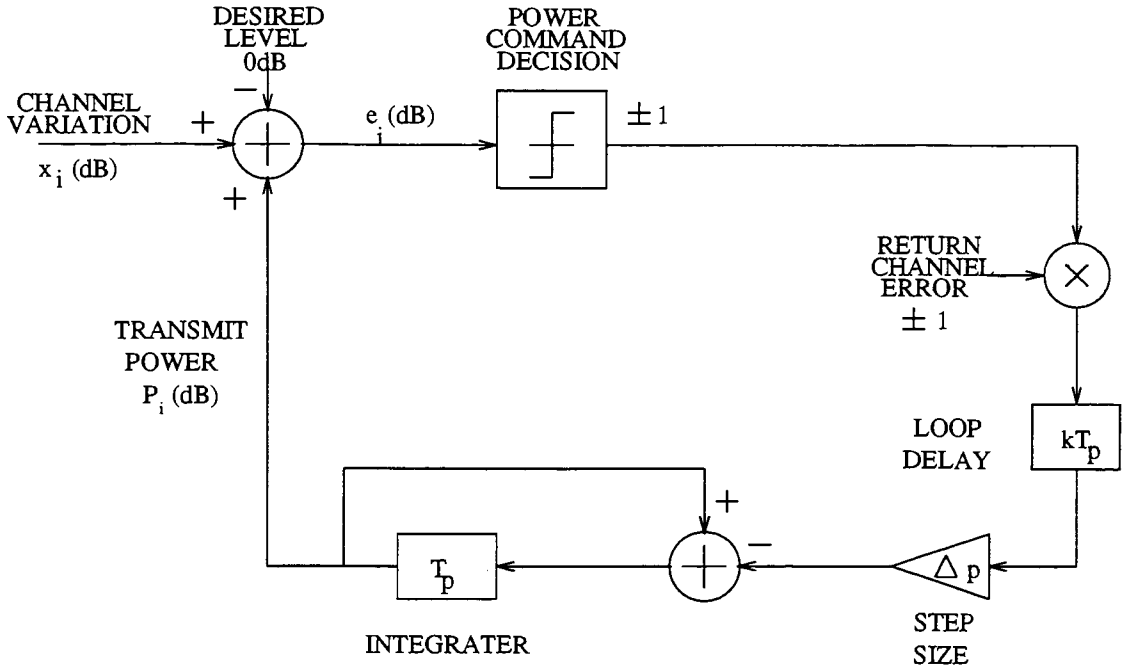

Figure 2.7: Feedback power control model.

eliminate the uncertainty and differences in the characteristics of individual receivers. It has been found recently that power control based on the ratio of signal power to interference power (SIR) is more realistic. It is actually desirable from the radio link performance perspective, since it is the SIR that determines the received bit error probability. Usually feedback algorithms that allow power command decisions to be made at the base station receiver are considered.

Figure 2.7 shows a simple model of feedback power control used in uplink. The user transmitting signal power p_i dB is updated by a fixed step Δp dB every T_p seconds. T_p is called the power control sampling period. During ith period, the signal power received at the base station is $(p_i + x_i)$ dB where x_i dB is the channel variation.

The received signal power is compared to a desired threshold at the base station, and a hard quantized power command bit is transmitted back to the user over the return channel. The model in Figure 2.7 also includes the possibility of return channel errors and the extra loop delay kT_p (k:integer) which accounts for the propagation and time delays involved in generating, transmitting, and executing a power control command. Usually the power control command bit is assumed to be unprotected, since the usual long delay due to coding/interleaving is inconsistent with the need for fast power control.

2.4.3 Multipath Diversity and RAKE receiver

As we have mentioned, a mobile communication system experiences a multipath propagation environment. This means there is more than one path linking the transmitter to the receiver. These different paths might consist of several discrete paths, each one with a different attenuation and time delay relative to the others, or they might be a continuum of paths. In relatively narrowband modulation systems such as analog FM modulation employed by the first generation cellular system, the existence of multiple paths causes severe fading. Diversity techniques are widely used to mitigate fading and to achieve a highly reliable digital data transmission without excessively increasing transmitter power. There are several ways that we can provide the receiver with several independently fading replicas of the same information-bearing signal: time, frequency, and space. Time diversity can best be obtained by the use of interleaving and error correction coding. Frequency diversity is achieved by transmitting the signal on different carriers where the separation between successive carriers exceeds the

coherence bandwidth of the channel. Space diversity is obtained by employing extra transmitting or receiving antennas.

With wideband CDMA modulations, the transmitted signal has a bandwidth much greater than the coherent bandwidth of the channel. Such a signal with bandwidth W will resolve the multipath components and provide the receiver with several indepedetly fading signal paths. Thus, the use of a wideband signal with this inherent multipath effect may be viewed as a sophisticated method for frequency diversity. The optimum receiver for processing the wideband signal will achieve the the performance of an equivalent diversity communications system.

When the relative delay between two resolved paths is larger than the chip duration T_c, these two paths are considered to be independent and they arrive at the receiver through different fading processes. However, if the delay between any two paths is smaller than T_c, they can be treated as a single path. This assumption has been confirmed by field test [3]. Multipath processing takes the form of parallel correlators for the PN waveform. The receiver employs several parallel correlators. There is one for each identified multipath, and this technique allows individual path arrivals to be tracked independently. Afterwards, the sum of their received signal strengths is used to demodulate the signal. Fading processes of different arrivals are independent, and the demodulation based on the sum of the signals is much more reliable. These parallel correlators are also called RAKE receivers, and they are the optimum receivers mentioned above for wideband signals.

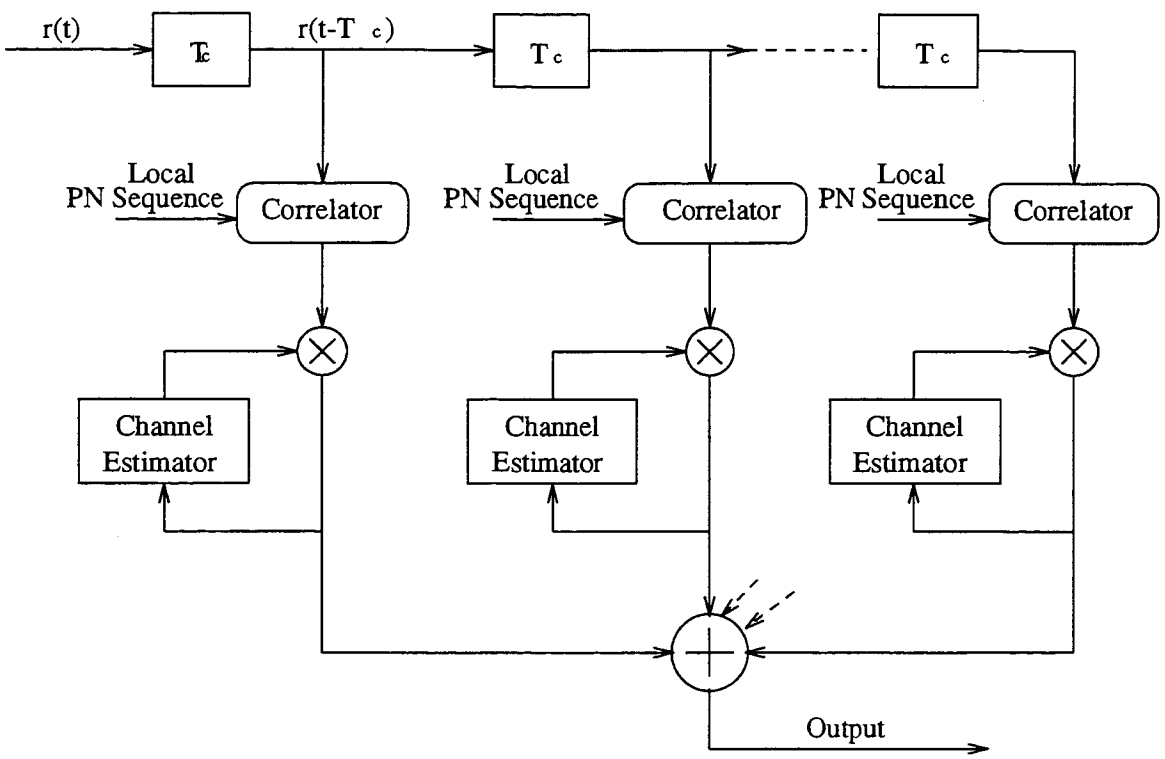

Figure 2.8: Model of RAKE receiver with maximal ratio combining.

Many types of RAKE receivers have been suggested in [3, 14]. Usually it employs coherent detection with maximum ratio combining or differential detection with equal gain combining. It is known that the coherent detection provides a 3dB gain over differential detection in a flat Rayleigh fading environment. This gain is achieved with the perfect estimation of the channel state information (CSI). In this thesis, we consider both equal gain combining for differential detection and maximal ratio combining for coherent detection. The RAKE receiver used in simulation has the structure of a tapped delay lind followed by a group of correlators and a combining unit. The receiver detects the incoming multipath signals and despreads the wideband signal with local PN sequences. The despread signals from independent paths will be demodulated and combined to form the decision variable. We assume the relative delays are always the multiples of the chip duration and by despreading the received signal with local PN sequences, signals through independent multipaths can be detected respectively. There are many taps at the RAKE receiver, but only several of them contain signal energy, while the others are only multiple access interference and noise.

2.5 Characteristics of Interference

As mentioned in Section 2.4, there are many users in a cellular CDMA system with different PN sequences. At the receiver, the received signal includes all the multipath signals from all users within certain areas (usually a cell). While each tap of a designated RAKE receiver is synchronized to a certain multipath of the signal of the designated user, the received signal includes the desired information as well as various

interferences and noises.

Here we consider a simple BPSK system to give basic results for the characteristics of the interferences. The received signals is

$$r(t) = \sum_{k=1}^{K} \sum_{l=1}^{L} A_k^l PN_k(t - \tau_k^l) s_k(t - \tau_k^l) \cos(\omega_c t + \phi_k^l) + n(t) \tag{2.19}$$

where $r(t)$ is the received signal, K is the total number of active users, L is the total number of multipaths of each user, A_k^l is the amplitude of the l_{th} path of the k_{th} user, $s_k(t)$ is the information sequence of the k_{th} user at bit-rate R_b, $PN_k(t)$ is the spreading chip sequence of the k_{th} user at chip-rate, R_c, $n(t)$ is the additive white Gaussian noise, $G = T/T_c$ is the processing gain, T is bit period and T_c is chip period. τ_k^l and ϕ_k^l are the time delay and the phase of the k_{th} user's l_{th} path, which are assumed to be known to the receiver. The information bits and chips are rectangular. Their values are all i.i.d. random values with probability 0.5 of ± 1. The τ_k^l and ϕ_k^l are all i.i.d. uniform random variables in $[0, T]$ and $[0, 2\pi]$ respectively.

We assume knowledge of the spread sequence of the designated user at the receiver. Without loss of generality, we consider the receiver for the first user. After being processed by the RAKE receiver and the low pass filter, the correlation value from the n_l^{th} correlator of user 1 is

$$\begin{aligned} y_1^{n_l}(i) &= \int_{\tau_1^{n_l}}^{T+\tau_1^{n_l}} r(t) PN_1(t - \tau_1^{n_l}) dt \qquad (2.20) \\ &= A_1^{n_l} s_1(i) + I_1(l) + I_I(l) + N_I(l) \\ &= A_1^{n_l} s_1(i) \\ &\quad + \frac{1}{T} \sum_{l=1, l \neq n_l}^{L} \int_{\tau_1^{n_l}}^{T+\tau_1^{n_l}} A_1^l s_1(t - \tau_1^l) PN_1(t - \tau_1^l) PN_1(t - \tau_1^{n_l}) \cos \phi_1^l dt \end{aligned}$$

$$+\frac{1}{T}\sum_{k=2}^{K}\sum_{l=1}^{L}\int_{\tau_1^{n_l}}^{T+\tau_1^{n_l}} A_k^l s_k(t-\tau_k^l)PN_k(t-\tau_k^l)PN_1(t-\tau_1^{n_l})\cos\phi_k^l dt$$
$$+\frac{1}{T}\int_{\tau_1^{n_l}}^{T+\tau_1^{n_l}} n(t)PN_1(t-\tau_1^{n_l})\cos\phi_1^{n_l} dt$$

where the second term $I_1(l)$ in equation (2.21) is the self-interference to the n_lth branch of the RAKE receiver due to the multipath; the third term $I_I(l)$ is the multiple access interference from other users; and $N_I(l)$ is the term due to the presence of AWGN.

The characteristics of multipath interference and multiuser interference in mobile CDMA system have been studied in [34] - [42]. The self-interference is mainly decided by the shifted auto-correlation of the spreading sequence $PN_1(t)$, and the multiple access interference is determined by the cross-correlation properties among spreading sequences. If a long period spreading sequence is adopted, it can be modeled as a random binary sequence, and the properties of auto-correlation and cross-correlation would be quite similar. Analysis [41] based on the moments of the multipath and multiuser interference random variables have shown that with the large processing gain G, the interference variables can be treated as Gaussian. Furthermore, as for the asynchronous case, where τ_k^l and ϕ_k^l are uniformly distributed over $[0,T]$ and $[0,2\pi]$ respectively, the variance of the cross-correlation is given by [39, 40]

$$\sigma^2 = Var[\frac{1}{T}\int_0^T PN(t-\tau_1)PN(t)\cos\phi dt] \approx \frac{1}{3G} \qquad (2.21)$$

We will model the self-interference as Gaussian noise in our simulation in Chapter 3.

2.6 Summary

In this chapter, we have introduced some terminologies commonly used in mobile communications. We also introduced spread spectrum techniques and their applications in a cellular CDMA system. The RAKE receiver and power control technique, which are important factors in land mobile communication, have been illustrated. Finally, the additive white Gaussian characteristics of the multipath and multiuser interferences have been described. We will use these models and concepts in our research work in the following chapters.

Chapter 3

An Analysis of PSAM for Rayleigh Fading Channels in CDMA

In this chapter, we will discuss the combining of different rate convolutional coding schemes with PSAM and M-ary PSK modulation techniques in CDMA environment. We will examine their performance in the frequency-selective Rayleigh fading channel in the presence of self-interference. The performance of this system is analyzed and the exact expression for the pairwise error event probability is given. An upper bound for the PSAM with convolutional coding is also calculated. With the total transmission bandwidth fixed, our results show the trade off between coding rate, processing gain, and selection of modulation schemes for the system.

The organization of this chapter is the following: Section 3.1 introduces the system model of coded PSAM in CDMA, descriptions of the transmitted signal, coding and spreading schemes, and receiver processing. Section 3.2 gives the exact pairwise error

event probability and the calculation of upper error bound in a coded system. Section 3.3 considers the pilot symbol insertion scheme and the selection of parmeters. Section 3.4 compares the performance of different coding, spreading and modulation schemes.

3.1 System Model

The system block diagram of the coded communication system used in the thesis is given in Figure 3.1 Ideal interleaving is assumed in the system. This assumption is justified for continuous data transmissions under moderately fast fading conditions. As shown in [44], an interleaving depth (given in number of symbols) of about one quarter the inverse of the normalized Doppler frequency provides almost the same effect as ideal interleaving.

3.1.1 General Description

The block diagram of our system is given in Figure 3.1. The input to the convolutional encoder is a sequence of binary digits denoted as

$$\mathbf{a} = (a_1, ..., a_k, ...) \tag{3.1}$$

and the coded output data are mapped to a MPSK symbol in the symbol set. The M-PSK symbols are denoted as

$$\mathbf{c_i} = (c_{i1}, ..., c_{ik}, ...) \tag{3.2}$$

which is the ith codeword of the scheme. Each symbol c_{ik} in $\mathbf{c_i}$ is a point in the complex plane, and the set of distinct symbols forms the signal constellation. The sequence of modulation symbols is passed to an interleaver with a depth greater than

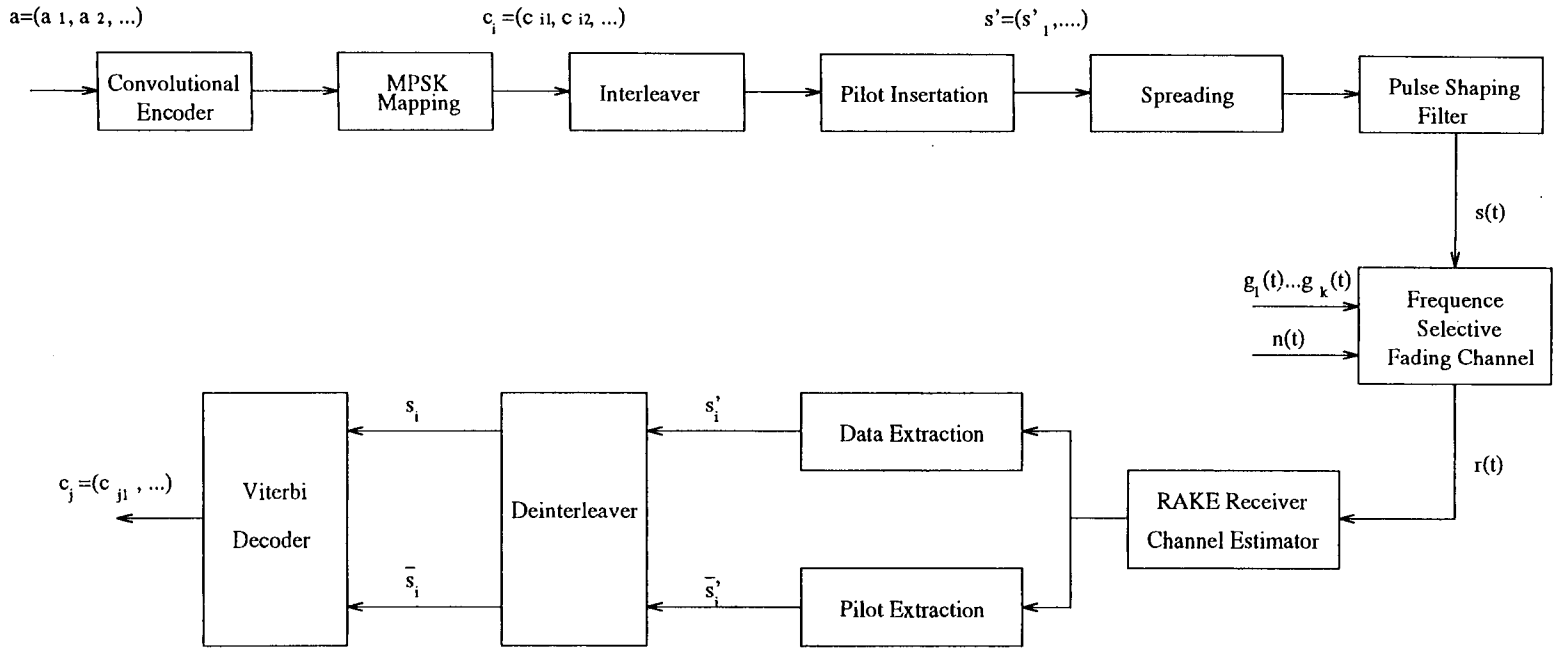

Figure 3.1: System Block Diagram

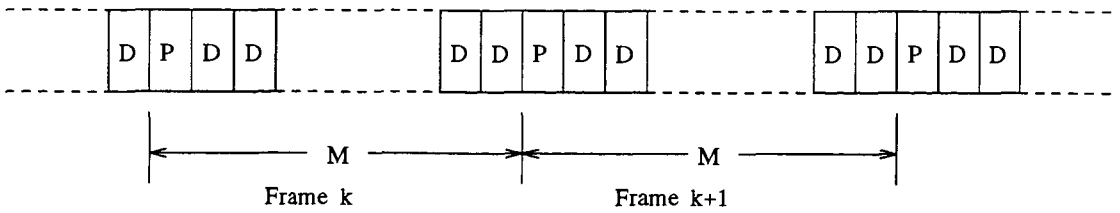

Figure 3.2: Transmitted frame structure.

the memory of the channel fading processs. Its output is denoted as

$$\mathbf{c}_i' = (c_{i1}', ..., c_{ik}', ...) \tag{3.3}$$

Pilot symbols are then inserted periodically into the sequence $\mathbf{c}_i'$. The symbols are formatted into frames of length M in which the pilot symbols at times $i = kM$ have a known value $\tilde{s}$. The frame structure is shown in Figure 3.2, where P denotes the pilot symbol and D is the data symbol. The resulting sequence is denoted as

$$\mathbf{s}' = (s_1', ..., s_k', ...) \tag{3.4}$$

The signal will be multiplied by a binary PN sequence to spread the transmission bandwidth. After the pulse shaping filter, the spreaded signal is transmitted in the usual way over a frequency-selective Rayleigh fading channel.

At the receiver, the received signal will pass through a RAKE receiver, which was described in Section 2.4.3. The samples are then split into two streams: one for the data, and the other for the pilot symbols. An estimate of the channel is obtained through interpolation of the received pilot symbols.

3.1.2 Coding and Spreading Schemes

In our study, we keep the information throughput and spreaded bandwidth constant, then compare the error performance of the system under different coding and spreading schemes. The information data rate is assumed to be 1 and the spreaded bandwidth of the transmitted signal is B. We consider rate $1/2$ and $1/3$ convolutional code with constraint lengths of 3 and 5, as well as BPSK, QPSK and 8PSK modulation. The encoder structure and spreading schemes are depicted in the following sections.

BPSK

The coding rate of convolutional encoder is k/n, i.e., k input information bits are encoded into n coded bits. While the spreading factor (processing gain) is G, we wish to keep the spreaded bandwidth of the transmitted signal $B = Gn/k$ constant. Obviously, there will be a trade off between the coding rate k/n and the processing gain G. Furthermore, while the pilot symbol is inserted into the transmitted data stream, and the frame size is M, the spreaded bandwidth will be

$$B = G\frac{n}{k}\frac{M}{M-1} \tag{3.5}$$

where we can see that the insertion of the pilot symbol also affects the processing gain of the PSAM system. The effect will be examined in following sections.

The constraint length for the convolutional codes studied in this thesis are 3 and 5. We use the good codes in [14]. The encoder generator polynomials (g_1, g_2) of constraint length 3 and rate $1/2$ code are (in octal form) $g_1 = 5$ and $g_2 = 7$; for constraint

length 5 rate 1/2 code, the generator polynomials are $g_1 = 23$, $g_2 = 35$. The encoder generator polynomials (g_1, g_2, g_3) of constraint length 3 and rate 1/3 code are, $g_1 = 5$, $g_2 = 7$ and $g_3 = 7$. For constraint length 5 rate 1/3 code, the generator polynomials are $g_1 = 25, g_2 = 33, g_3 = 37$. Figure 3.3 are the structures of the convolutional encoders.

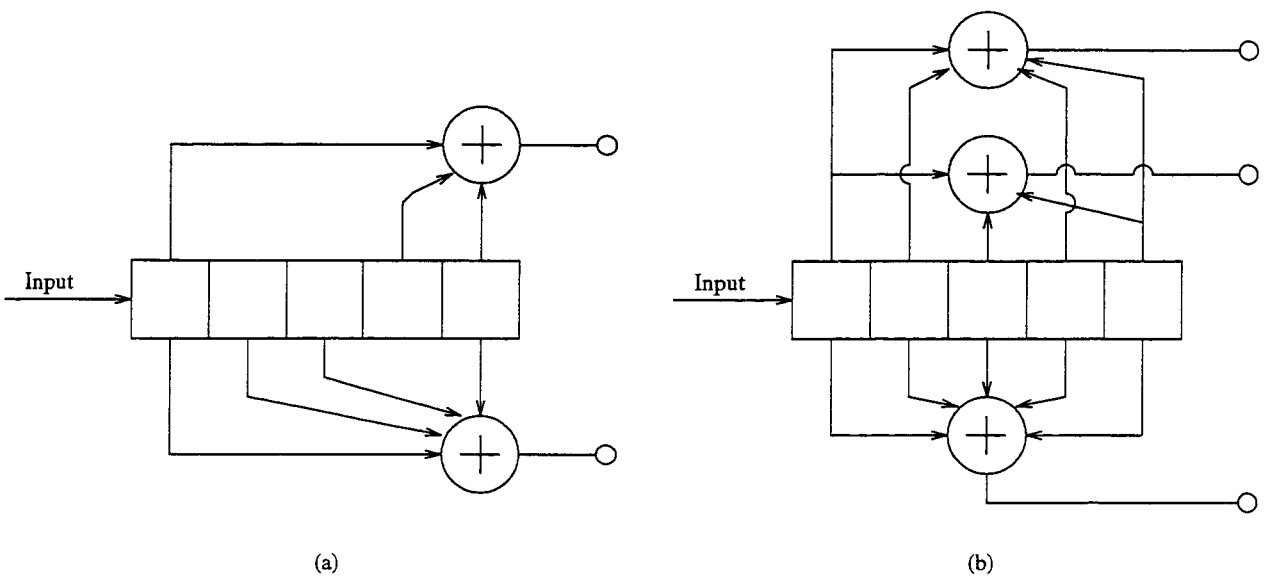

Figure 3.3: (a) Structure of $L = 5, k = 1, n = 2$ Convolutional Encoder. (b) Structure of $L = 5, k = 1, n = 3$ Convolutional Encoder.

The trellis diagram for the rate 1/3 L=5 convolutional code is plotted in Figure 3.4.

QPSK and 8PSK

To keep the information throughput and the spreading factor unchanged, we considered rate 1/2 convolutional code with QPSK modulation as well as rate 1/3 convolutional code with 8PSK modulation. For rate 1/2 QPSK and rate 1/3 8PSK, the code

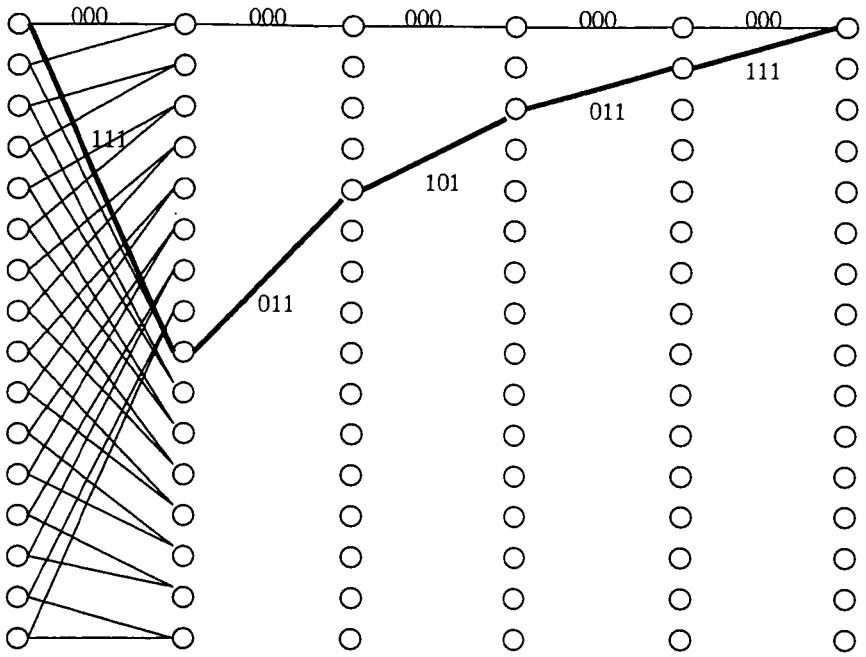

Figure 3.4: Trellis diagram of rate 1/3 $L = 5$ convolutional code.

rate and transmission bandwidth are fixed, and there is no trade off between the code rate and the processing gain as in BPSK. Only the insertion of the pilot symbol has an effect on the processing gain. The relationship of the processing gain G and the frame size M is $B = G\frac{M-1}{M}$.

Figure 3.5 shows the constellations of QPSK and 8PSK, which the Gray coding is adopted to convert the information bits to the transmitted PSK signal. The PSK signal in the kth signaling interval $k = 0, 1, ..., N$ can be expressed in a complex form as $s_k = exp(j\theta_k)$, where θ_k is the transmitted signal phase and will take one of the M values from the set $(2\pi m)/M; m = 0, 1, ..., M-1$.

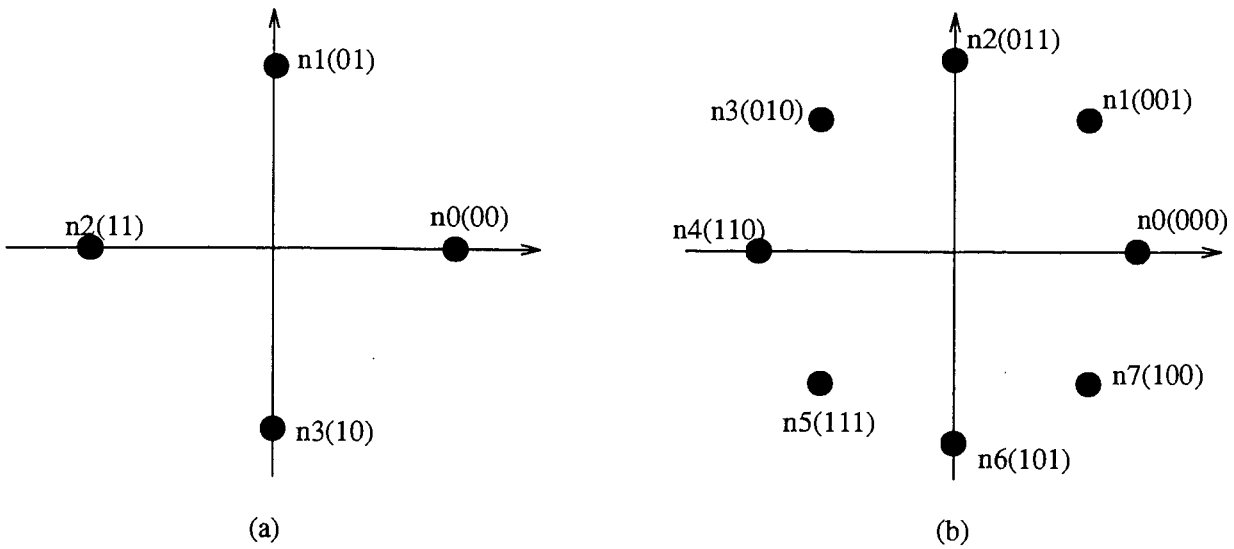

Figure 3.5: (a) Constellations of QPSK with Gray mapping. (b) Constellations of 8PSK with Gray mapping.

The baseband equivalent of the transmitted signal is given as

$$S(t) = A \cdot s(t)PN(t) \qquad 0 \leq t \leq T \tag{3.6}$$

where A is the amplitude, $s(t)$ is the data waveform which takes one of the M complex PSK symbol values, and T is the symbol duration.

$$PN(t) = \sum_{n=-\infty}^{+\infty} PN(n)\psi(t - nT_c) \tag{3.7}$$

$PN(t)$ is the pseudo-noise spreading waveform, $PN(n)$ is the n-th chip in the pseudo-random waveform, and $G = T/T_c$ is the processing gain. $\psi(t)$ is a unit energy rectangular pulse of chip duration T_c, and

$$\int_{-\infty}^{+\infty} |\ \psi(t)\ |^2\, dt = 1 \tag{3.8}$$

As long period PN sequences are suggested for spectrum spreading, we can assume $PN(t)$ is a truely random sequence.

3.1.3 Receiver Processing

The frequency-selective Rayleigh fading channel model is described in Section 2.2. When $S(t)$ is transmitted over a frequency-selective Rayleigh fading channel, the baseband equivalent of the received signal can be written as

$$r(t) = \sum_{k=1}^{K} \sum_{l=1}^{L} g_k^l(t) S_k(t - \tau_k^l) + n_w(t) \tag{3.9}$$

where $g_k^l(t)$ is a zero-mean complex Gaussin fading process with a variance of $\sigma_{g^l}^2$, and $n_w(t)$ is the complex envelope of the channel additive white Gaussian noise (AWGN). K is the number of users and L is the number of multipaths. $g_k^l(t)$ is the fading process related to the k_{th} user's l_{th} multipath. τ_k^l is the time delay and phase of the k_{th} user's l_{th} multipath, which is assumed to be known. First, we consider BPSK modulation, then we will extend the result to QPSK and 8PSK.

At the receiver, the output of the first user's l_{th} branch is

$$\begin{aligned} y_1^{n_l}(i) &= \frac{1}{T} \int_{\tau_1^{n_l}}^{T+\tau_1^{n_l}} r(t) PN(t - \tau_1^{n_l}) dt \qquad (3.10) \\ &= \frac{1}{T} \int_{\tau_1^{n_l}}^{T+\tau_1^{n_l}} A_1 g_1^{n_l}(t - \tau_1^{n_l}) s_1(t - \tau_1^{n_l}) PN_1(t - \tau_1^{n_l}) PN_1(t - \tau_1^{n_l}) dt \\ &\quad + \frac{1}{T} \sum_{l=1, l \neq n_l}^{L} \int_{\tau_1^{n_l}}^{T+\tau_1^{n_l}} A_1 g_1^l(t - \tau_1^l) s_1(t - \tau_1^l) PN_1(t - \tau_1^l) PN_1(t - \tau_1^{n_l}) dt \\ &\quad + \frac{1}{T} \sum_{k=2}^{K} \sum_{l=1}^{L} \int_{\tau_1^{n_l}}^{T+\tau_1^{n_l}} A_k g_k^l(t - \tau_k^l) s_k(t - \tau_k^l) PN_k(t - \tau_k^l) PN_1(t - \tau_1^{n_l}) dt \\ &\quad + \frac{1}{T} \int_{\tau_1^{n_l}}^{T+\tau_1^{n_l}} n_w(t) PN_1(t - \tau_1^{n_l}) dt \end{aligned}$$

We assume that the fading process $g_k^l(t)$ is slow enough that $g_k^l(t)$ remains roughly constant over each data symbol interval. This means that the term $g_k^l(t)s_k(t)$ can be written as $g_k^l(i)s_k(i)$, where $g_k^l(i)$ denotes the value of $g_k^l(t)$ during the i_{th} interval.

The output of the first user's RAKE receiver's l_{th} branch is sampled every T seconds to produce the $y_1^{n_l}(i)$ in

$$y_1^{n_l}(i) = A_1 g_1^{n_l}(i) s_1(i) + I_{11} + I_{1k} + N_1 \tag{3.11}$$

where I_{11} is the self-interference due to the multipath effect, I_{1k} is the multiple access interference and N_1 is the Gaussian noise.

As we discussed in Section 2.5, the interference terms can be modeled as AWGN and the variances were given as

$$Var\{I_{11}\} = \frac{A_1}{3G} \sum_{l=1, l \neq n_l}^{L} E\{[g_1^l]^2\} \tag{3.12}$$

$$Var\{I_{1k}\} = \frac{1}{3G} \sum_{k=1}^{K} A_k \sum_{l=1}^{L} E\{[g_k^l]^2\} \tag{3.13}$$

where $E[\bullet]$ denotes the mathematical expectation. The variance of the AWGN term N_1 is given as $\frac{N_0}{T}$.

It is convenient to introduce the conventional received SNR measures at this point. We define the ratio q of pilot power to data power as

$$q = \mid \tilde{s} \mid^2 / (M-1) E[\mid s \mid^2] \tag{3.14}$$

where the expectation is calculated over data symbols only. The expected total energy received over a frame after correlation combining is

$$E_f = \sigma_g^2 A^2 (\mid \tilde{s} \mid^2 + (M-1) E[\mid s \mid^2]) \tag{3.15}$$

where $\sigma_g^2 = \sum_{l=1}^{L} \sigma_{g^l}^2$ is the combined energy from different multipaths. With n bits per symbol and $M-1$ data symbols in a frame, the received energy per data bit is

$$E_b = \frac{E_f}{n(M-1)} = \frac{\sigma_g^2 A^2}{n(M-1)} \mid \tilde{s} \mid^2 (\frac{1+q}{q}) \tag{3.16}$$

While considering the single user situation, the received signal sample at the RAKE receiver's $1st$ branch output is given by equation (3.17) as

$$r(i) = Ag_1(i)s_1(i) + I_1(i) + N_1(i) \tag{3.17}$$

The self-interference term I_1 and Gausian noise samples are both white with variances $\frac{1}{3G}\sum_{l=2}^{L}\sigma_{g^l}^2$ and unity, respectively, and the signal to noise ratio $\gamma_b = E_b/N_0$. In our analysis, since the interference can be modeled as AWGN, we will use the term SIR (signal to interference ratio) instead of SNR.

3.1.4 Optimum Interpolater

Since we have a frequency-selective Rayleigh fading channel, each signal through different multipaths experienced independent fading processes. At the RAKE receiver, we will get the estimates of channel state information through pilot symbols for each RAKE receiver branch. After the channel estimation is acquired, maximal ratio combining is used to form the decision variable.

Without loss of generality, we take $s(0)$ as a pilot symbol and consider the detection of $s(k)$ $(-[M/2] \leq k \leq [(M-1)/2])$. The channel state estimator provides an estimate of the symbol gain $g(k)$ in equation (3.18) using the K nearest pilot samples

$$\hat{g}_l(k) = \underline{\mathbf{h}}_l^{\dagger}(k)\underline{\mathbf{r}}_l \tag{3.18}$$

$\hat{g}_l(k)$ is the estimated channel state information for the l_{th} multipath, where $\underline{\mathbf{h}}_l^{\dagger}(k)$ is an interpolation filter and its elements depend on the position k within the frame. The length K column vetor $\underline{\mathbf{r}}_l$ is defined as the set of pilot samples $r_l(iM)$ and the dagger denotes conjugate transpose. The estimation error is denoted by $e_l(k)$, so that

$$g_l(k) = \hat{g}_l(k) + e_l(k) \tag{3.19}$$

All the fading processes of multipaths are assumed independent; therefore, the estimation errors in different branches are independent in the RAKE receiver.

The KxK auto-correlation matrix is

$$\mathbf{\Phi}_{RR} = \frac{1}{2}E[\underline{\mathbf{r}}_l\underline{\mathbf{r}}_l^{\dagger}] \tag{3.20}$$

and the M-length K covariance vectors are

$$\mathbf{\Phi}_{g_lR} = \frac{1}{2}E[g_l^*(k)\underline{\mathbf{r}}_l] \tag{3.21}$$

If $\underline{\mathbf{h}}_l(k) = \mathbf{\Phi}_{g_lR}\mathbf{\Phi}_{RR}^{-1}$, the variance of the estimation error will be minimized and the estimator turns to be an optimum one.

$$E[\mid g_l - \hat{g}_l \mid^2] = E[\sigma_{g_l}^2 - \underline{\mathbf{h}}_l^{\dagger}(k)\underline{\mathbf{r}}_l\underline{\mathbf{r}}_l^{\dagger}\underline{\mathbf{h}}_l(k)] = \sigma_{g_l}^2 - \mathbf{\Phi}_{g_lR}\mathbf{\Phi}_{RR}^{-1}\mathbf{\Phi}_{Rg_l} \tag{3.22}$$

The expressions for the components of the arrays Φ_{RR} and Φ_{g_lR} are

$$\Phi_{RR}(ij) = A\sigma_{g_l}^2 J_0(2\pi f_D(i-j)MT) + (\sigma_I^2 + 1)\delta_{ij} \tag{3.23}$$

where σ_I^2 is the self-interference, δ_{ij} is the Kronecker delta function, f_D is the Doppler frequency of the fading channel and $J_0(\bullet)$ is the zeroth order Bessel function of the first kind.

$$\Phi_{g_lR}(i) = A\sigma_{g_l}^2 J_0(2\pi f_D(iM-k)T) \tag{3.24}$$

The sequence of received data symbols at the l_{th} branch of RAKE receiver can be written as

$$r_{lk} = g_{lk}c_{ik} + I_k + n_k \tag{3.25}$$

with variance

$$\sigma_{r_l}^2 = \mid c_{ik} \mid^2 \sigma_{g_l}^2 + \sigma_I^2 + 1 \tag{3.26}$$

Using the above results of the interplator, it can be shown that the variance of $\hat{g}_l$, the covariance of g_l and $\hat{g}_l$, and the covariance of r_l and $\hat{g}_l$ are

$$\sigma_{\hat{g}_l}^2 = \underline{\mathbf{h}}_l^{\dagger}(k)\mathbf{\Phi}_{RR}\underline{\mathbf{h}}_l(k) \tag{3.27}$$

$$\sigma_{g_l\hat{g}_l}^2 = \frac{1}{2}E[g_l\hat{g}_l^*] = \sigma_{\hat{g}_l}^2 \tag{3.28}$$

$$\sigma_{r_l\hat{g}_l} = \frac{1}{2}E[r_l\hat{g}_l^*] = c\sigma_{g_l\hat{g}_l}^2 \tag{3.29}$$

where c is the transmitted signal point. These expressions will be used later to calculate the pairwise error probability.

3.2 Bit Error Performance Analysis

In this section, we will give the exact expression for pairwise error probability and introduce the residue method to calculate the error event probability.

3.2.1 The Decoding Metric

The channel estimator in Figure 3.1 will extract from the received signal information about the channel's complex gains. We denoted the sequence at the estimator output as $(\hat{g}_l(1), ..., \hat{g}_l(k), ...)$, and the expression is given in equation (3.18). In the most

ideal situation, the estimator provides perfect channel state information (CSI) which implies

$$\hat{g}_l(k) = g_l(k) \qquad Perfect\ CSI \tag{3.30}$$

coherent detection. On the other hand, for differential detection such as DPSK, we are using the sample received in the last signalling interval to provide the channel state information for the current interval. The result is

$$\hat{g}_l(k) = g_l(k-1)s(k-1) + I_{11}(k-1) + N_1(k-1) \tag{3.31}$$

The Viterbi decoder will select the codeword $\hat{\mathbf{c}} = (\hat{c}_1, ..., \hat{c}_k, ..., \hat{c}_M)$ whose metric

$$\begin{aligned} M(\hat{c}) &= \sum_{l=1}^{L} \sum_{k} \mid r_{lk} - \hat{c}_k \hat{g}_{lk} \mid^2 \\ &= \sum_{l=1}^{L} \sum_{k} \{ \mid r_{lk} \mid^2 + \mid \hat{g}_{lk} \mid^2 - r_{lk} \hat{g}_{lk}^* \hat{c}_k^* - r_{lk}^* \hat{g}_{lk} \hat{c}_k \} \end{aligned} \tag{3.32}$$

is the smallest.

3.2.2 The Pairwise Error Event Probability

Let the transmitted codeword be $\mathbf{c}_i = (c_{i1}, ..., c_{ik}, ...)$. According to equation (3.32), the decoder will pick the erroneous codeword $\mathbf{c}_j = (c_{j1}, ..., c_{jk}, ...)$ if

$$\begin{aligned} D = M_j - M_i &= \sum_{k} D_k \leq \delta \\ &= \sum_{k=1}^{M} \{ r_k g_k^* (c_k^* - \hat{c}_k^*) + r_k^* g_k (c_k - \hat{c}_k) \} \end{aligned} \tag{3.33}$$

where

$$D_k = A_k \mid r_k \mid^2 + B_k \mid g_k \mid^2 + C_k r_k g_k^* + C_k^* r_k^* g_k \tag{3.34}$$

are independent random variables when conditioned on the codeword and the channel information of the RAKE receiver's branch. Note that D is simply a quadratic form of

complex Gaussian random variables, and in the case of PSK, this expression simplifies to

$$A_k = 0 \tag{3.35}$$

$$B_k = \mid c_{jk} \mid^2 - \mid c_{ik} \mid^2 \tag{3.36}$$

$$C_k = c_{ik}^* - c_{jk}^* \tag{3.37}$$

and $\delta = 0$.

The probability of confusing the codeword $\mathbf{c}_j$ with the codeword $\mathbf{c}_i$, denoted by $P(C_i \rightarrow C_j)$, is simply the probability that the random variable D in equation (3.33) is less than δ. Let $\phi_k(s)$ be the two-sided Laplace transform of the pdf of the random variable D_k. We assume ideal interleaving in this study and because of the independence of the $D_k's$, the characteristic function of D is simply the product of the $\phi_k(s)$

$$\Phi_D(s) = \prod_k \phi_k(s) \tag{3.38}$$

where

$$\phi_k(s) = \frac{p_{1k}p_{2k}}{(s - p_{1k})(s - p_{2k})} \tag{3.39}$$

$$p_{1k} = w_k - \sqrt{w_k^2 - \frac{1}{4x_k y_k}} \tag{3.40}$$

$$p_{1k} = w_k + \sqrt{w_k^2 - \frac{1}{4x_k y_k}} \tag{3.41}$$

$$w_k = -\frac{A_k\sigma_{\tau_k}^2 + B_k\sigma_{\hat{g}_k}^2 + C_k\sigma_{\tau_k\hat{g}_k}^2 + C_k^*\sigma_{\tau_k\hat{g}_k}^{2*}}{4x_k y_k} \tag{3.42}$$

$$x_k = \sigma_{\tau_k}^2\sigma_{\hat{g}_k}^2 - \mid \sigma_{\tau_k\hat{g}_k}^2 \mid^2 \tag{3.43}$$

$$y_k = A_k B_k - \mid C_k \mid^2 \tag{3.44}$$

All the terms $\sigma_{\tau_k}^2$, $\sigma_{\hat{g}_k}^2$ and $\sigma_{\tau_k \hat{g}_k}$ are given in equation (3.26)-(3.29). The probability density function of D is simply the inverse Laplace transform of $\Phi_D(s)$. This means in principle we could invert $\Phi_D(s)$ by residues, and perform an appropriate integration to obtain the error probability. Thus, the pairwise error probability, defined as the probability that D is less than zero, is an integration of its pdf from $-\infty$ to 0. This can be related to the characteristic function as

$$\begin{aligned} P(\mathbf{c}_i \rightarrow \mathbf{c}_j) &= Prob[D \leq 0] \\ &= -\sum Residue[e^{s\delta}\Phi_D(s)/s]_{RP_{poles}}, \quad \delta \leq 0 \\ &= \sum Residue[e^{s\delta}\Phi_D(s)/s]_{LP_{poles}}, \quad \delta > 0 \end{aligned} \tag{3.45}$$

where $\Phi_D(s)/s$ is the Laplace transform of the cumulative pdf of the random variable D, and the summation is taken over all distinct RP or LP poles.

Equation(3.39) is the expression for a flat fading channel. While multipath fading is present, the Rayleigh fading channel is frequency-selective and the expression for $\phi_k(s)$ becomes complicated. For example, if the delay power profile is (0, 0, 0)dB, the order i of the poles in $\phi_k(s)$ will be i^3 and

$$\phi_k(s) = \frac{p_{1k}^3 p_{2k}^3}{(s-p_{1k})^3(s-p_{2k})^3} \tag{3.46}$$

If the delay power profile is (0, -10, -10)dB, $\phi_k(s)$ will be

$$\phi_k(s) = \frac{p_{11k}p_{12k}^2 p_{21k}p_{22k}^2}{(s-p_{11k})(s-p_{12k})^2(s-p_{21k})(s-p_{22k})^2} \tag{3.47}$$

where p_{11k} and p_{21k} are obtained from the 0dB path, and p_{12k} and p_{22k} are obtained from the -10dB paths. The selective fading channel makes the residue calculation complicated.

3.2.3 Upper Bound Calculation

In most digital communication systems, the average bit error probability is of greater interest than the pairwise error event probability. Because of the form of $P(\mathbf{c}_i \rightarrow \mathbf{c}_j)$, we are not able to get an upper bound on the bit error probability via the classical transfer function bound approach. Therefore, we are restricted to find an approximation of the bit error probability rather than accounting for error event paths of all lengths. In our study, we estimate the bit error probability by considering only a small set of short error events as follows

$$P_b \approx \frac{1}{n} \sum_j m_{ij} P(\mathbf{c}_i \rightarrow \mathbf{c}_j) \tag{3.48}$$

with

$$L_{merge}(\mathbf{c}_i, \mathbf{c}_j) \leq N \tag{3.49}$$

where n is the number of information bits per channel symbol; m_{ij} is the number of information bit errors associated with an error event. The sum is over the set of dominant error events, and $L_{merge}(\mathbf{c}_i, \mathbf{c}_j)$ is the number of encoding intervals it takes for $\mathbf{c}_j$ to merge with $\mathbf{c}_i$ in the trellis diagram. The error events truncated depend on the value of N in equation (3.49). This parameter should be chosen so that the amount of computation will not be excessive (the computational complexity will grow approximately exponentially with N) and yet most of the dominant error events at the SNR of interest are included. For our coding schemes, we set N up to 7. For most good codes, the shortest Hamming distance event will be included in the approximation in equation (3.48), as long as N is greater than or equal to the free Hamming distance L_{min}.

The error events used in the BER calculation are listed in Table 3.1-3.4 for convolutional coded BPSK, QPSK and 8PSK modulation with constraint length 3 and 5. All the error events are obtained by hand from the trellis diagrams of coding schemes illustrated in Figure 3.4. Note that in Table 3.1-3.4, L_{merge} represents the merge length of the error event; $n_i, i = 0, 1, ..., M$ represents the number of complex MPSK symbols in the erroneous word with a value equal to $exp(j\frac{\pi}{M}i)$; L is the total number of modulation symbols in the erroneous word that are different from the transmitted codeword; m_{ij} is the number of bit errors associated with the error event; and $N_i, i = 1, 2, 3$ is the number of poles in $\Phi_D(s)$ of order i. Since there are 3 branches at the RAKE receiver in our analysis, the order of the poles are increased, and the residue calculation via differentiation is very complicated. If the fading profile is (0, 0, 0)dB, the order of the poles in $\Phi_D(s)$ is N_i^3.

L_{merge}	n_0	n_1	n_2	n_3	L	m_{ij}	N_1	N_2	N_3	N_4
3	0	0	2	0	3	1	1	1	0	0
4	0	0	2	2	4	2	0	2	0	0
5	1	2	2	0	4	2	0	2	0	0
	0	1	2	2	5	3	0	1	1	0
6	1	1	2	2	5	3	0	1	1	0
	0	2	2	2	6	4	0	1	0	1
	1	1	2	2	5	3	0	1	1	0

Table 3.1: List of Error Events (Relative to the All Zero Phase Codeword) for rate 1/2 (L=3) QPSK Scheme

3.3 Pilot Symbol Insertion Scheme

Pilot symbols are inserted into the transmitted signal stream with spacing M at the transmitter. The receiver extracts the pilot symbols, and estimats the CSI with an interpolator. Then the size of the structured frame, the interpolation position and

L_{merge}	n_0	n_1	n_2	n_3	L	m_{ij}	N_1	N_2	N_3	N_4
5	0	2	2	1	5	1	0	1	1	0
6	1	1	3	1	5	2	0	1	1	0
7	1	1	3	2	6	3	0	0	2	0
	0	1	3	3	7	2	0	0	1	1

Table 3.2: List of Error Events (Relative to the All Zero Phase Codeword) for rate 1/2 (L=5) QPSK Scheme

L_{merge}	n_0	n_1	n_2	n_3	n_4	n_5	n_6	n_7	L	m_{ij}	N_1	N_2	N_3
3	0	0	1	0	0	2	0	0	3	1	1	1	0
4	0	0	0	0	0	2	0	2	4	2	0	2	0
5	1	0	2	0	0	2	0	0	4	2	0	2	0
	0	0	1	0	0	2	0	2	5	3	1	2	0
6	1	0	1	0	0	2	0	2	5	3	1	2	0
	0	0	2	0	0	2	0	2	6	4	0	3	0
	1	0	1	0	0	2	0	2	5	3	1	2	0

Table 3.3: List of Error Events (Relative to the All Zero Phase Codeword) for rate 1/3 (L=3) 8PSK Scheme

L_{merge}	n_0	n_1	n_2	n_3	n_4	n_5	n_6	n_7	L	m_{ij}	N_1	N_2	N_3	N_4
5	0	0	2	0	0	2	1	0	5	1	0	1	1	0
6	0	0	0	0	2	2	0	0	6	2	0	3	0	0
7	0	2	0	0	0	2	1	2	7	3	1	1	0	1
	1	0	2	2	0	2	0	0	6	2	0	1	0	1

Table 3.4: List of Error Events (Relative to the All Zero Phase Codeword) for rate 1/3 (L=5) 8PSK Scheme

interpolator size will have an effect on the performance of the system. We have some simulation results for uncoded BPSK to show the effect of these parameters and their selection. The channel delay power profile for simulation is (0, 0, 0)dB.

3.3.1 Effect of Interpolation Position

From equation (3.18), we see that the position k of a symbol within the frame determines the estimation error as well as the BER. The numerical experimentation showed a small position dependence at normal operation parameters. For example, for an interpolator of size $K = 11$, in a $M = 7$ symbol frame, with $f_DT = 0.01$, $SNR = 20dB$ and processing gain is 380, there was only a 1% variation in BER across the frame. With $f_DT = 0.05$ and $SNR = 40dB$, there is a variance of 4% across the 7-symbol frame. However, for normal operating parameters and K being greater than 11, we say that the position dependence is negligible. In the following sections, we only evaluate the BER for $k = 1$, i.e., for the symbol immediately following the pilot symbol.

3.3.2 Effect of Pilot Symbol Frame Size

The frame size M has an optimum value, which represents a trade off between extra energy in unnecessary pilot symbols and insufficient amount of sampling of the fading process for good estimation. Figure 3.6 illustrates the effect for BPSK at $SNR = 20dB$, with a variety of fade rates and a 11-tap interpolator. It is obvious that the BER rises steeply when the frame size causes sampling rate to fall below the Nyquist rate, that is, when $M < 1/2f_DT$.

We selected the frame size $M = 7$ as the benchmark for our research in this thesis. Although it represents a 14% loss of capacity, it does accommodate fade rates up to $f_D T = 0.05$ (which is 5% of the symbol rate). If slower fade rates are expected, such as $f_D T = 0.01$ or $f_D T = 0.005$, then much larger frames can be adopted to reduce the loss of capacity.

3.3.3 Effect of Interpolator Size

The size of an interpolator is a significant issue in PSAM as it affects processing delay and computational load, as well as BER. We show the dependence on the number of coefficients K for BPSK with a size 7 frame. From the curves in Figure 3.7, we can see that the improvement beyond five to ten coefficients is very slight. Therefore, we choose the interpolator size to be $K = 11$ in our research.

3.4 Numerical Results

In this section, we present the numerical results for the pilot symbol assisted modulation discussed in above sections. The frequency-selective Rayleigh fading channel is a 3-ray model and the spreaded bandwidth is fixed at 380 (assuming the input information rate is 1). At the transmitter, the pilot symbol is inserted every 6 data symbols and the data frame size is $M = 7$. At the receiver, the number of pilot symbols used in the interpolator for channel estimation is $K = 11$. These values of M and K have been shown above to provide a good compromise among accuracy

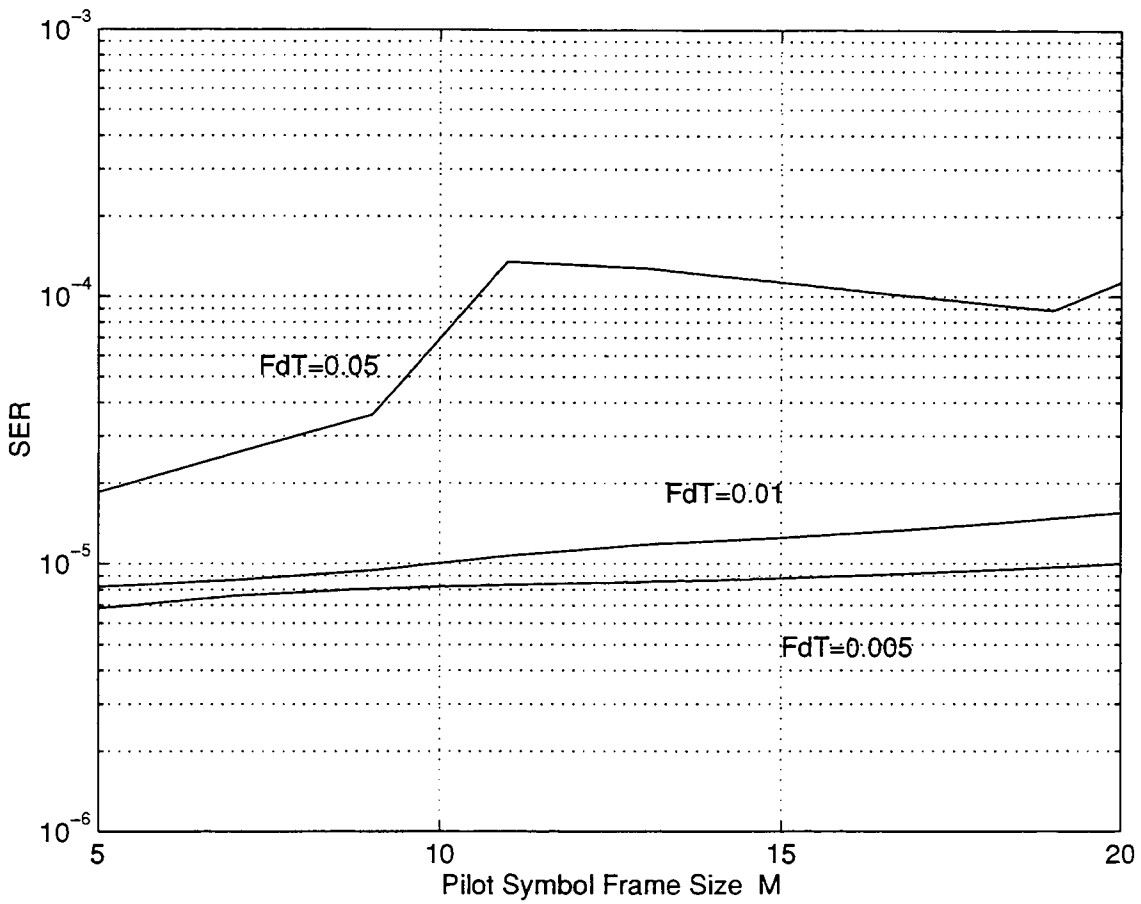

Figure 3.6: Effect of frame size on BPSK (SNR=20dB, K=11, (0, 0, 0)dB delay power profile and Processing Gain is 380).

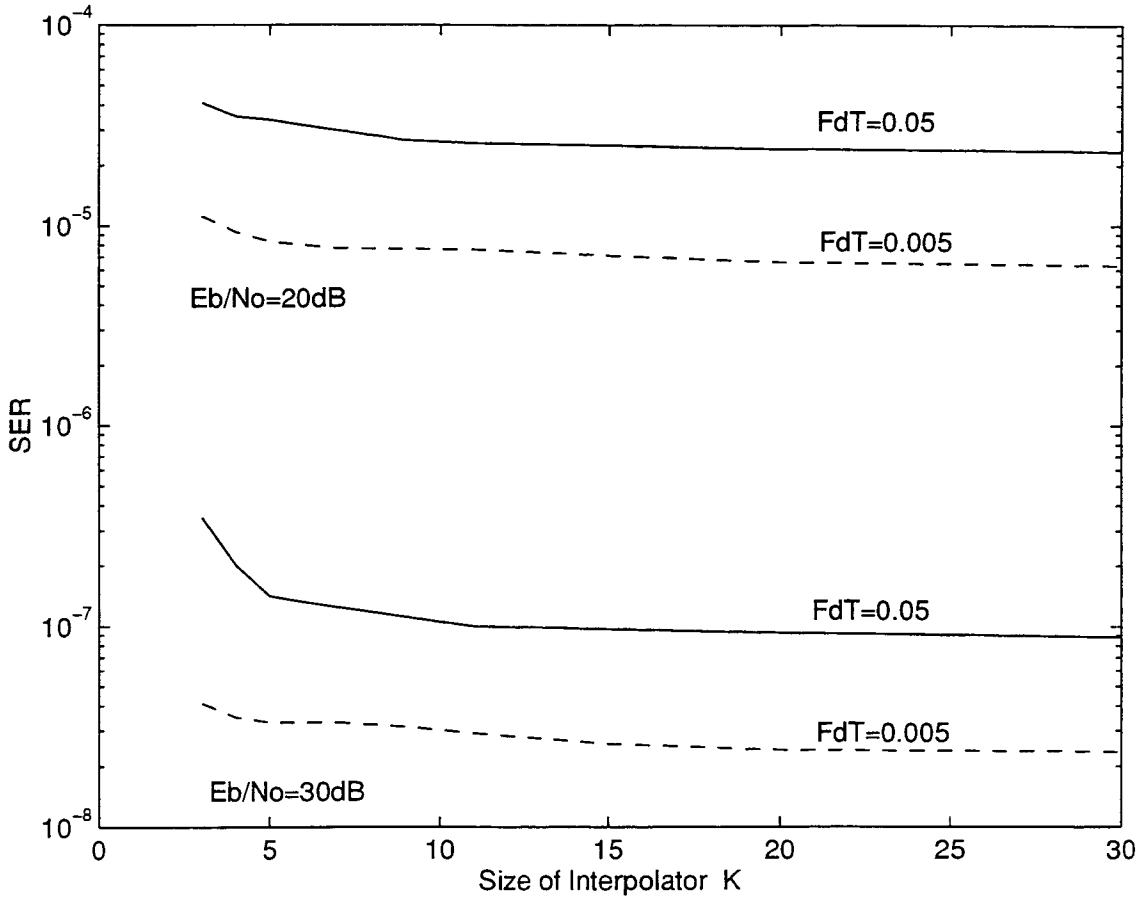

Figure 3.7: Effect of interpolator size on BPSK (M=7).

in the channel estimates, the decoding delay, as well as the decoding complexity for all the fade rates of interest. For BPSK modulation, error performance of rate 1/2 and 1/3 convolutional codes (with contraint length 3 and 5) are compared under different channel conditions. Then the results for rate 1/2 convolutional code with QPSK modulation are illustrated, as well as the results for rate 1/3 convolutional code with 8PSK modulation. The comparison of different modulation schemes are presented with the unchanged information throughput. In all illustrations, the results of coherent detection and differential detection are plotted for comparison.

3.4.1 Pilot Symbol Assisted BPSK

The calculation of the upper bound of BPSK is obtained through equation (3.45). The transmitted information bits are random binary sequence with probability 0.5 of ± 1. For coherent and differential detection, while the spreaded bandwidth is fixed at 380 and the information rate is 1, the spreading factor (processing gain G) for rate 1/2 code is 190 and 127 for rate 1/3 code respectively. In terms of PSAM, the insertion of pilot symbol increases the bandwidth of the transmitted signal, thus the spreading factor is reduced to 163 for rate 1/2 code and 109 for rate 1/3 code.

Rate 1/2 Convolutional Code PSAM BPSK

Figure 3.8 and Figure 3.9 show the error performance of rate 1/2 (constraint length 3) BPSK under fade rate 0.05 and 0.005. The channel is frequency-selective and the delay power profiles are (0, 0, 0)dB and (0, -3, -6)dB. When the BER is 10^{-6}, we can see at fast fading ($f_D T = 0.05$), and the PSAM has only 0.3dB improvement compared with differential detection. But at slow fading ($f_D T = 0.005$), the PSAM

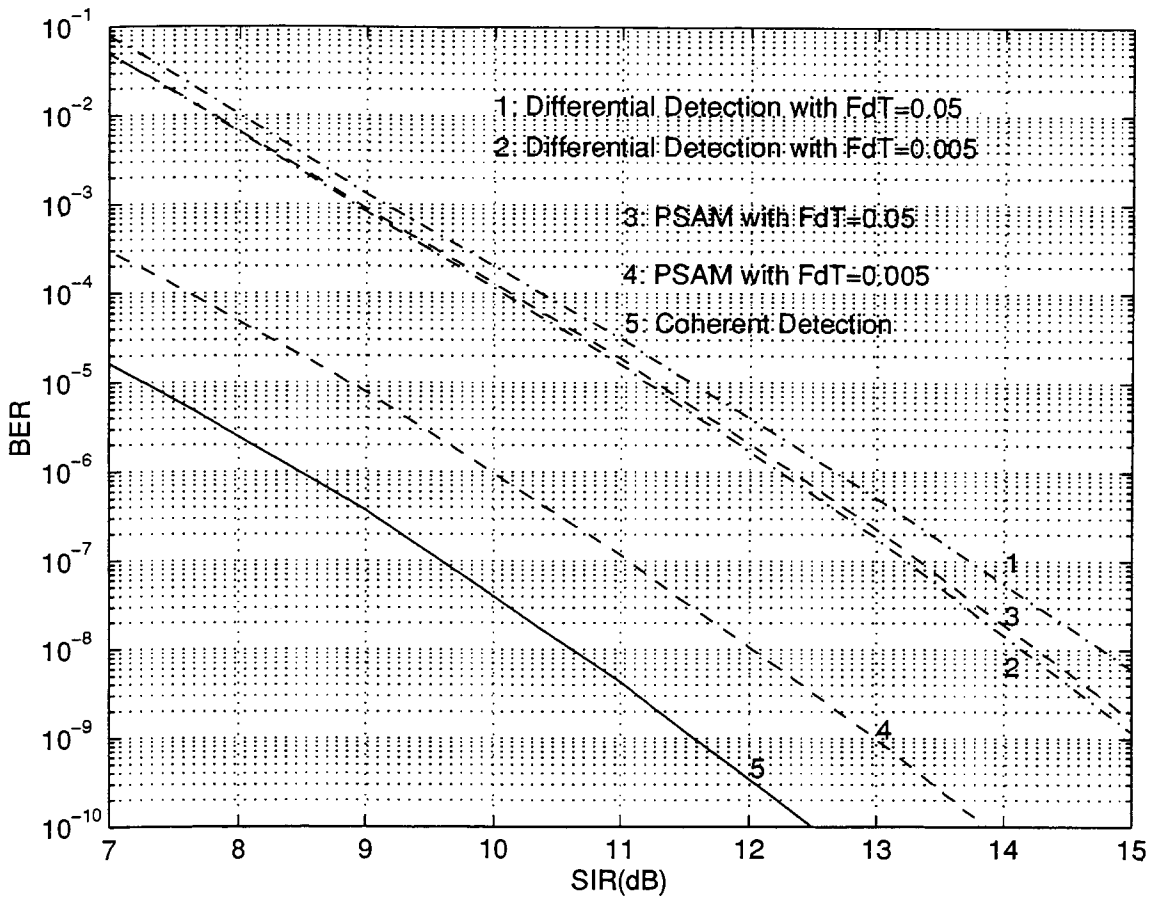

Figure 3.8: Bit error performance of constraint length 3 rate 1/2 convolutional coding pilot symbol assisted BPSK. Delay power profile is (0, 0, 0)dB.

has over 2dB improvement than differential detection.

Figure 3.10 illustrates the error performance of rate 1/2 (constraint length 3) code at fade rates 0.05 and 0.005. Although the channel is still frequency-selective Rayleigh fading, the (0, -10, -10)dB delay power profile makes it more like a "flat" fading one. The error performance appears differently from Figure 3.8-3.9.

Through Figure 3.10, we find that compared with differential detection, PSAM

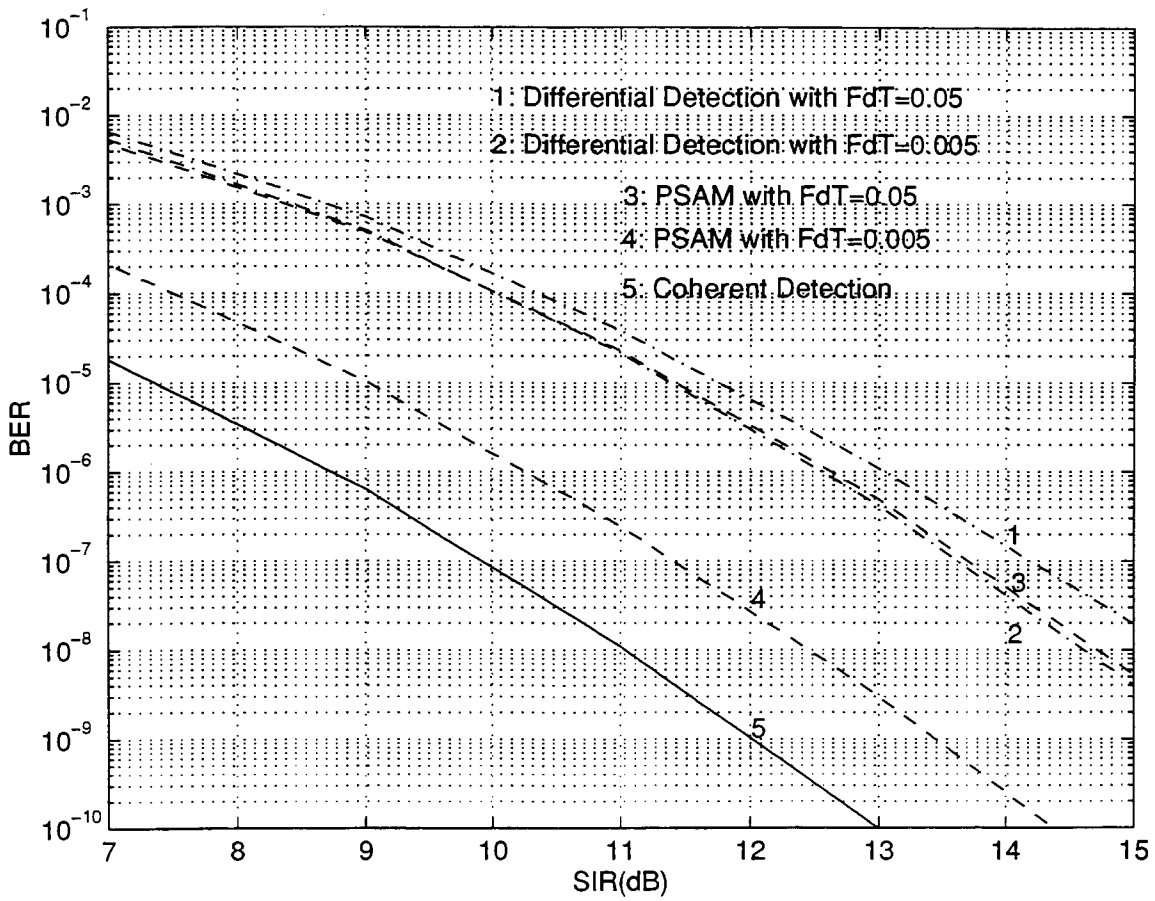

Figure 3.9: Bit error performance of constraint length 3 rate 1/2 convolutional coding pilot symbol assisted BPSK. Delay power profile is (0, -3, -6)dB.

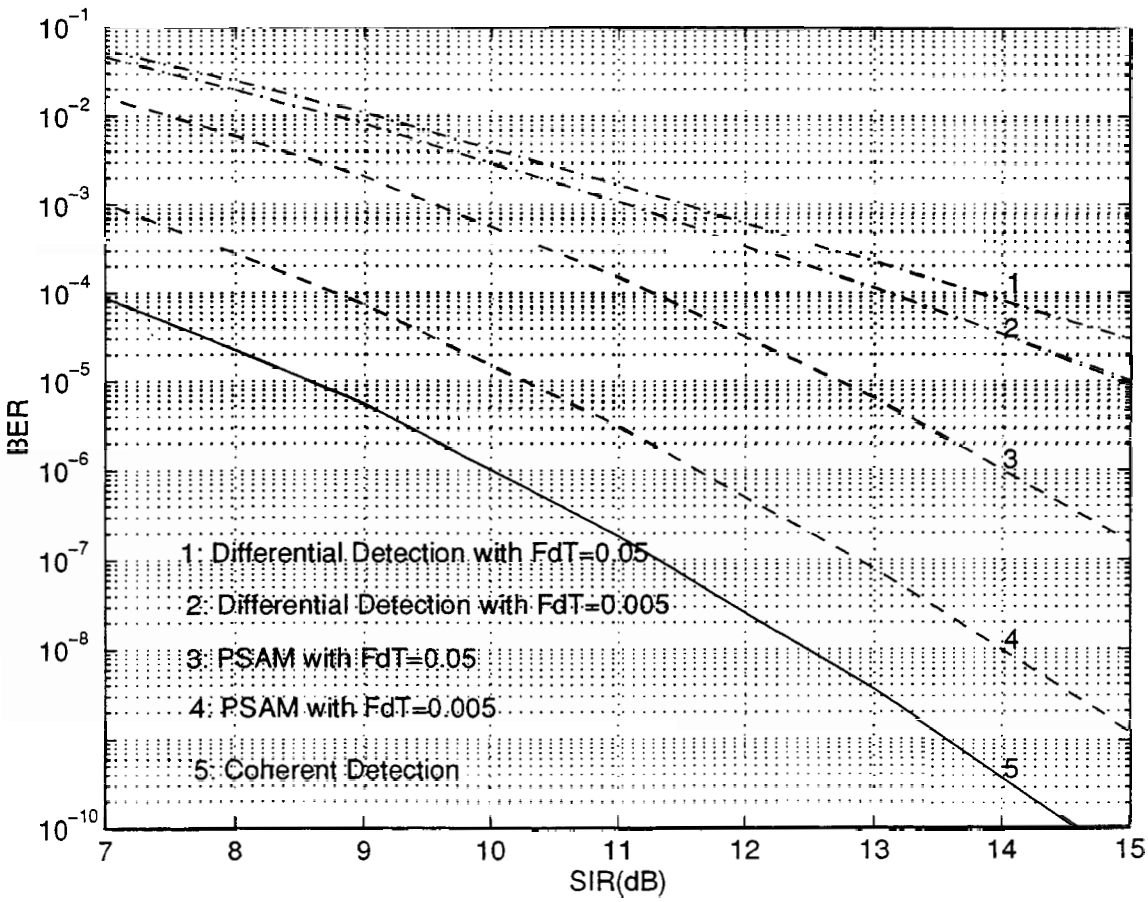

Figure 3.10: Bit error performance of constraint length 3 rate 1/2 convolutional coding pilot symbol assisted BPSK. Delay power profile is (0, -10, -10)dB.

at fast fading ($f_DT = 0.05$)improves the performance by over 2dB at 10^{-4}. At slow fading ($f_DT = 0.005$), the improvement is around 4dB at 10^{-4} and the performance of PSAM is only 1.5dB poorer than ideal coherent BPSK. Comparing Figure 3.10 to Figure 3.8 and 3.9, we can see that unlike a very selective fading channel where PSAM only works at slow fading, PSAM can also improve the performance of differential detection at a fast fading rate. In a less selective fading channel, while the signals' power of the 2nd and 3rd path are much less (-10dB) than the main path (the 1st path), the channel can be approximated as a "flat" fading channel. The received signal-to-interference ratio (SIR) at the RAKE receiver's 1st branch is larger because of a small self-interference power caused by weak paths. This gives the better performance of channel estimator and improves the PSAM performance than differential detection. On the other hand, the SIR at the other RAKE receiver taps are smaller due to the large interference from the strongest path. This reduces the diversity effect after combining and causes a decrease in the overall performance. Although the performance in a "flat" fading channel is inferior to that in a more selective fading channel due to the loss of the diversity effect, we should say that PSAM works more effectively than differential detection in a "flat" fading channel than in a selective fading channel with the presence of self-interference.

The performance of rate 1/2 (constraint length 5) and rate 1/3 (constraint length 3 and 5) convolutional codes BPSK have the same behavior as above under similar channel conditions. We can say at a very selective fading channel such as (0, 0, 0)dB delay power profile, the self-interference caused by the multipath effect is large, and PSAM can improve the performance compared with differential detection only at a

slow fading rate. When the channel presents flat fading properties, self-interference is smaller at certain taps of RAKE receiver, and PSAM can improve the performance better than differential detection at both fast and slow fading.

Comparision of Rate 1/2 to Rate 1/3 PSAM BPSK

We compare the error performances of rate 1/2 to 1/3 convolutional code in combination with pilot symbol assisted BPSK modulation. Under different fade rates and delay power profiles, rate 1/2 and 1/3 codes with different constraint lengths and processing gains present different performances. First, we will be discussing the very selective fading channel, and the delay power profile is (0, 0, 0)dB.

Figure 3.11 plotted the curves at fade rate 0.05. From (a) we can see that while the constraint length is 3 for both codes, the rate 1/2 PSAM outperforms rate 1/3 PSAM by about 0.75dB at 10^{-6}. Rate 1/2 code also outperforms rate 1/3 code with coherent or differential detection. On the other hand, when the constraint length is 5, Figure 3.11(b) shows that rate 1/3 PSAM outperforms rate 1/2 PSAM by 0.5dB at 10^{-6}. The rate 1/3 code outperforms rate 1/2 code at lower BER ($< 10^{-4}$) with coherent or differential detection. This phenomenon is caused by the properties of convolutional codes. The rate 1/2 code with constraint length 3 has free distance 5, and rate 1/2 code with constraint length 5 only has free distance 7. Whereas the rate 1/3 code with constraint length 3 has free distance 6, the rate 1/3 code with constraint length 5 has free distance up to 12. The rate 1/2 code and rate 1/3 code with constraint length 3 have similar error-correcting ability, but a larger processing

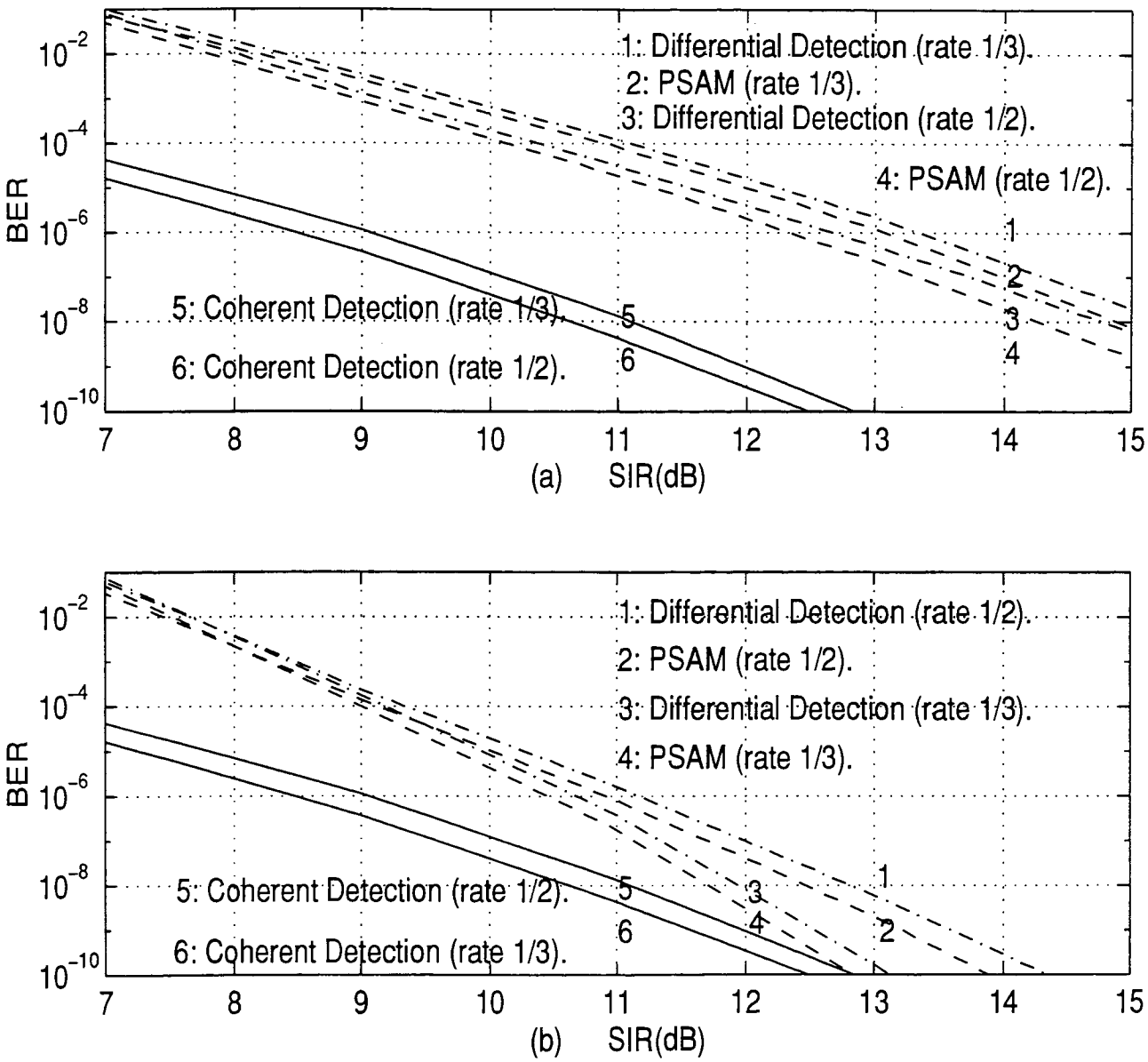

Figure 3.11: Comparison of error performance of rate 1/2 to rate 1/3 convolutional coding pilot symbol assisted BPSK. Delay power profile is (0, 0, 0)dB and fade rate is 0.05. (a) Constraint length is 3. (b) Constraint length is 5.

gain with rate 1/2 code reduces the self-interference caused by selective fading channel and the performance of rate 1/2 BPSK is getting better. For constraint length 5 codes, although the processing gain for rate 1/2 BPSK is larger than that of rate 1/3 BPSK, the error-correcting power of rate 1/2 code is much less compared to rate 1/3 code, and the performance of rate 1/3 BPSK is better. Without increasing the decoding complexity, the rate 1/3 code which has a larger constraint length and smaller processing gain, performs better than rate 1/2 code with the same constraint length and a larger processing gain. This shows the trade off between the coding rate and the processing gain while the information throughput and transmission bandwidth are fixed.

At slow fading ($f_D T = 0.005$), Figure 3.12 shows that rate 1/2 BPSK and rate 1/3 BPSK have similar behavior as above. However, the improvement of rate 1/3 code to rate 1/2 code is obvious when a larger constraint length code is adopted.

Now we present the error performance at a less frequency-selective Rayleigh fading channel, and the delay power profile is (0, -10, -10)dB.

Figure 3.13 shows the error performance of rate 1/2 and rate 1/3 BPSK modulation with constraint length 3 at both fast and slow fading channels. We can see that the error performance of rate 1/2 and 1/3 codes are quite similar. At a BER of 10^{-6}, there is less than 0.5dB difference between rate 1/2 BPSK and rate 1/3 BPSK. With constraint length 3, although the rate 1/2 code with a larger processing gain outperforms rate 1/3 code with a smaller processing gain, the error-correcting abilities of these two codes are similar, and we see that the difference is not big. Comparing

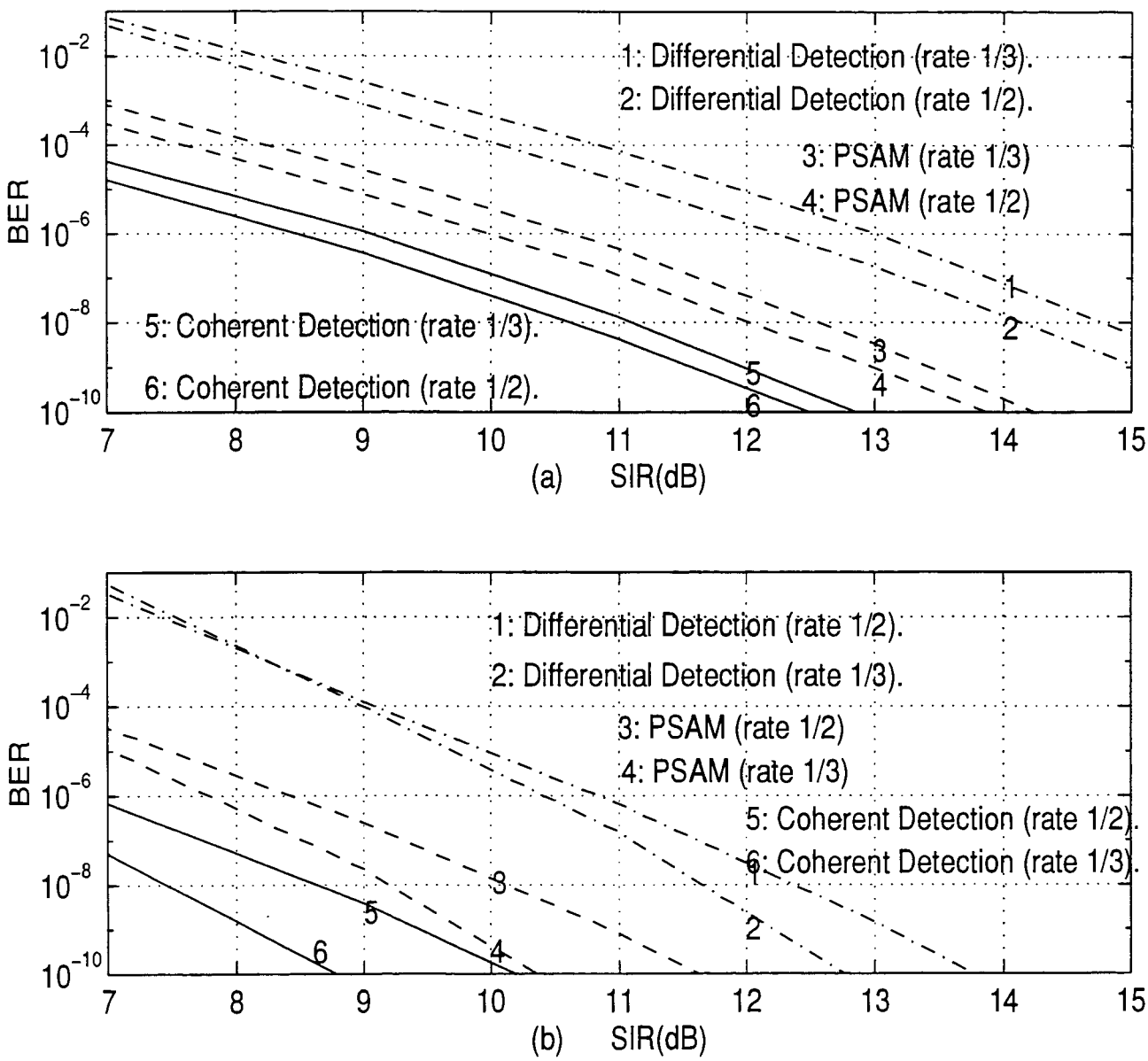

Figure 3.12: Comparison of error performance of rate 1/2 to rate 1/3 convolutional coding pilot symbol assisted BPSK. Delay power profile is (0, 0, 0)dB and fade rate is 0.005. (a) Constraint length is 3. (b) Constraint length is 5.

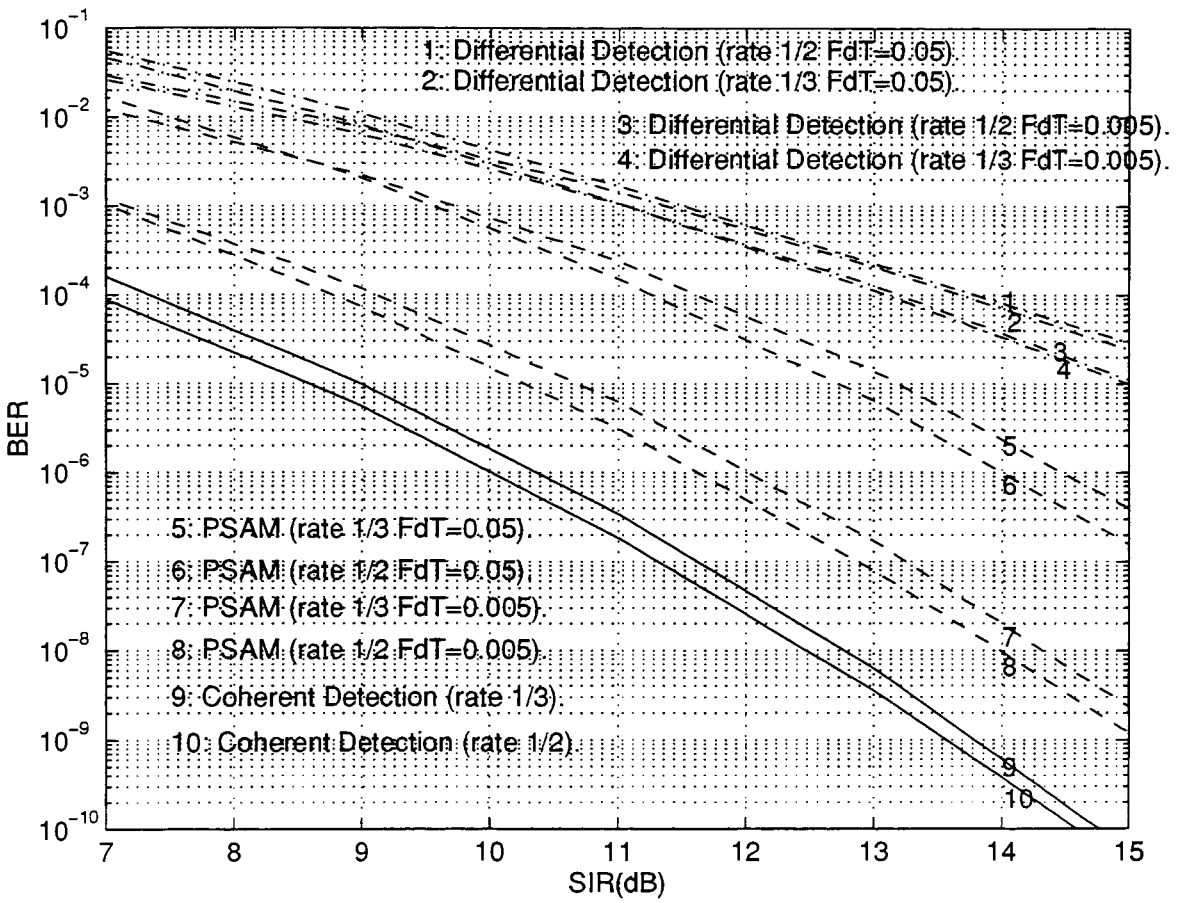

Figure 3.13: Comparison of bit error performance of constraint length 3 rate 1/2 to rate 1/3 convolutional coding pilot symbol assisted BPSK. Delay power profile is (0, -10, -10)dB.

Figure 3.11(a), Figure 3.12(a) and Figure 3.13, we see that no matter whether the channel is fast or slow fading, frequency-selective or "flat" fading, rate 1/2 convolutional code with short constraint length 3 only outperforms rate 1/3 code by about 0.5dB.

Figure 3.14 shows the error performance of rate 1/2 BPSK and rate 1/3 BPSK when the constraint length of convolutional code is 5. At both fast and slow fading channels, rate 1/3 BPSK has 1dB improvement at 10^{-6} over rate 1/2 BPSK scheme due to the powerful error correcting ability of the rate 1/3 code. Comparing Figure 3.11(b), Figure 3.12(b) and Figure 3.14, the rate 1/3 BPSK has only 0.5dB improvement over the rate 1/2 BPSK in a very selective fading channel, but the improvement is up to 1dB in a less selective fading channel due to less multipath interference. We can say that while the information throughput and transmission bandwidth are fixed, rate 1/3 code with constraint length 5 outperforms rate 1/2 code in both fast and slow fading channels. The less selective the channel is, the more improvement the rate 1/3 code achieves.

3.4.2 Pilot Symbol Assisted QPSK and 8PSK

In this section, we will present the error performance of rate 1/2 convolutional code with PSAM QPSK, as well as the error performance of rate 1/3 convolutional code with PSAM 8PSK. The transmitted signal constellations are shown in Figure 3.5, and the signals have the value $s_k = exp(j\theta_k)$. θ_k is the transmitted signal phase and will take one of the M ($M = 4$ for QPSK and $M = 8$ for 8PSK) values from the set $(2\pi m)/M; m = 0, 1, ..., M-1$. We assume the pilot symbols to be real in both

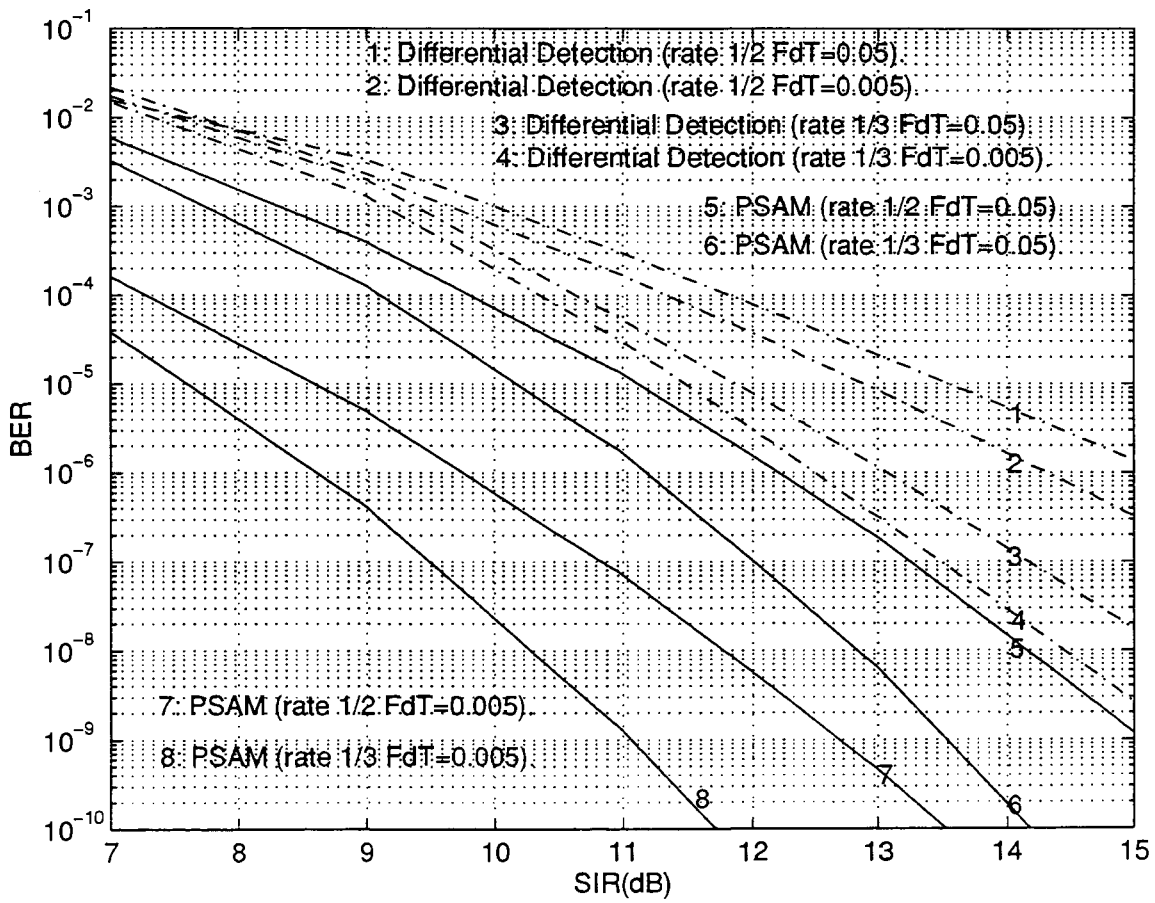

Figure 3.14: Comparison of bit error performance of constraint length 5 rate 1/2 to rate 1/3 convolutional coding pilot symbol assisted BPSK. Delay power profile is (0, -10, -10)dB.

cases with the value $\tilde{s} = 1$. The BER calculation is much like that of BPSK. For QPSK, one input information bit is encoded to two bits and then mapped to a QPSK symbol with Gray code. For 8PSK, one input information bit is encoded to three bits and then mapped to a 8PSK symbol with Gray code. The insertion of pilot symbols will reduce the processing gain of QPSK and 8PSK. With a seven-symbol frame and spreaded bandwidth 380, the processing gain for PSAM QPSK and 8PSK is actually 326. On the other hand, the spreading factor for coherent or differential QPSK and 8PSK is still 380.

First, we consider PSAM QPSK. Figure 3.15 shows the error performance of rate 1/2 PSAM QPSK with constraint length 3. The channel is frequency-selective Rayleigh fading and the delay power profile is (0, 0, 0)dB. The curves present similar performance with that of PSAM BPSK. Compared with differential detection, the improvement of PSAM is less than 1dB at fast fading. On the other hand, the improvement of PSAM QPSK is nearly 2dB at slow fading. Rate 1/2 PSAM QPSK with constraint length 5 presents similar behavior.

Figure 3.16 shows the error performance of PSAM QPSK at a less frequency-selective fading channel with a delay power profile of (0, -10, -10)dB. Compared with differential detection, the PSAM has around 1dB improvement at fast fading while at slow fading, the improvement can be over 2dB. Comparing Figure 3.16 with Figure 3.15, the improvement of PSAM over differential detection is quite similar at both slow and fast fading. Compared to DPSK, when the channel is less selective,

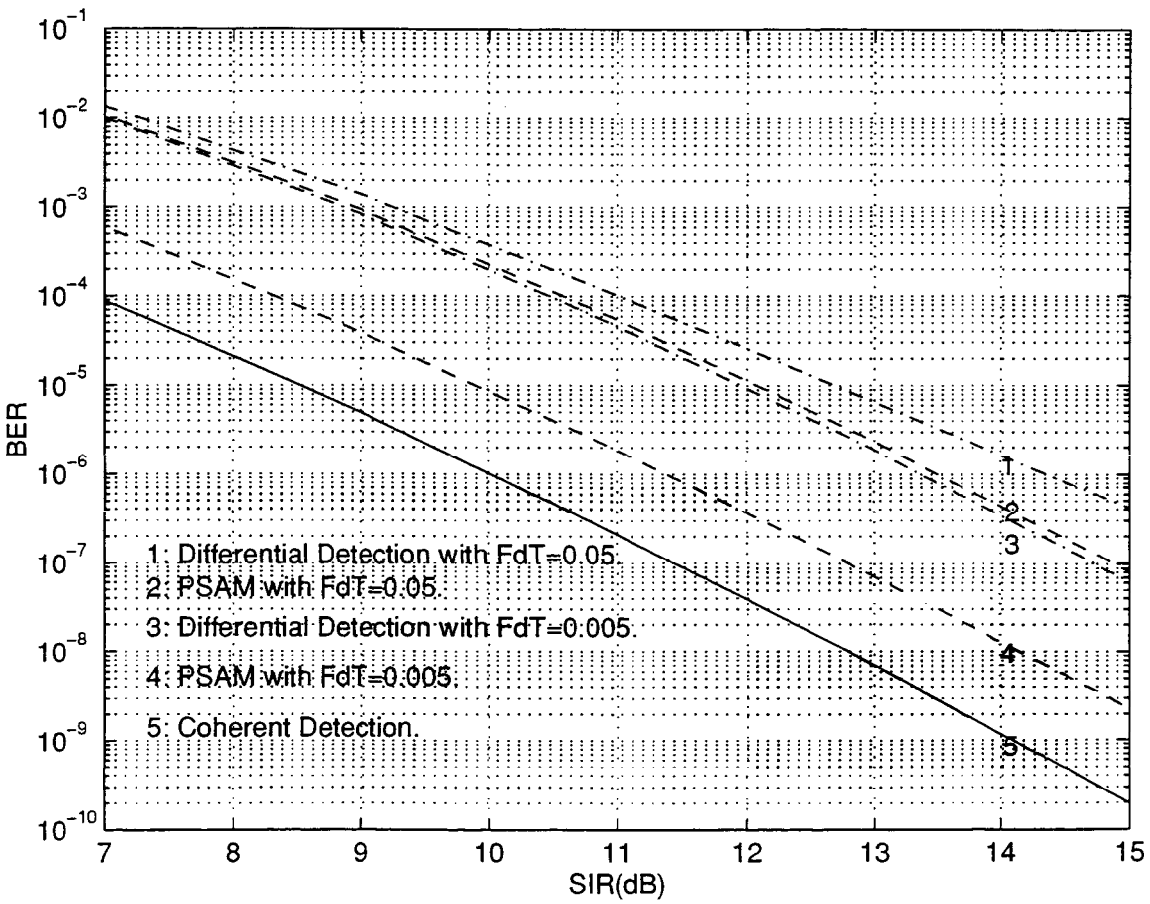

Figure 3.15: Bit error performance of rate 1/2 (constraint length 3) convolutional code PSAM QPSK. Delay power profile is (0, 0, 0)dB.

the improvement shows that it is getting better, but at the same time, the diversity effect is also decreasing and the overall performance is reducing. This tells us that when the self-interference is getting stronger at a certain tap of RAKE receiver, the signal-to-interference ratio of the corresponding multipath is lower and it does not provide the diversity effect as expected. Rate 1/2 code PSAM QPSK with constraint length 5 presents similar behavior.

For rate 1/3 PSAM 8PSK, the behavior is quite similar to rate 1/2 PSAM QPSK, and the curves of constraint length 3 are shown in Figure 3.17. Compared to differential detection, we noted at fast fading, the improvement is less than 1dB; however, at slow fading, the improvement is approximately 2dB. We also noticed that when the channel is getting less selective, the performance is getting poorer as the effect of multipath diversity is reduced. The 1/3 PSAM 8PSK with constraint length 5 presents similar behavior.

3.4.3 Comparision of Pilot Symbol Assisted BPSK, QPSK and 8PSK

We have illustrated the error performance of the pilot symbol assisted BPSK, QPSK and 8PSK in various fading channels. In this section, we compare several pilot symbol assisted modulation schemes with the same net information throughput of 1 bit/symbol and fixed spreading bandwidth 380: uncoded BPSK, rate 1/2 and 1/3 coded BPSK, rate 1/2 coded QPSK and rate 1/3 coded 8PSK. In all cases, the length of each data block is $M = 7$, and the number of pilot symbols (interpolator size)

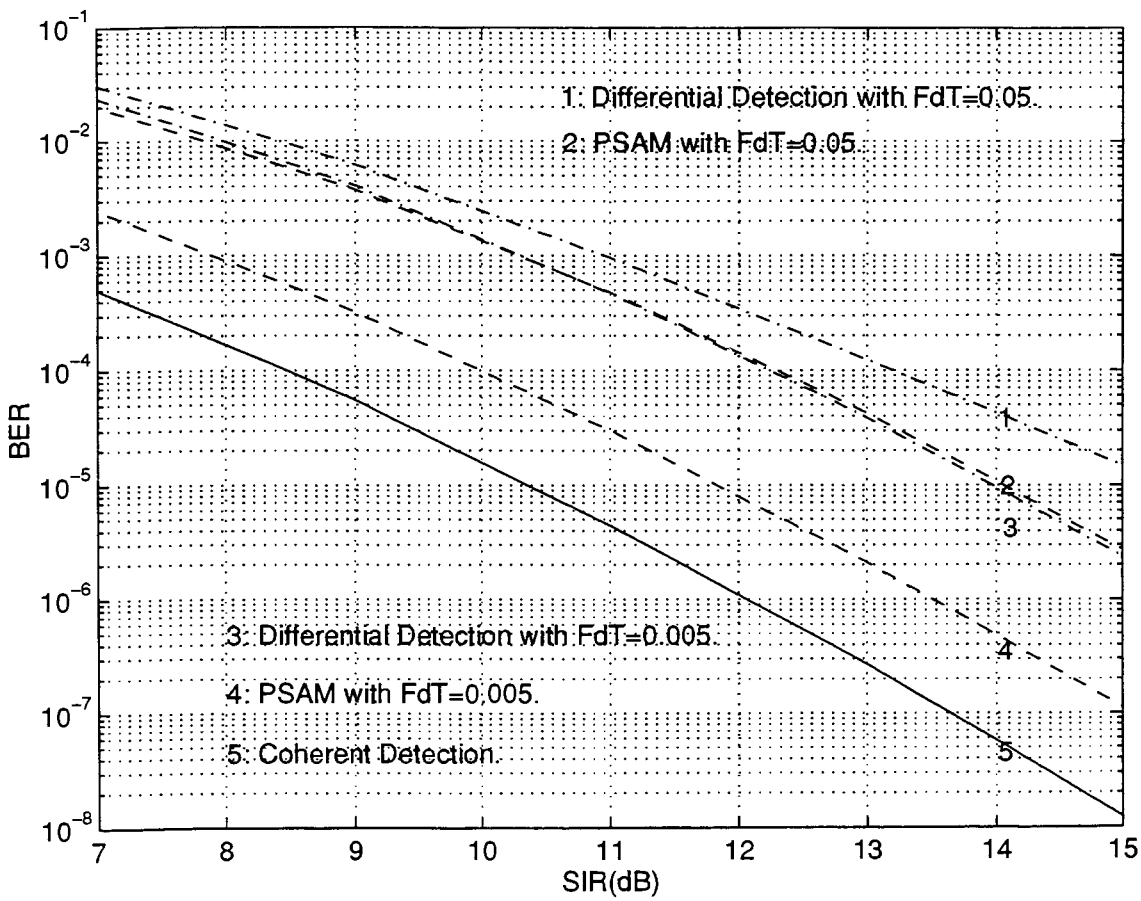

Figure 3.16: Bit error performance of rate 1/2 (constraint length 3) convolutional code PSAM QPSK. Delay power profile is (0, -10, -10)dB.

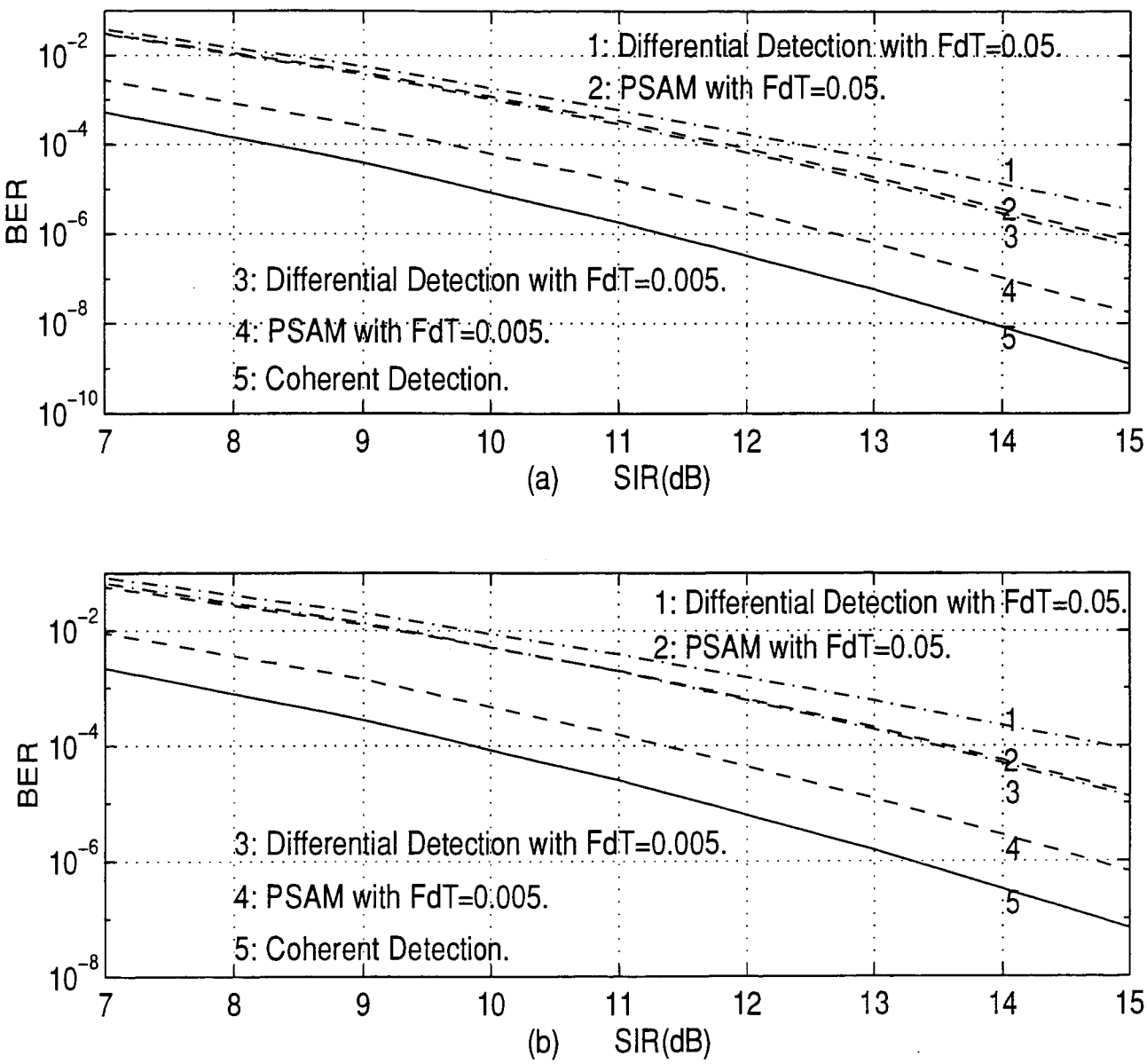

Figure 3.17: Bit error performance of rate 1/3 (constraint length 3) convolutional code PSAM 8PSK. (a) Delay power profile is (0, 0, 0)dB. (b) Delay power profile is (0, -10, -10)dB.

used for interpolation is $K = 11$. As mentioned above, different code rates and the insertion of pilot symbols make the processing gain of these modulations different. The processing gain is 326 for uncoded BPSK, rate 1/2 QPSK and rate 1/3 8PSK, 163 for rate 1/2 BPSK and 109 for rate 1/3 BPSK respectively.

Figure 3.18 and Figure 3.19 show the comparison of constraint length 3 code under fade rates of 0.05 and 0.005. The channel is frequency-selective fading with a delay power profile of (0, 0, 0)dB. Rate 1/2 QPSK always outperforms rate 1/3 8PSK at all fade rates. The improvement is about 1-1.2dB. Rate 1/3 BPSK performs better than rate 1/3 8PSK, and rate 1/2 BPSK also outperforms rate 1/2 QPSK. The advantage of BPSK is not obvious at fast fade rate ($f_D T = 0.05$) and at a higher BER ($> 10^{-4}$) in Figure 3.18. At slow fade rate ($f_D T = 0.005$) and all BER ranges considered, Figure 3.19 shows that both the rate 1/2 and 1/3 BPSK schemes outperform the rate 1/2 QPSK and rate 1/3 8PSK schemes.

Figure 3.20 shows the comparison of constraint length 5 code under a fade rates of 0.05 and 0.005. We noticed that rate 1/2 QPSK still outperforms rate 1/3 8PSK at all fade rates, but the difference is becoming smaller. Rate 1/3 code with constraint length 5 outperforms rate 1/2 code in BPSK. In Figure 3.20(a), at lower SIR, rate 1/2 QPSK and rate 1/3 8PSK with a larger processing gain have less self-interference from multipaths, and they outperform rate 1/2 and 1/3 BPSK with a smaller processing gain. When SIR increases, the self-interference also increases and the performance of

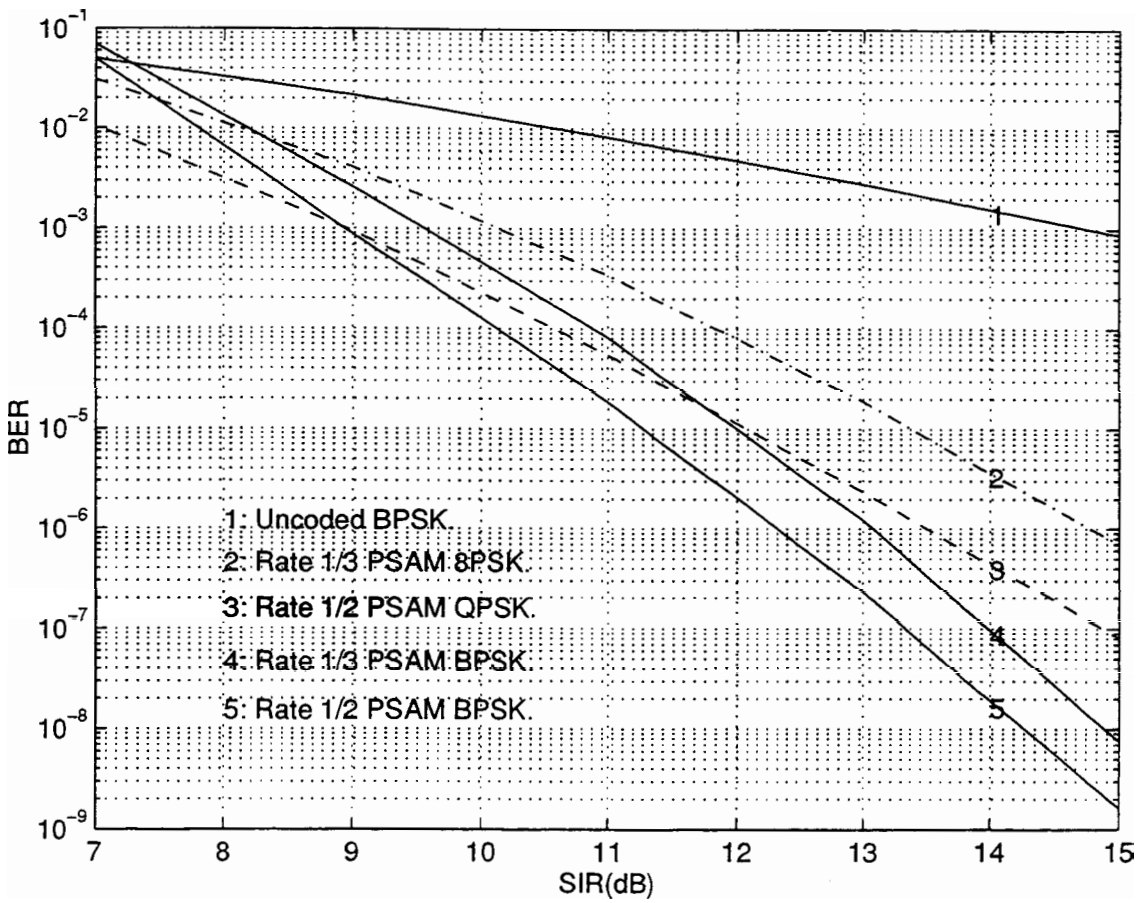

Figure 3.18: Bit error performance comparison of uncoded PSAM BPSK, rate 1/2 and 1/3 coded PSAM BPSK, rate 1/2 coded PSAM QPSK and rate 1/3 coded PSAM 8PSK. Constraint length of convolutional code is 3. Delay power profile is (0, 0, 0)dB and fade rate is 0.05.

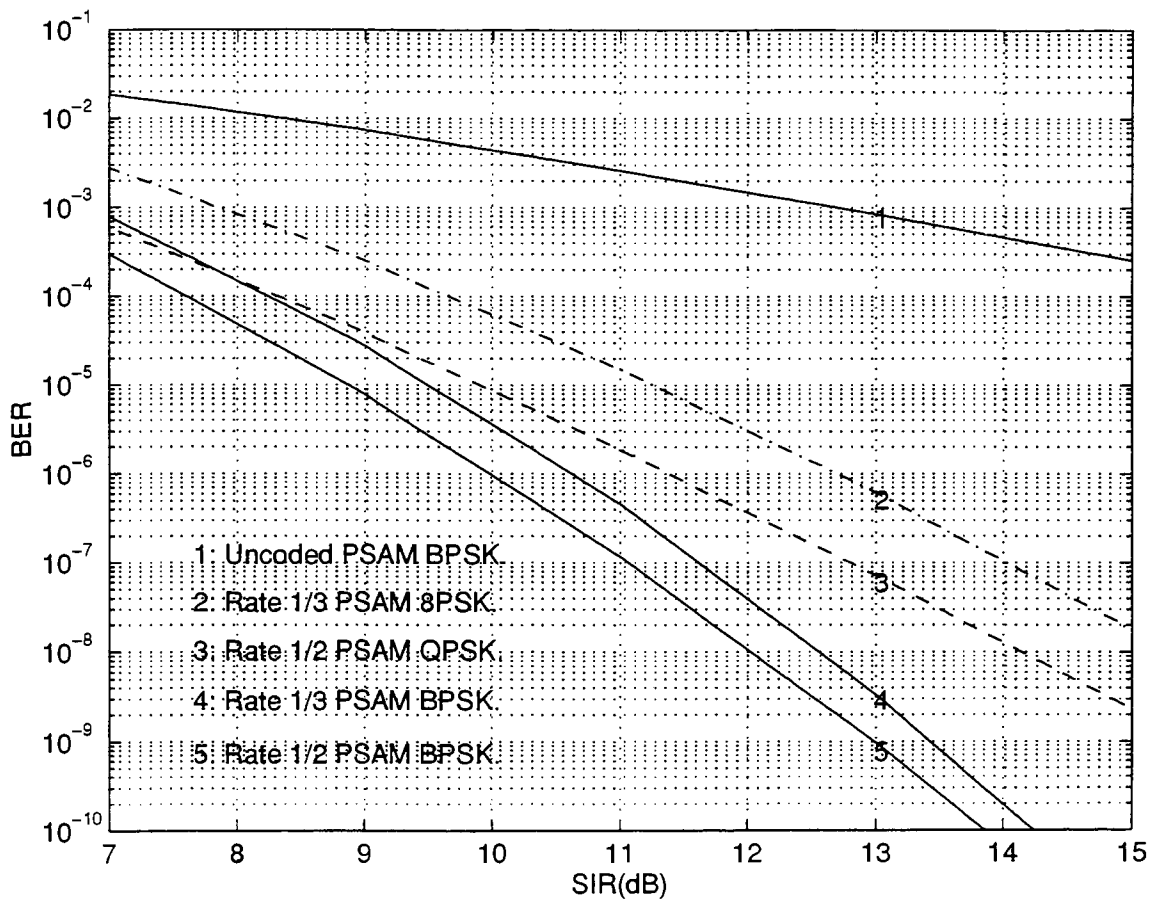

Figure 3.19: Bit error performance comparison of uncoded PSAM BPSK, rate 1/2 and 1/3 coded PSAM BPSK, rate 1/2 coded PSAM QPSK and rate 1/3 coded PSAM 8PSK. Constraint length of convolutional code is 3. Delay power profile is (0, 0, 0)dB and fade rate is 0.005.

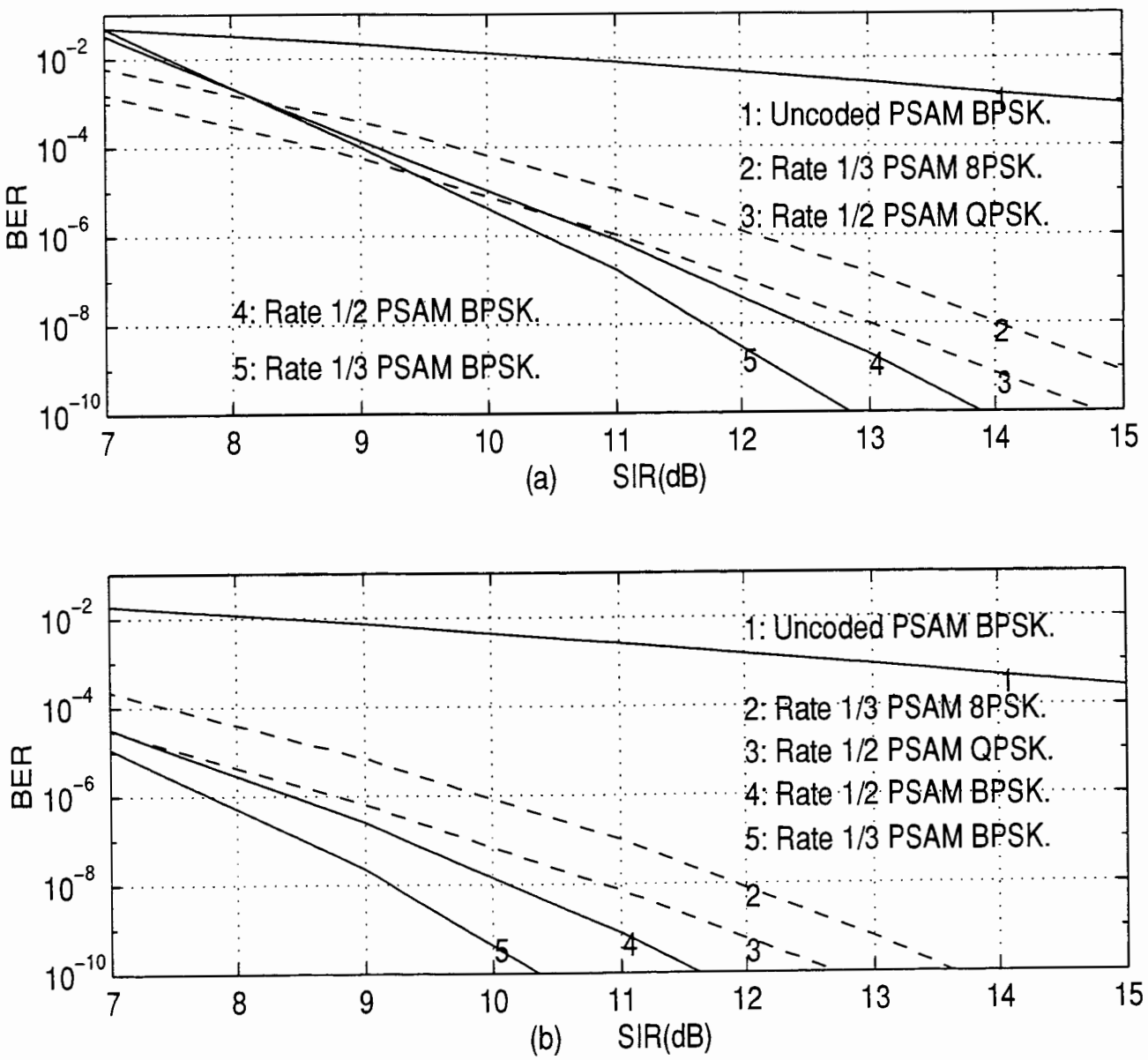

Figure 3.20: Bit error performance comparison of uncoded PSAM BPSK, rate 1/2 and 1/3 coded PSAM BPSK, rate 1/2 coded PSAM QPSK and rate 1/3 coded PSAM 8PSK. Constraint length of convolutional code is 5. Delay power profile is (0, 0, 0)dB. (a) Fade rate is 0.05. (b) Fade rate is 0.005.

the dense constellation modulation becomes poor. BPSK modulation with a strong error-correcting code presents better performance.

Now we consider the error performance at a less frequency-selective fading channel with a delay power profile of (0, -10, -10)dB. Figure 3.21 shows the error performance of constraint length 3 code, and Figure 3.22 shows the error performance of constraint length 5 code at fade rates 0.05 and 0.005. They have similar behavior as those of (0, 0, 0)dB selective fading channel.

3.5 Summary

In this chapter, we presented the analysis and numerical results of different rate convolutional coding schemes with PSAM and M-ary PSK modulation techniques in CDMA environment. The residue method is adopted in the analysis to calculate the upper bound of different modulation schemes. The parameters of pilot symbol insertion were decided from simulation results. A frame size $M = 7$ is selected as well as interpolation size $K = 11$.

In the numerical calculations, the transmitted data rate and spreading bandwidth are assumed to be fixed. The trade off between code rate, modulation scheme and processing gain is then illustraded. First, we considered pilot symbol assisted BPSK. The performance of rate 1/2 and rate 1/3 codes (constraint length 3 and 5) present

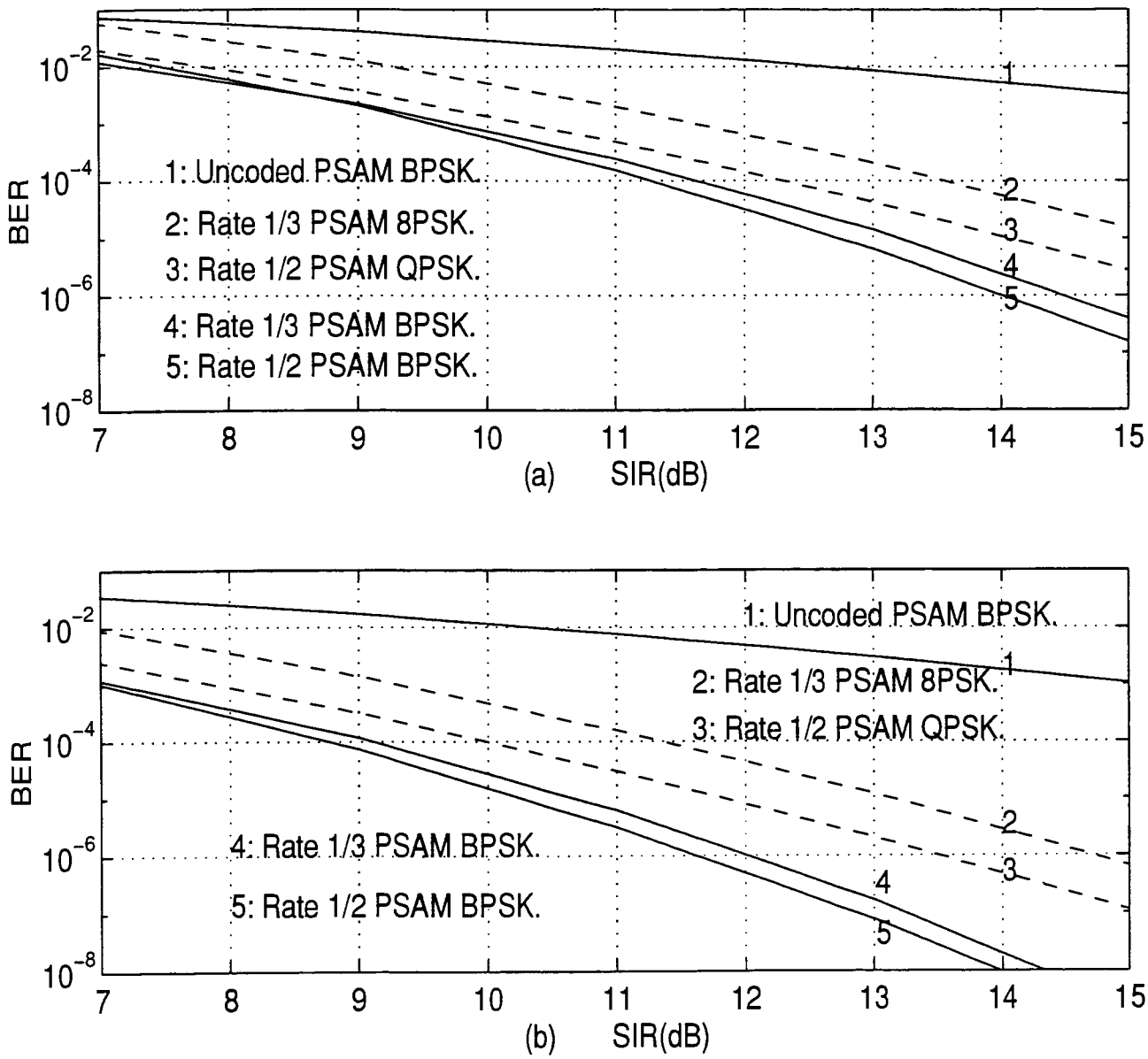

Figure 3.21: Bit error performance comparison of uncoded PSAM BPSK, rate 1/2 and 1/3 coded PSAM BPSK, rate 1/2 coded PSAM QPSK and rate 1/3 coded PSAM 8PSK. Constraint length of convolutional code is 3. Delay power profile is (0, -10, -10)dB. (a) Fade rate is 0.05. (b) Fade rate is 0.005.

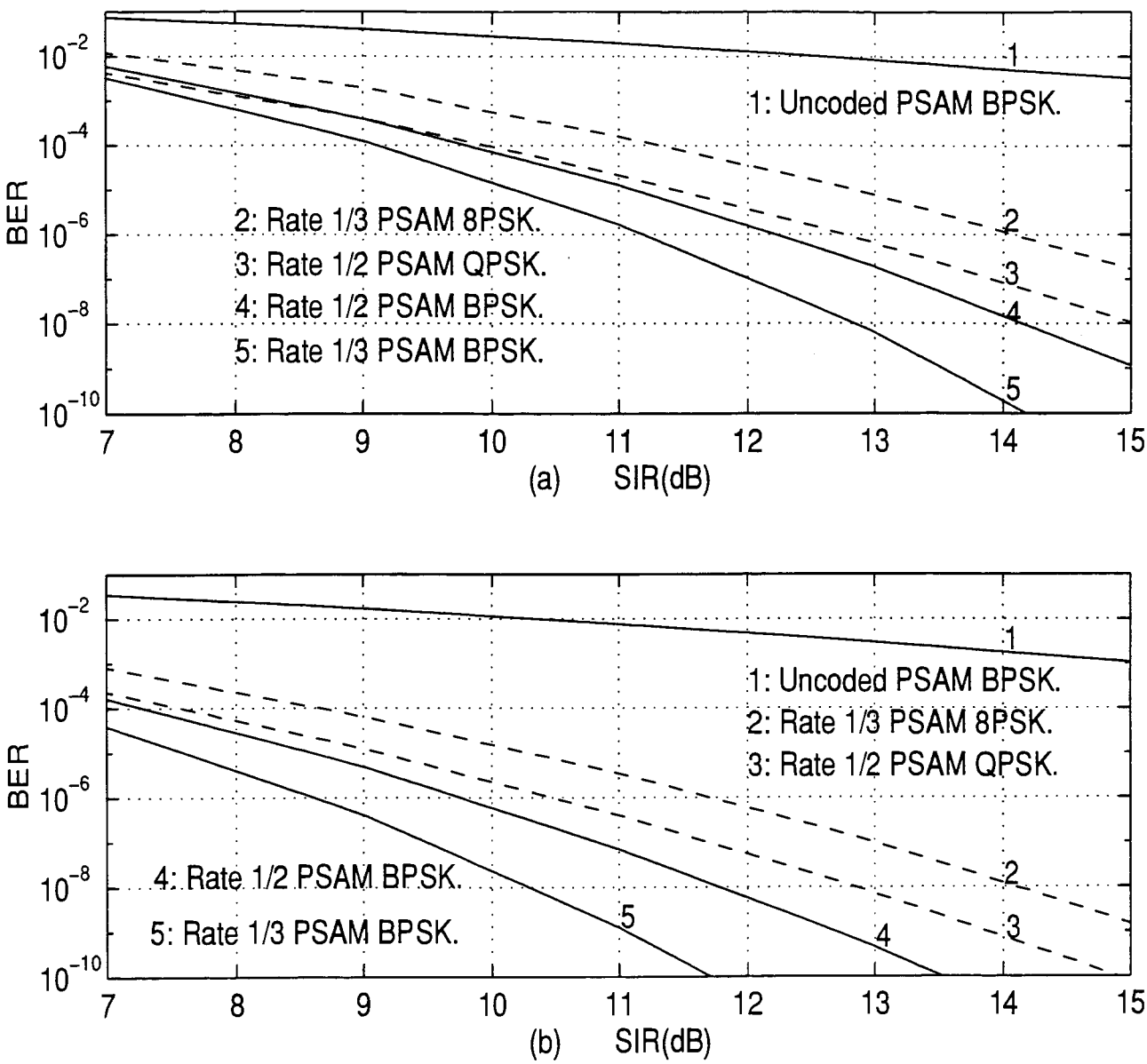

Figure 3.22: Bit error performance comparison of uncoded PSAM BPSK, rate 1/2 and 1/3 coded PSAM BPSK, rate 1/2 coded PSAM QPSK and rate 1/3 coded PSAM 8PSK. Constraint length of convolutional code is 5. Delay power profile is (0, -10, -10)dB. (a) Fade rate is 0.05. (b) Fade rate is 0.005.

similar behavior. In a very selective fading channel, the self-interference is larger and PSAM can improve the performance compared with differential detection only at a slower fading rate. When the channel is less selective and presents "flat fading" properties, PSAM can improve the performance better than differential detection at both fast and slow fading. Comparing rate 1/2 and rate 1/3 PSAM BPSK, different phenomena are observed. Constraint length 3 rate 1/2 code and rate 1/3 code have similar error correcting capabilities. The smaller self-interference due to a larger processing gain makes rate 1/2 BPSK outperform rate 1/3 BPSK slightly. Constraint 5 rate 1/3 code has a much better error-correcting capability than rate 1/2 code, and it outperforms rate 1/2 code in both fast and slower fading channels. The less selective the channel is, the more improvement the rate 1/3 code achieves.

Afterwards, the performance of pilot symbol assisted rate 1/2 QPSK and rate 1/3 8PSK are investigated. The PSAM QPSK and 8PSK present similar behavior in both more and less selective fading channels. At fast fading ($f_D T = 0.05$), the PSAM has about 1dB improvement over differential detection. On the other hand, the improvement can be over 2dB at slower fading ($f_D T = 0.005$). When the channel is getting less selective, the overall performance is decreasing due to the reduced diversity effect. Finally, with fixed data throughput and spreading bandwidth, comparisons have been made between uncoded BPSK, rate 1/2 and 1/3 coded BPSK, rate 1/2 coded QPSK and rate 1/3 coded 8PSK. They present similar behavior in both more and less selective fading channels. When constraint length is 3, rate 1/2 QPSK always outperforms rate 1/3 8PSK at all fade rates considered. At a slower fade rate, both the rate 1/2 and 1/3 BPSK outperforms rate 1/2 QPSK and rate 1/3 8PSK

schemes. When the constraint length is 5, rate 1/2 QPSK still outperforms rate 1/3 8PSK. Rate 1/2 QPSK and 1/3 8PSK outperform BPSK at lower SIR due to less self-interferences. When the self-interference increases and the performance of dense constellation modulation becomes poorer, BPSK with a strong error-correcting code presents better performance.

Chapter 4

Error Performance Simulation of Cellular CDMA

In this chapter, we consider the bit-error-rate (BER) performance and frame-error-rate (FER) performance on the uplink (portable-to-base) of a cellular CDMA system. The CDMA system uses convolutional code, orthogonal signaling, symbol interleaving, multipath diversity with noncoherent combining and fast closed-loop power control. The transmitted information data rate is 64kb/s and the processing gain is 128. The exact analytical expression for the required signal-to-noise ratio (SNR) at a given decoded BER and FER is quite difficult to derive because of its dependence on the fading rate, the interleaving size, and the detection scheme at the receiver. Instead of deriving these performance bounds analytically, computer simulation is used to obtain the channel performance. The organization of this chapter is as follows: Section 4.1 introduces the system model of combined orthogonal/convolutional coding scheme for CDMA communication. Section 4.2 illustrates the simulation results and the influence of parameter selection. Section 4.3 presents a simple performance comparison of this combined orthogonal/convolutional coding scheme to Pilot Symbol Assisted

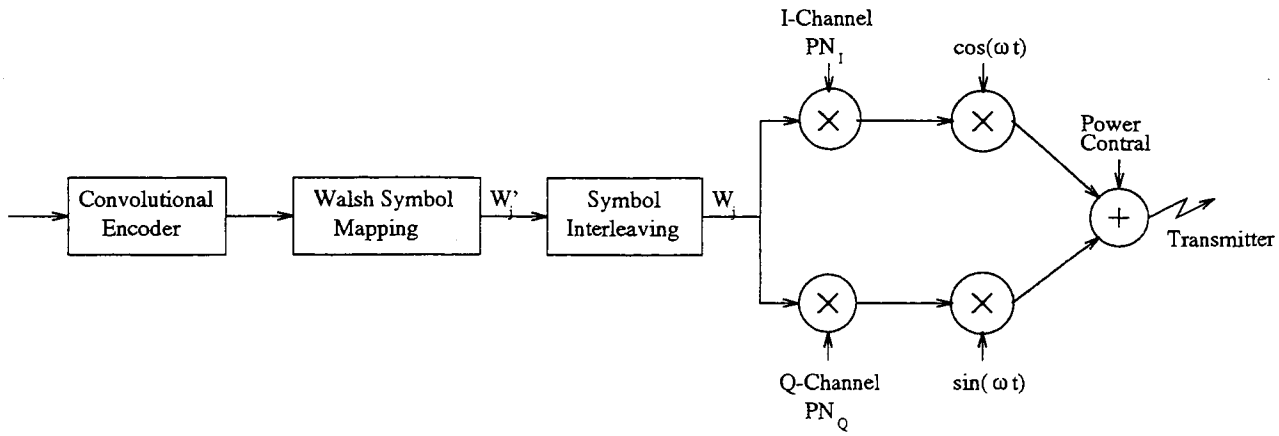

Figure 4.1: Block diagram of the transmitter structure of DS/CDMA system.

Modulation.

4.1 System Model of Combined Orthogonal and Convolutional Coding Scheme

A combined orthogonal/convolutional coding scheme, which is adequate for noncoherent reception over the uplink, is suggested in [13]. The information bits to be transmitted are organized in groups of k information bits, which are coded by a rate k/n convolutional encoder to generate n coded bits. These groups of n coded bits are further encoded into M-ary Walsh symbols, or, in general, M-orthogonal waveforms; $M = 2^n$. Then the M-ary symbols within a block are symbol interleaved to combat fading. Such a scheme achieves a spreading factor of kM/n. Further spreading using PN sequences is usually needed to provide spectrum spreading and user separation. The resulting spread spectrum sequence is then modulated and transmitted. In this

case, the code optimality and the definition of distance in orthogonal/convolutional code are different from the binary convolutional coding. We must measure the distance in units of Hadamard symbols. For instance, the optimal binary constraint length 9, rate 1/3 convolutional code has a minimum binary distance of 18. The same code used in the 2/6/64 coding yields a minimum distance of 5 (of 64-ary Hadamard words). The transmitter structure is depicted in Figure 4.1.

4.1.1 Convolutional Code Encoder and Hadamard Mapping

This approach is called the orthogonal/convolutional coding scheme and $k/n/M$ code. In this thesis, we use 2/6/64 code, which has promising performance at the cost of complexity. The rate 2/6 encoder can be implemented in the same way, using the same 3 generators as a rate 1/3 encoder. Theoretically, a rate 2/6 code may be designed to use six different generators and has a better distance property than using the rate 1/3 code generators twice. However, there is no systematic way to design an optimal code, and computer searching will be very time consuming when the constraint length is long. Practically, people find that running a rate 1/3 encoder twice as a rate 2/6 encoder is a quite satisfactory solution, and this is how our simulations are realized.

A rate 1/3, constraint length 9 convolutional code is used in simulation, and the three generator polynomials are $g_1 = 557$, $g_2 = 663$, and $g_3 = 711$. The structure of the encoder is depicted in Figure 4.2.

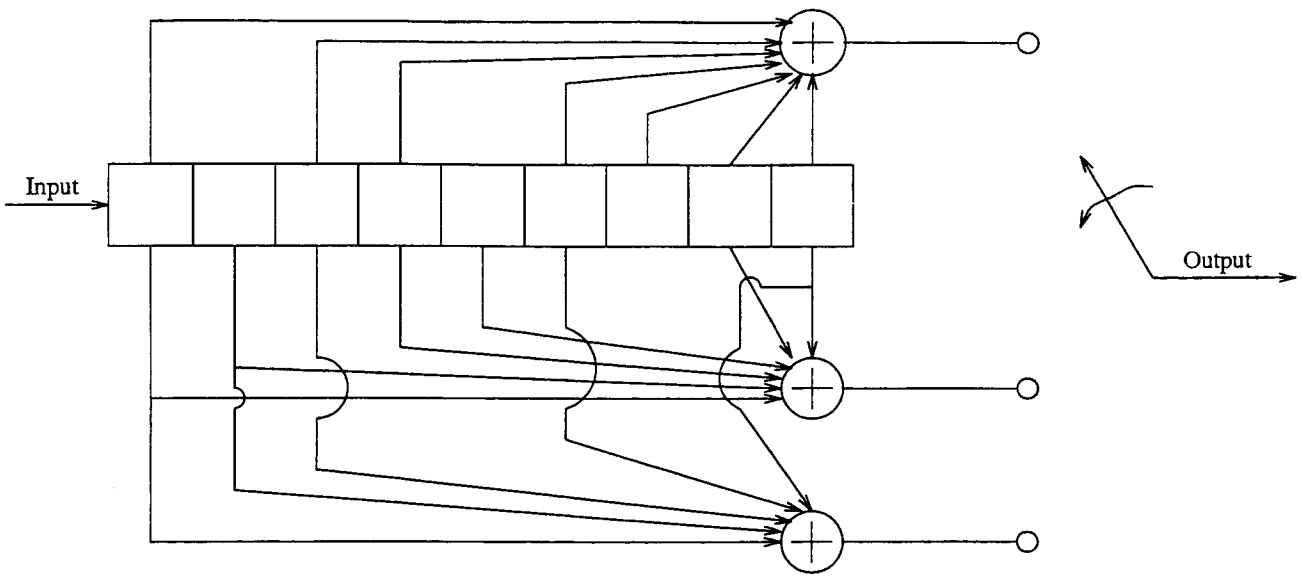

Figure 4.2: Structure of $L = 9$, $k = 1$, $n = 3$ convolutional encoder.

The output of the encoder is comprised of 6 coded bits per 2 input information bits. The 6 coded bits are further mapped into one of the 64 Hadamard codewords (Walsh symbols) using a 64x64 Hadamard matrix (i.e., each Hadamard code word consists of 64 binary bits). This process produces 64 orthogonal signals. The Hadamard matrix consists of 1s and -1s, with the property that every row of the matrix is orthogonal to any other row of the matrix. The formation of the Hadamard matrix is as follows

$$H_0 = [1] \tag{4.1}$$

$$H_k = \begin{bmatrix} H_{k-1} & H_{k-1} \\ H_{k-1} & -H_{k-1} \end{bmatrix} \tag{4.2}$$

With the use of the Hadamard signals (rows from the Hadamard matrix H_6) in the uplink of this CDMA system, the word-by-word interleaving technique implies interleaving based on a Hadamard word.

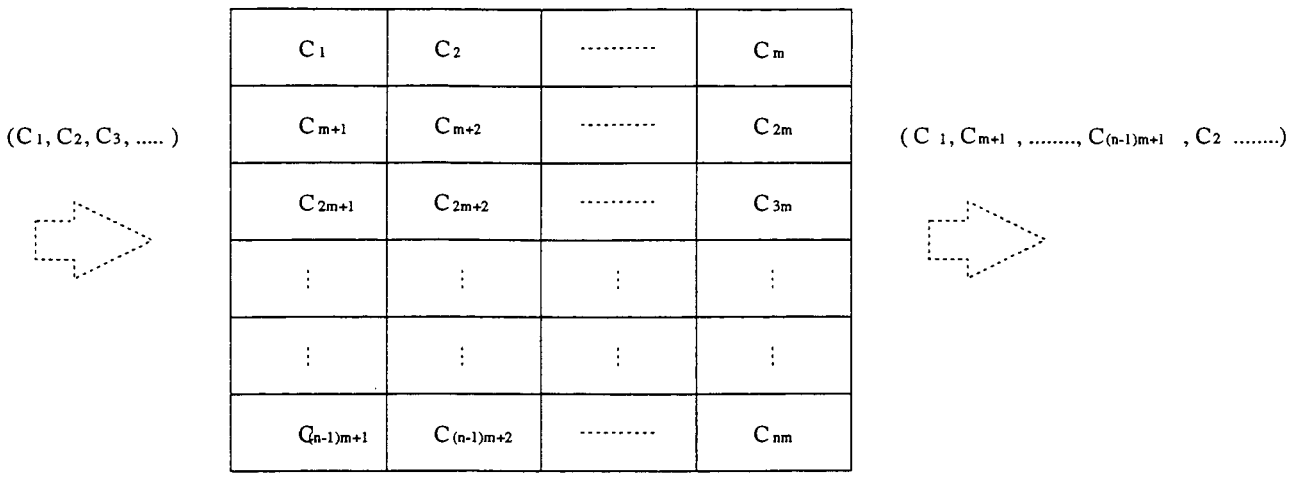

Figure 4.3: A block interleaver with n rows and m columns.

4.1.2 Symbol Interleaving

The successive received code symbols are correlated, and interleaving is usually applied to achieve time diversity to mitigate fading. An interleaver shown in Figure 4.3 is a device which can rearrange the ordering of the encoded symbols so that two consecutive symbols are separated by certain spaces (interleaving depth) after interleaving. The interleaver is able to break up the burst errors caused by multipath fading, and the individual symbols received will have independent fading gains. Since data are organized in blocked bits, a block interleaver is usually used. There are two types of block interleaving available: bit interleaving, where the encoded bits are first interleaved and then mapped into Hadamard orthogonal symbols; and symbol interleaving, where interleaving follows orthogonal mapping. It has been shown that symbol interleaving results in at least 1dB improvement in the required SNR [43], so we adopted symbol interleaving in this simulation.

We performed our simulation on two interleaving sizes: 6 by 16 and 16 by 16 symbol interleaving. At the transmitter, the symbols are written into the interleaver row by row and transmitted out column by column. At the receiver, the demodulated symbols are written into the deinterleaver column by column and read out row by row. Because we have two input information bits mapped into a Walsh symbol, the overall interleaving delay is $192T_b$ for 6 by 16 symbol interleaving, and $512T_b$ for 16 by 16 symbol interleaving respectively, where T_b is the time duration of information bit. The frame size considered for FER calculation is the same as the interleaver size.

4.1.3 Modulation and Demodulation

In our simulation, we consider quaternary direct-sequence systems where the same data is modulated onto the in-phase and quadrature channels using different PN codes. It is also called balanced quadriphase modulation. The receiver structure of such a system is shown in Figure 4.4(a), and it is basically a RAKE receiver as introduced in Section 2.4.3.

Although the modulation is done by QPSK, the data modulation may be regarded as a binary PSK. It's suggested that PN codes with long periods should be applied in this system. Because of the large period of the PN codes considered, it can be assumed to be a random sequence.

The received signal is demodulated and despreaded, and its in-phase (I) and

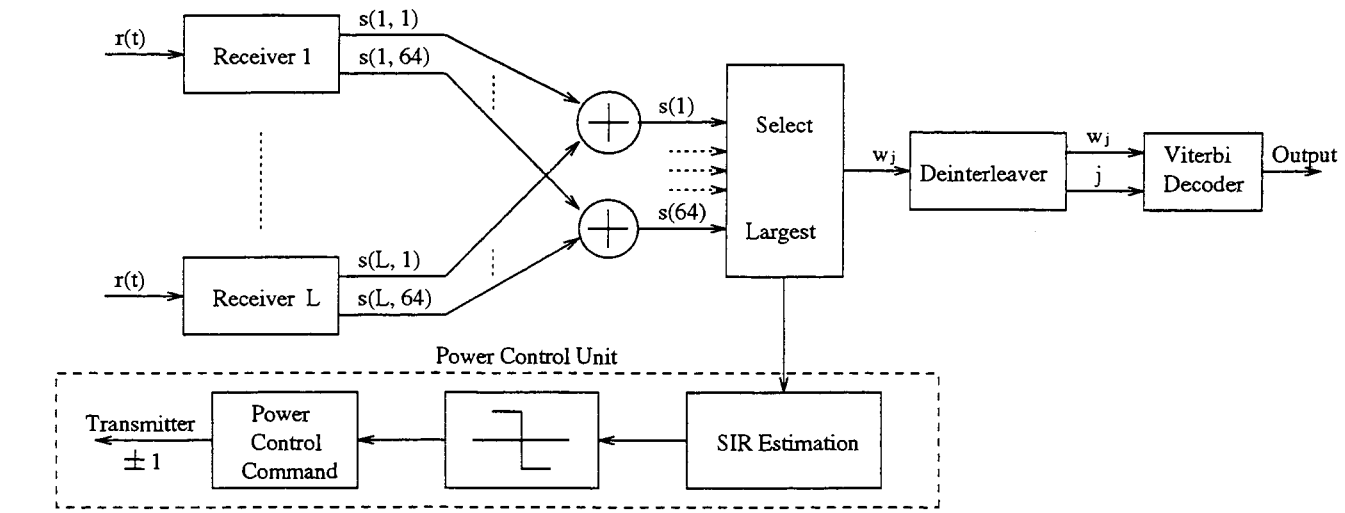

(a)

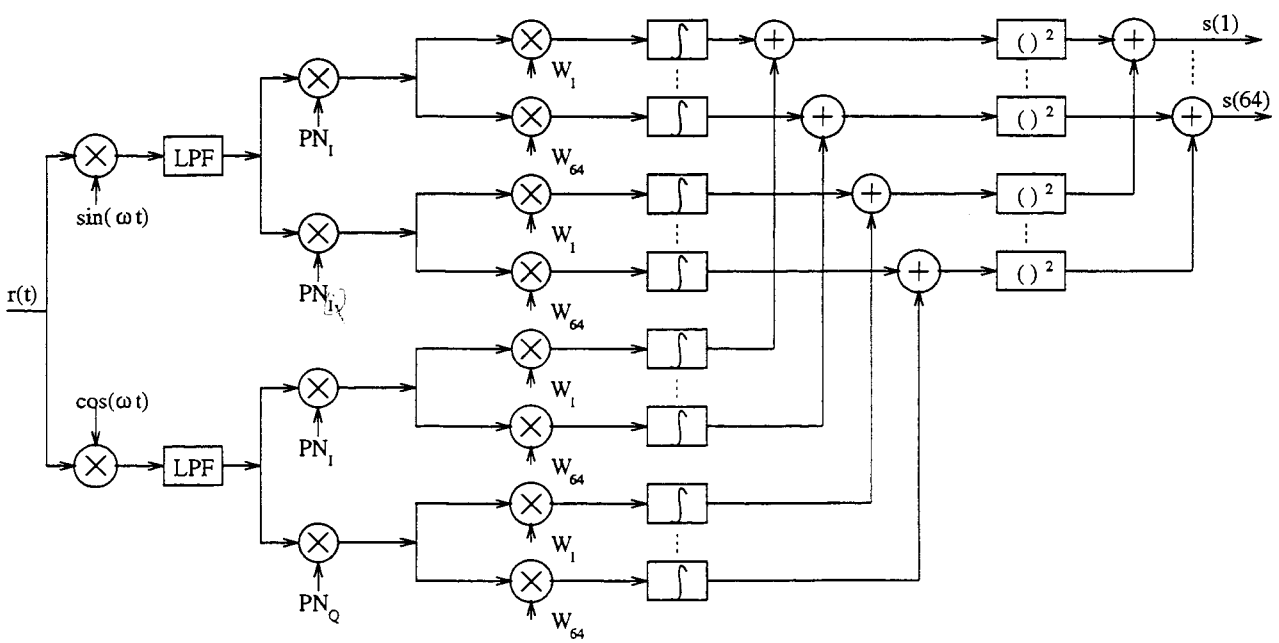

(b)

Figure 4.4: Receiver structure of DS/CDMA system. (a) Block diagram of L branch RAKE receiver and decoder. (b) The receiver model for the l^{th} RAKE branch.

quadrature (Q) components are separated. The resulting I and Q samples are correlated with each of the 64 orthogonal waveforms independently (Hadamard correlator). The corresponding outputs of the I and Q correlators are squared and added together. The outputs of the corresponding Hadamard correlators from other diversity branches are square-law combined, weighed with equal gain as well.

The channel is frequency-selective Rayleigh fading with a delay power profile of (0, -3, -6)dB or (0, -10, -10)dB. Slow fading is considered in our simulation. The normalized Doppler frequency f_dT is 0.0002 and 0.002, which is based on $2GHz$ carrier frequency and vehicle speed $7 - 70km/hr$.

4.1.4 Power Control

Due to the delay by deinterleaving, information to be used for feedback power control must be extracted before deinterleaving. The output of the square-law combiner consists of 64 values, which will be used for power control and for the Viterbi decoder. These 64 metrics correspond to one of the 64-ary orthogonal signals. Because of the orthogonality of the 64-ary signals, on the average at relative high SIR, the maximum metric value should indicate the signal power. The rest of the metrics correspond to noise and interference power. Therefore, a hard decision is performed to select the maximum value of the 64 output values from the square-law combiner. Therefore, the quantity

$$\lambda = \sum_{j=1}^{m} \frac{\max(w_{j,1}, ..., w_{j,64})}{\sum_{i \neq max} w_{j,i}} \tag{4.3}$$

represents the estimated short-term average SIR, where $w_{j,i} = 1, ..., 64$ are the outputs from the square-law combiner for the j^{th} information bit period T_b; and m is the power control updating rate. The numerator represents the signal power over an information bit period, and the denominator represents the noise and interference over an information bit period. Because interferences are noise-like and have constant power level, the signal-to-interference ratio (SIR) and signal-to-noise (SNR) are treated the same in our simulation.

The unique mapping $f(\lambda)$ between a given SIR (in dB) and the corresponding value presented in Equation 4.3 can be found by simulation. The estimated SIR $\Lambda = f(\lambda)$ is then compared to the set power control threshold Γ. If $\Lambda > \Gamma$, the portable is requested to reduce its power by δdB; otherwise, it increases its power by δdB. If the criterion for the uplink performance is a 10^{-3} decoded bit error rate, the SIR should be around 7dB. The error rate suffered by the unprotected power control bits is assumed to be 10%.

4.1.5 Viterbi Decoder

The outputs of the square-law combiner $w_{j,1}, ..., w_{j,64}$ are used as metric values in the Viterbi decoding process. It advances two nodes for each received signal, and the metric value between the received signal and 6-bit coded symbol $(a_5, a_4, ..., a_0)$ is w_k, where $k = 2^5 a_5 + ... + 2a_1 + a_0$. The maximum value w_{max} and its corresponding index k are then used in the Viterbi decoding process. For example, if $w_{max} = w_{18}$,

then the binary representation of the value 18 (i.e., 010010) will be treated as the estimated transmitted coded signal. The value of w_{18} is used as the weight for each of the corresponding binary coded bits. The decoding depth is chosen to be 6 times of the constraint length. The use of w_{max} as the soft metric does not degrade the system performance compared to the use of the optimum soft metric in the decoding process (i.e., the log-likelihood function of w_{max}).

4.2 Simulation Results

The transmitted data rate is 64kb/s with a carrier frequency 2GHz. The processing gain is 128 and the channel is a three-ray frequency-selective fading channel. We are interested in the performance for a slowly fading channel with normalized fading rate $f_DT = 0.0002$. Results of $f_DT = 0.002$ has also been studied for comparison. Two delay power profiles have been simulated for the fading channel, (0, -3, -6)dB and (0, -10, -10)dB.

The block diagram has been shown in Figure 4.1 and 4.4. Some assumptions on power control were applied to the simulation results. The power control command bits are generated every $T_p = 1.25msec$, and the present SIR is estimated through 8-bit short term estimation. The power control processing and transmission delays are $2T_p$ and the power control step size is set at 0.5 dB. The power control bits do not go through coding and interleaving, and they suffer a 10% random error rate. Two symbol interleaving sizes of 6x16 and 16x16 have been adopted for simulation. The data frame size is also the same as the interleaving size, i.e., 192 and 512 information

bits for 6x16 and 16x16 interleaving respectively. At the receiving end, the RAKE receiver captures signal power from all three paths.

4.2.1 At fading rate 0.0002

Figure 4.5 and Figure 4.6 illustrate the BER and FER with a delay power profile of (0, -3, -6)dB. The interleaving size in Figure 4.5 is 6x16. From the curves we can see the power control technique can reduce the BER and FER dramatically. A frame is counted as an error frame as long as there is one single error bit within it.

While reading the simulation results of power control, the BER and FER performances should not be related to the SNR, since the power control scheme maintains a constant level of receiving SIR at the receiver end. This applies to all the power control simulation results within this chapter.

Figure 4.6 illustrates the BER and FER with interleaving size 16x16. The effect of power control is obvious. Comparing Figure 4.5 to Figure 4.6, the BER and FER are almost the same for both interleaving sizes without power control. With the power control technique, the larger interleaving size 16x16 presents a similar performance as interleaving size 6x16 does. This indicates that for a very slow fading channel, the interleaving size should be large enough to randomize the channel so that the use of a powerful error-correcting code would be effective.

Figure 4.7 - Figure 4.8 illustrate the BER and FER with a delay power profile of (0,

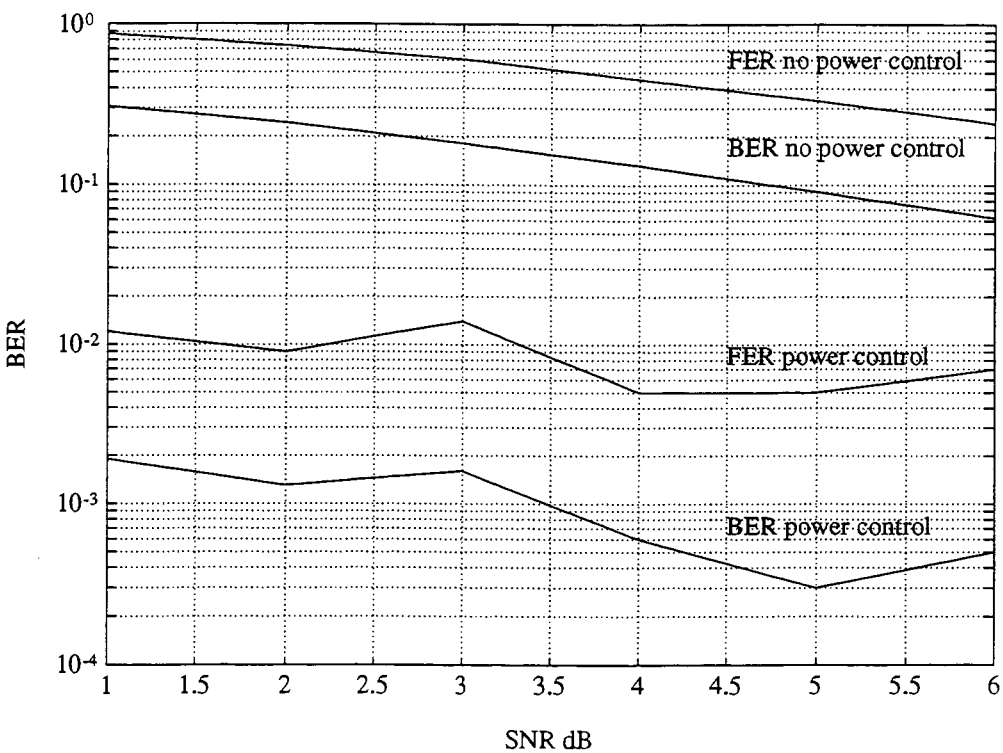

Figure 4.5: The performance of BER and FER. Interleaving size is 6x16, delay power profile is (0, -3, -6)dB and f_dT=0.0002.

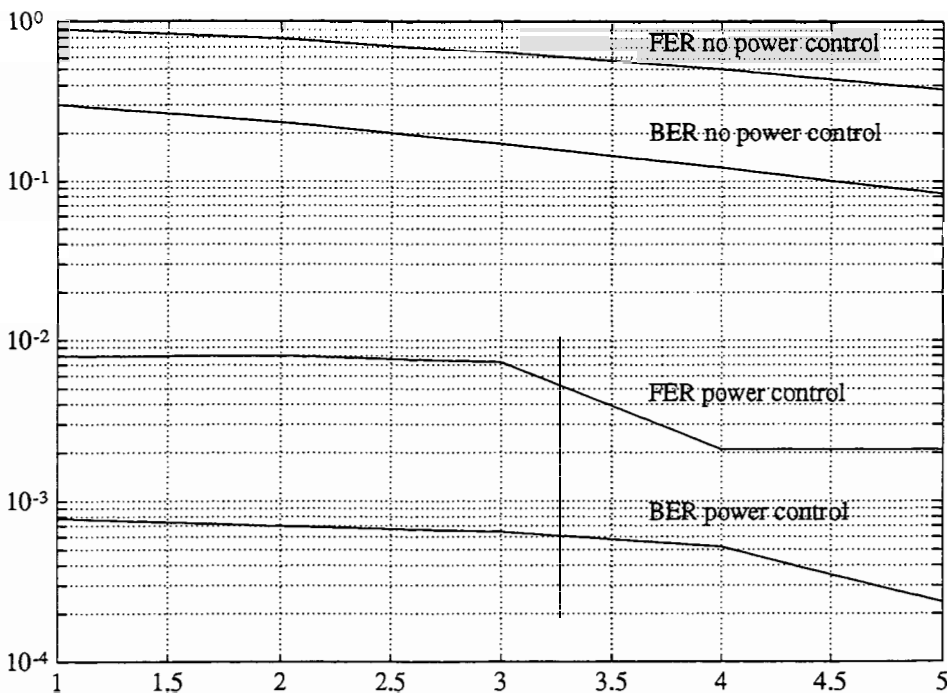

Figure 4.6: The performances of BER and FER. Interleaving size is 16x16, delay power profile is (0, -3, -6)dB and f_dT=0.0002.

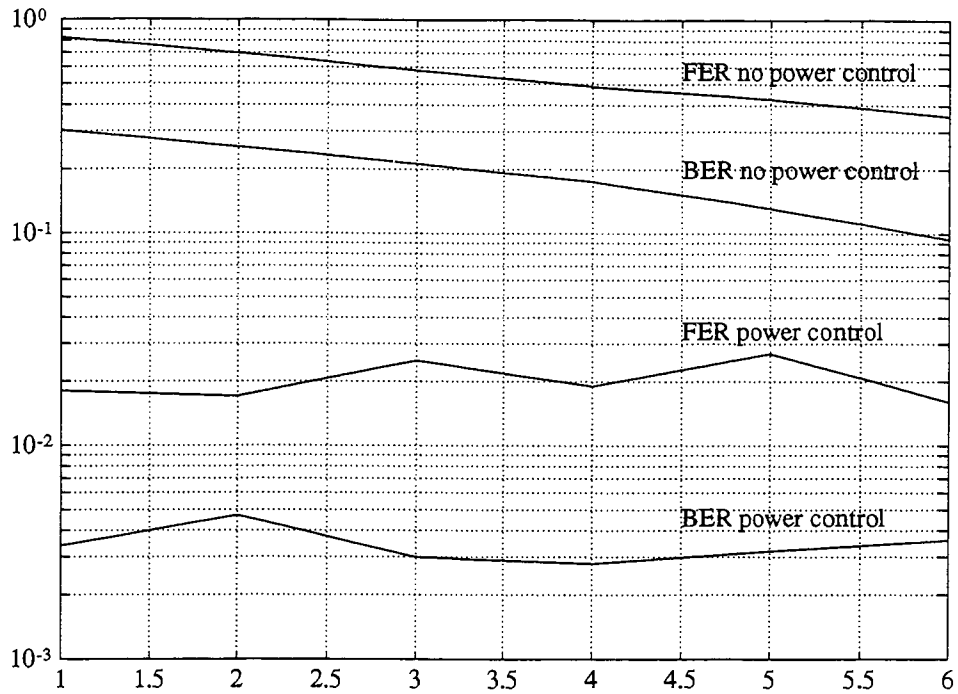

Figure 4.7: The performances of BER and FER. Interleaving size is 6x16, delay power profile is (0, -10, -10)dB and f_dT=0.0002.

-10, -10)dB and different interleaving size. The weak multipaths make the frequency selective channel look like a flat fading one. The interleaving size in Figure 4.7 is 6x16 and although power control technique reduces the BER and FER, its performance is not as good as that of (0, -3, -6)dB. This is because the channel is more like a flat fading channel and has a less diversity effect.

The interleaving size in Figure 4.8 is 16x16 and the results are similar to Figure 4.6. This also confirms that at a very slow fading rate, the interleaving size 6x16 and 16x16 randomize the burst error similarly. Comparing Figure 4.6 to Figure 4.8, we find that

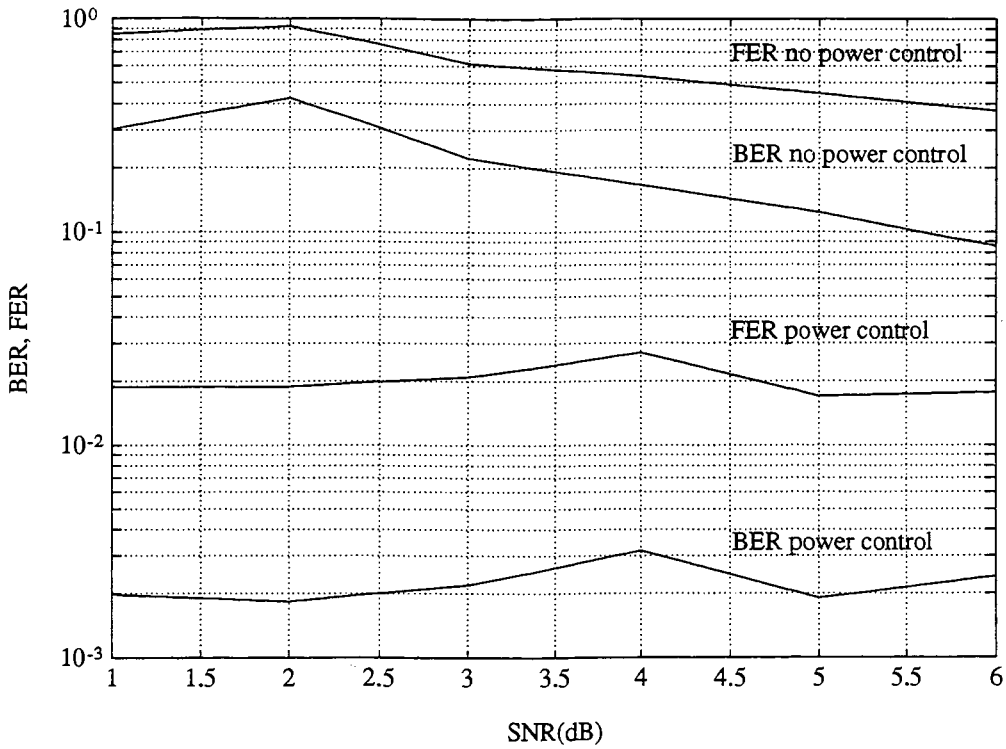

Figure 4.8: The performances of BER and FER. Interleaving size is 16x16, delay power profile is (0, -10, -10)dB and f_dT=0.0002.

under the same interleaving size, the performance of (0, -3, -6)dB is better than that of (0, -10, -10)dB with or without power control. This indicates that when the channel is getting less frequency selective, the diversity effect of the spread spectrum also decreases.

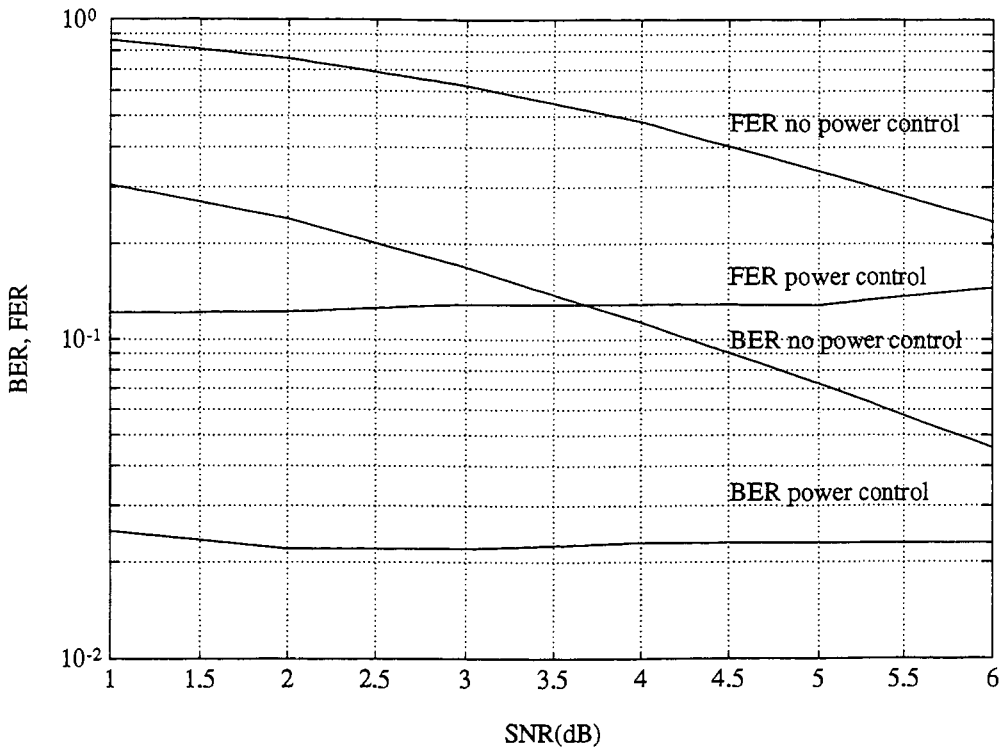

Figure 4.9: The performances of BER and FER. Interleaving size is 6x16, delay power profile is (0, -3, -6)dB and f_dT=0.002.

4.2.2 At fading rate 0.002

Figure 4.9 - Figure 4.12 illustrate the BER and FER performances of different interleaving sizes and delay power profiles with the considered fading rate to be 0.002. Compared to fading rate 0.0002, we call this the fast fading case. While the interleaving size is 6x16 and the delay power profile is (0, -3, -6)dB, the results are depicted in Figure 4.9. From the curves we can tell that although power control still reduces the BER and FER, the performance does not improve as much as for theslow fading channel.

The results of a 16x16 interleaving size are shown in Figure 4.10 and compared with Figure 4.9, we find that a larger interleaving size performs better than a smaller interleaving size at a fast fading rate. This indicates that unlike in a very slow fading rate, a 16x16 interleaving size can randomize the burst error much better than the 6x16 interleaving, so the use of an error-correcting code is effective. However, the same power control technique used in slow fading does not work well in the fast fading environment. The adjustment in transmitting power could not follow the variation of a fast fading channel. Although increasing the interleaving size can reduce the BER, the increased data packet contains more information bits, and the FER does not improve or even drops down.

Figure 4.11 - Figure 4.12 show the results of a delay power profile of (0, -10, -10)dB. The behaviors of BER and FER are similar to those with a delay power profile (0, -3, -6)dB. The BER performance is improved with a larger interleaving size but the FER performance drops down due to the larger packet size. The power control technique improves the performance but does not work as well as in slow fading channels. Comparing the curves in Figure 4.11 and Figure 4.12 to those in Figure 4.9 and Figure 4.10, we find that when the channel is getting less selective, the diversity effect decreases as well.

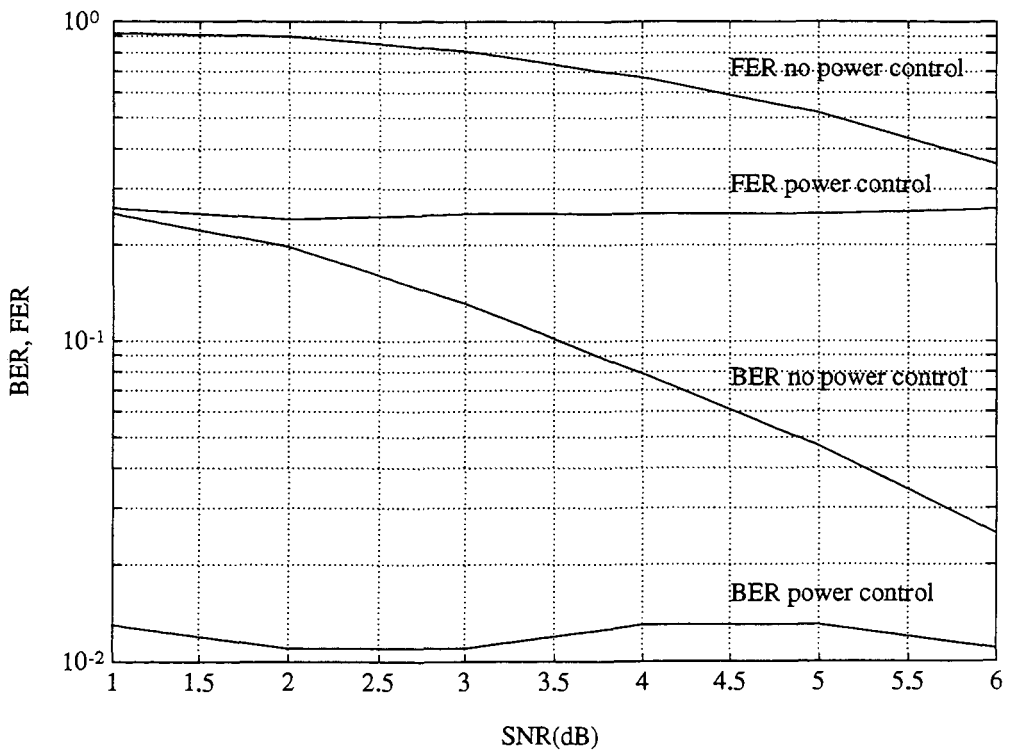

Figure 4.10: The performances of BER and FER. Interleaving size is 16x16, delay power profile is (0, -3, -6)dB and f_dT=0.002.

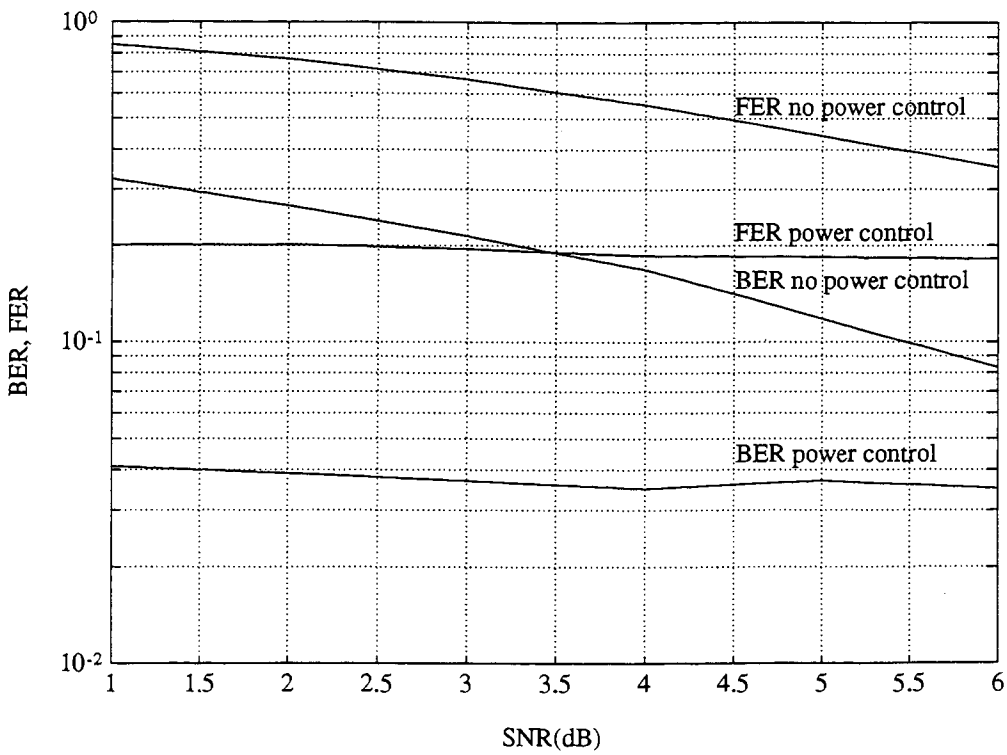

Figure 4.11: The performances of BER and FER. Interleaving size is 6x16, the delay power profile is (0, -10, -10)dB and f_dT=0.002.

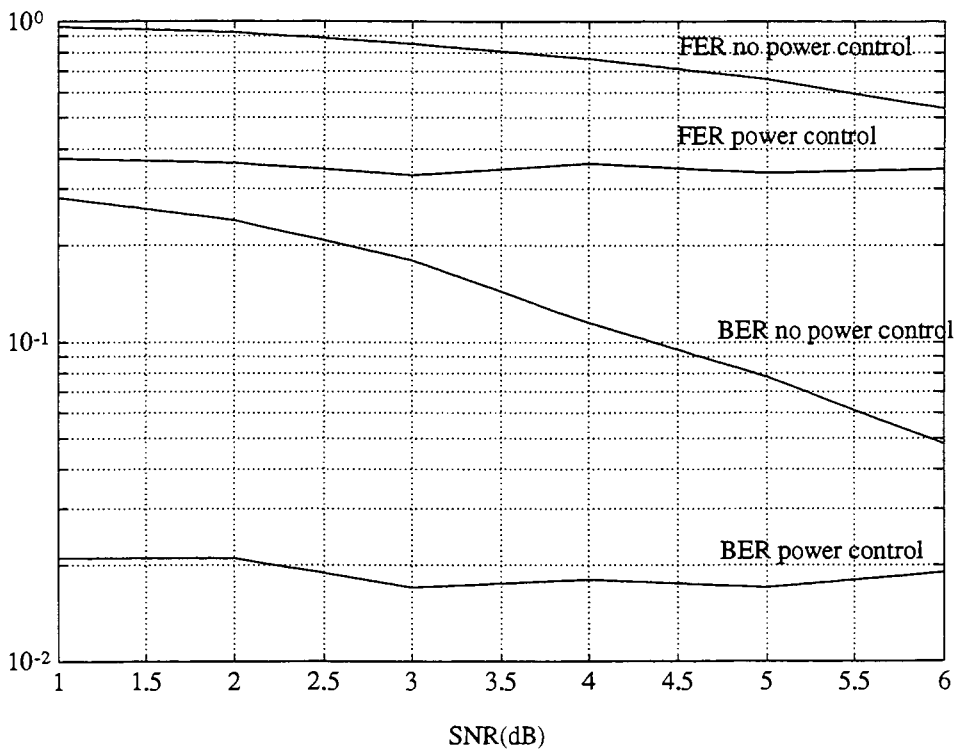

Figure 4.12: The performances of BER and FER. Interleaving size is 16x16, the delay power profile is (0, -10, -10)dB and f_dT=0.002.

4.3 Comparison of Pilot Symbol Assisted Modulation and Combined Orthogonal/Convolutional Coding Scheme

In Chapter 3, we gave the error bound analysis of Pilot Symbol Assisted Modulation. The performances of diffferent rate convolutional coding schemes with PSAM and MPSK modulation techniques were presented. In this section, we are going to present a simulation performance comparison between PSAM and non-coherent detection. The channel is frequency-selective Rayleigh fading and the delay power profile is (0, -3, -6)dB. Fading rate $F_D T$=0.005 and 0.0005 are simulated.

For the PSAM, a rate 1/3 convolutional code with contraint length 9 and BPSK modulation are considered. The pilot symbol insertion scheme is the same one introduced in Chapter 3. The transmitted data frame length is 7 and the interpolator size at the receiver end is 11. The bandwidth spreading factor is 128. After pilot symbol insertion, the actual processing gain decreases to 109. A 12 by 16 bit interleaving scheme is adopted to break up the burst errors caused by multipath fading. The interleaving delay is $192T_b$, where T_b is the time duration of the information bit.

The pilot symbols used in BPSK have the value +1, and the data symbols are ± 1. The receiver makes decisions by phase correcting the RAKE receiver output with the channel estimate and comparing the result to zero. Referring to equation (3.19, 3.25), $Re[r_l(k)g_l(k)]$ is the output of the l^{th} branch. The outputs from all branches are combined together to form the decision variable, which will be deinterleaved and

decoded. If the real part of the decision variable is positive, a +1 is sent to Viterbi decoder, otherwise a -1 is sent. In our simulation, the Viterbi decoder performs hard-decision decoding to recover the transmitted data.

The orthogonal/convolutional coding scheme is the same one introduced in Section 4.1 except that there is no power control implemented, and the constraint length of the convolutional code is 9. A 6 by 16 symbol interleaving is adopted with interleaving delay $192T_b$.

Figure 4.13 shows the performances of PSAM and non-coherent detection at a fade rate of 0.005. The delay power profile is (0, -3, -6)dB. We can see that the PSAM performs better than non-coherent detection. At BER 10^{-3}, PSAM has approximately $3dB$ advantage over non-coherent detection. Figure 4.14 shows the performances of PSAM and non-coherent detection at a slower fade rate of 0.0005. The curves indicate that PSAM has more of an advantage over non-coherent detection. Even though the simulation is not very accurate at lower BER, the PSAM seems to outperform non-coherent detection at a slower fading rate.

4.4 Summary

We presented in this chapter the simulation results of a combined orthogonal/convolutional coding scheme in cellular CDMA system. The 2/6/64 code and the Walsh symbol

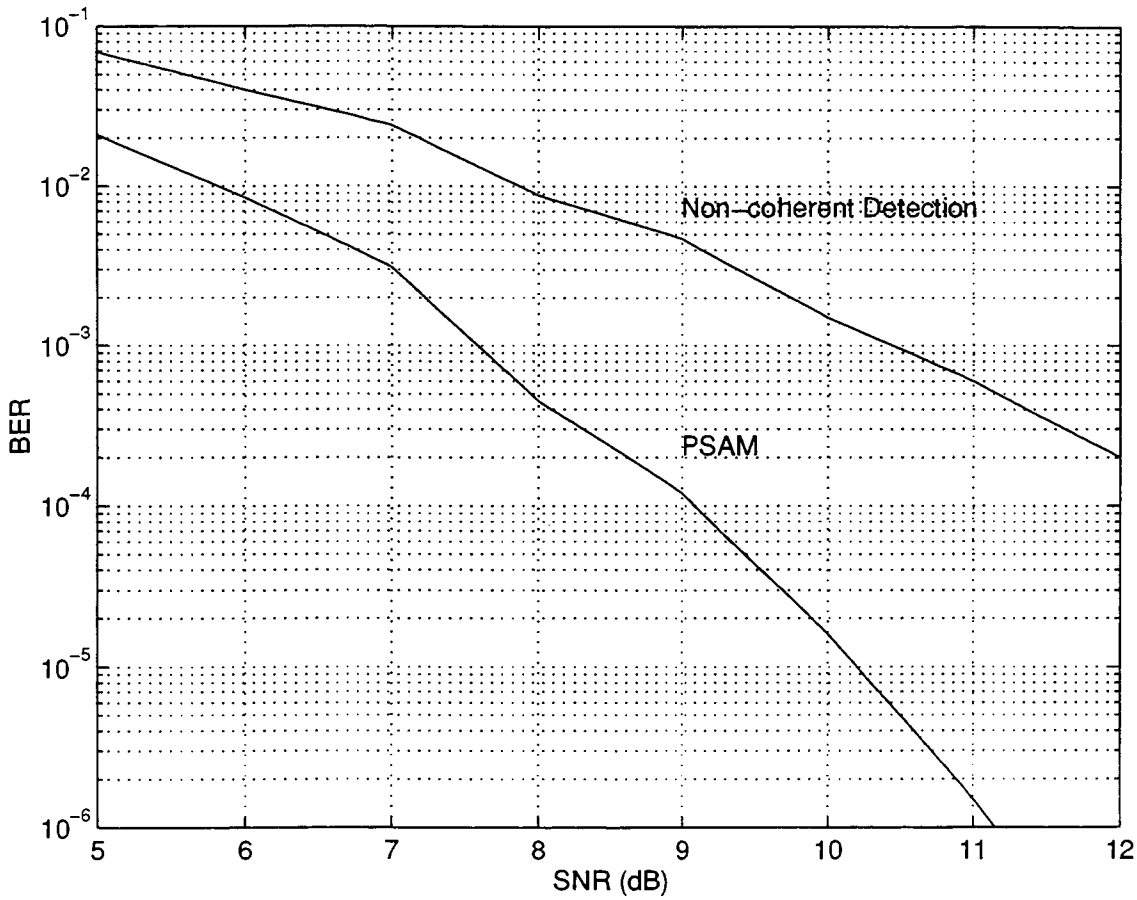

Figure 4.13: The BER performances of PSAM and Non-coherent detection. Interleaving delay is $192T_b$, the delay power profile is (0, -3, -6)dB and f_dT=0.005.

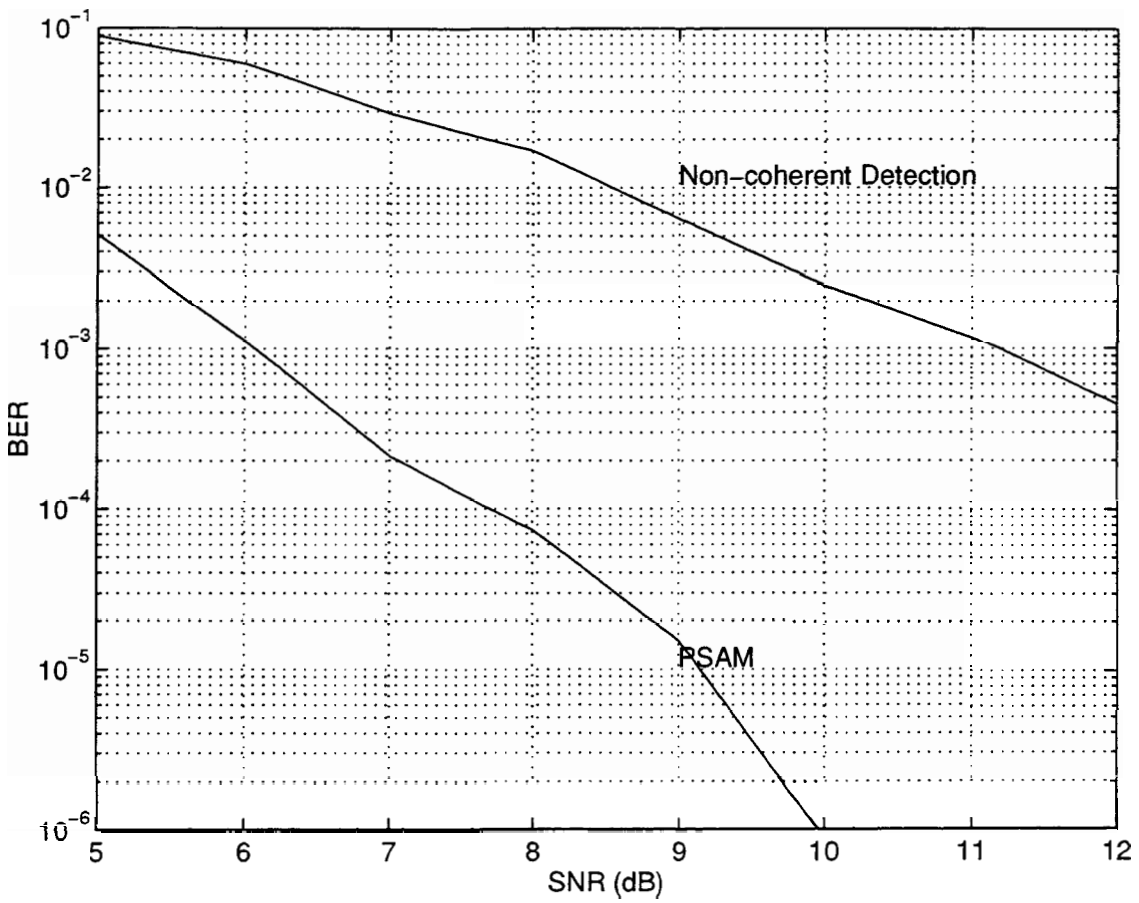

Figure 4.14: The BER performances of PSAM and Non-coherent detection. Interleaving delay is $192T_b$, the delay power profile is (0, -3, -6)dB and f_dT=0.0005.

interleaving are adopted in the transmitter. Balanced quadriphase modulation, where the same data is modulated onto the in-phase and quadrature channels using different PN sequences, is also considered. The power control, RAKE receiver and Viterbi decoder are implented at the receiver. When the power control update step can follow the variation of the channel, the effect is obvious. The more selective the channel is, the better the performance is achieved due to the diversity effect. At a faster fading rate ($f_D T = 0.002$), 16x16 interleaving size provides better performance than 6x16 interleaving size. On the other hand, at a slower fading rate ($f_D T = 0.0002$), 16x16 and 6x16 interleaving present similar results, which indicate that a larger interleaving size is needed at slower fading to randomize the burst error. Finally, the simple simulation comparison illustrates that PSAM has better performance than the non-coherent without power control technique.

Chapter 5

Conclusions

5.1 Conclusions

In this thesis, we studied the error performance of Pilot Symbol Assisted Modulation (PSAM) of M-ary PSK signals in a cellular CDMA system. A three-ray channel model is adopted to represent the frequency-selective Rayleigh fading encountered in cellular CDMA environment. One characteristic of cellular CDMA is the presence of self-interference and multiple access interference. The error performance of pilot symbol assisted modulation is affected by these interferences.

For BPSK modulation, the coding rate is k/n for convolutional encoder. We wanted to keep the transmission bandwidth $B = Gn/k$ constant, where G is the processing gain. Apparently, there is a trade off between the coding rate k/n and processing gain G. Furthermore, the insertion of pilot symbols also reduces the actual processing gain of the system. If the pilot symbols are inserted into the data stream

with frame size M, the transmission bandwidth will be

$$B = G\frac{n}{k}\frac{M}{M-1} \tag{5.1}$$

where the effect of frame size M is obvious. For rate 1/2 QPSK and rate 1/3 8PSK modulation, the actual processing gain is only affected by the insertion of pilot symbols.

Pilot symbol assisted BPSK modulation is analyzed first. The transmission bandwidth is fixed at 380, and we considered rate 1/2 PSAM BPSK with processing gain 163 and rate 1/3 PSAM BPSK with processing gain 109 respectively. PSAM always outperforms differential detection at both fast and slow fading. The slower the channel fading is, the better performance PSAM achieves. When the channel is less frequency-selective, the received SIR at the 1st branch of the RAKE receiver is larger because of the less amount of self-interference caused by the weaker paths. The improvement of PSAM over differential detection is getting larger. But the overall performance decreases due to less diversity effect.

At a channel with a delay power profile of (0, 0, 0)dB, we can see that when the constraint length is 3 for both codes, the rate 1/2 PSAM outperforms rate 1/3 PSAM. On the other hand, when the constraint length is 5, rate 1/3 PSAM outperforms rate 1/2 PSAM. This phenomenon is caused by the properties of the convolutional codes. The rate 1/2 and 1/3 codes with constraint length 3 have similar error-correcting abilities. However, rate 1/3 code with constraint length 5 has much stronger error-correcting ability than constraint length 5 rate 1/2 code. The larger processing gain with rate 1/2 code reduces the self-interference caused by the selective fading channel

and improves the performance. As for the constraint length 5 codes, although the processing gain for rate 1/2 BPSK is larger than that of rate 1/3 BPSK, the error-correcting power of rate 1/2 code is comparatively less than rate 1/3 code, and the performance of rate 1/3 BPSK is better.

Rate 1/3 PSAM 8PSK has a similar performance as rate 1/2 PSAM QPSK. We have illustrated the comparison of several PSAM schemes with the same net information throughput of 1 bit/symbol and fixed spreading bandwidth 380: uncoded BPSK, rate 1/2 and 1/3 coded BPSK, rate 1/2 coded QPSK and rate 1/3 coded 8PSK. When the constraint length is 3, rate 1/2 BPSK has the best performance among those schemes. However, when the constraint length is 5, rate 1/3 code outperforms the other schemes. When SIR increases, the self-interference also increases and the performance of dense constellation modulation becomes poorer. BPSK modulation with strong error-correcting code presents better performance.

Uplink error performance simulation has been made on a combined orthogonal/convolutional coding scheme for a cellular CDMA system. Balanced quadriphase modulation and Hadamard signals are adopted for modulation, and the closed loop power control and RAKE receiver were implemented at the receiver. Simulations were run through frequency-selective fading channels with delay power profiles of (0, -3, -6)dB and (0, -10, -10)dB. Bit error rate (BER) and frame error rate (FER) were simulated, where the frame size was the same as the interleaving size. The power control techniques can reduce the BER dramatically while the upgrade speed follows the variation of the fading channel. The result also indicates that a larger interleaving size is

needed to randomize the burst error in a slow fading channel. When the channel gets less selective, the overall performance decreases as well due to the less diversity effect. Finally, a simulation performance comparison of PSAM and non-coherent detection was presented. The coding scheme, interleaving size and spreading bandwidth are the same. Without the power control technique, the PSAM shows a consistant better performance than that of non-coherent detection.

5.2 Suggestions for Further Research

Some suggestions for further work are given below:

- When the multipath number is increasing and the coding scheme is getting complicated, the calculation of error bound with residue method becomes very difficult and time consuming. Some more effective methods should be found to make the calculation of bit error bound easier.

- More analysis and simulation results of the performance of the PSAM and non-coherent detection on the reverse link should be approached. Although including a pilot signal for each user will reduce the power efficiency, the better performance of PSAM might compensate it.

- Different pilot symbol insertion schemes could be considered for cellular CDMA environment to improve the performance.

Bibliography

[1] R. A. Scholtz, "The Origins of Spread-Spectrum Communications", IEEE Trans. Commun., Vol.30, No.5, May 1982.

[2] R. L. Pickholtz, D. L. Schilling and L. B. Milstein, "Theory of Spread-Spectrum Communications–A Tutorial", IEEE Trans. Commun., Vol.30, No.5, May 1982.

[3] G. L. Turin, "Introduction fo Spread-Spectrum Antimultipath Techniques and Their Application to Urban Digital Radio", Proc. of The IEEE, Vol.68, No.3, march 1980.

[4] G. R. Cooper and R. W. Nettleton, "A Spread-Spectrum Technique for high-Capacity Mobile Communications", IEEE Trans. Veh. Technol., Vol.27, No.4, November 1978.

[5] W. C. Y. Lee, "Spectrum Efficiency in Cellular", IEEE Trans. Veh. Technol., Vol.38, No.2, May 1989.

[6] A. J. Viterbi, "Very Low Rate Convolutional Codes for Maximum Theoretical Performance of Spread-Spectrum Multiple-Access Channels", IEEE Journal in SAC, Vol.8, No.4, May 1990.

[7] ————, "Spread Spectrum Communications–Myths and Realities", IEEE Communications Mag., Vol.18, No.5, May 1979.

[8] ————, "When Not to Spread Spectrum–A Sequel", IEEE Communications Mag., Vol.23, No.4, April 1985.

[9] W. C. Y. Lee, "Overview of Celllar CDMA", IEEE Trans. Veh. Technol., Vol.40, No.2, May 1991.

[10] K. S. Gilhousen, I. M. Jacobs, R. Padovani and L. A. Weaver, "Increased Capacity Using CDMA for Mobile Satellite Communications", IEEE Journal in SAC, Vol.8, May 1990.

[11] A. Salmasi and K. S. Gilhousen, "On the System Design Aspects of CDMA Applied to Digtial Cellular and Personal Communications Networks", IEEE Proc. of GlobeCom'91.

[12] R. L. Pickholtz, L. B. Milstein and D. L. Schilling, "Spread Spectrum for Mobile Communications", IEEE Trans. Veh. Technol., Vol.40, No.2, May 1991.

[13] QUALCOMM Incorporated, "An Overview of the Application of Code Division Multiple Access (CDMA) to Digital Cellular Systems and Personal Cellular Networks", submitted to TIA, Document Number EX60-10010, March 28, 1992.

[14] J. G. Proakis, "Digital Communications", New York: McGraw Hill, 1989.

[15] K. Feher, "Advanced Digital Communication Systems and Signal Processing Technology", Prentice-Hall, 1987.

[16] J. K. Cavers, "An Analysis of Pilot Symbol Assisted Modulation for Rayleigh Fading Channels", IEEE Trans. Veh. Technol., Vol.40, No.4, November 1991.

[17] S. Sampei and T. Sunaga, "Rayleigh Fading Compensation Method for 16 QAM in Digital Land Mobile Radio Channels," Proc. of IEEE 39th Veh. Tech. Conf., San Fran., pp.640-646, May 1989.

[18] M. L. Moher and J. H. Lodge, "TCMP-A Modulation and Coding Strategy for Rician Fading Channels", IEEE J. Select. Areas Commun., Vol.7, No.9, December 1989.

[19] C. D'Amours, J. Wang and A. Yongacoglu, "Differential and Pilot Symbol-Aided Detection of DS-CDMA in Frequency-Selective Rayleigh Fading Channels", IEEE Proc. GlobeCom'92.

[20] C. L. Liu and K. Feher, "Pilot-Symbol Aided Coherent M-ary PSK in Frequency-Selective Fast Rayleigh Fading Channels", IEEE Trans. Commun., Vol.42, No.1, January 1994.

[21] J. K. Cavers and P. Ho, "Analysis of the Error Performance of Trellis-Coded Modulations in Rayleigh-Fading Channels", IEEE Trans. Commun., Vol.40, No.1, January 1992.

[22] K. S. Gilhousen, I. M. Jacobs, et al, "On the Capacity of a Cellular CDMA System", IEEE Trans. Veh. Technol., Vol.40, No.2, May 1991.

[23] Q. Bi, "Performance Analysis of a CDMA Cellular System", IEEE Proc. of ICC'93.

[24] L. M. A. Jalloul and J. M. Holtzman, "Performance Analysis of DS/CDMA with Noncoherent M-ary Orthogonal Modulation in Multipath Fading Channels", IEEE J.Select.Areas Commun., Vol.12, No.5, June 1994.

[25] K. I. Kim, "On the Error Probability of a DS/SSMA System with a Noncoherent M-ary Orthogonal Modulation", IEEE Prod. of VTC'92.

[26] F. Ling and D. D. Falconer, "Combined Orthogonal/Convolutional Coding for a Digital Cellular CDMA System", IEEE Proc. of VTC'92.

[27] D. J. Torrieri, "Performance of a Direct Sequence Systems with long Pseudonoise Sequences", IEEE Journal SAC, Vol.10, No.4, May 1992.

[28] R. Price and P. E. Green, Jr., "A Communication Technique for Multipath Channels", Proc. IRE, Vol. 46, Mar. 1958.

[29] L. F. Chang and S. Ariyavisitakul, "Performance of a CDMA Radio Communications System with Feed-Back Power control and Mulipath Dispersion", IEEE Proc. of GlobeCom'91.

[30] S. Ariyavisitakul and L. F. Chang, "Signal and Interference Statistics of a CDMA System with Feedback Power Control", IEEE Trans. Commun., Vol.41, No.11, Novermber 1993.

[31] S. Ariyaisitakul, "SIR-Based Power Control in a CDMA System", IEEE Proc. of GlobeCom'92.

[32] R. S. Kennedy, "Fading Dispersive Communication Channels", New York: Wiley, 1969.

[33] W. C. Jakes, Jr., Ed., "Microwave Mobile Communications", New York: Wiley, 1974.

[34] J. S. Lehnert and M. B. Pursley, "Multipath Diversity Reception of Spread-Spectrum Multiple-Access Communications", IEEE Trans. Commun., Vol.35, No.11, November 1987.

[35] M. B. Pursley, D. V. Sarwate and W. E. Stark, "Error Probability for Direct-Sequence Spread-Spectrum Multiple-Access Communications–Part I:Upper and Lower Bounds", IEEE Trans. Commun., Vol.30, No.5, May 1982.

[36] E. A. Geraniotis and M. B. Pursley, "Error Probability for Direct-Sequence Spread-Spectrum Multiple-Access Communications–Part II: Approximations", IEEE Trans. Commun., Vol.30, No.5, May 1982.

[37] J. S. Lehnert and M. B. Pursley, "Error Probabilities for Binary Direct-Sequence Spread-Spectrum Communications with Random Signature Sequences", IEEE Trans. Commun., Vol.35, No.1, January 1987.

[38] R. K. Morrow, Jr. and J. S. Lehnert, "Bit-to-Bit Error Dependence in Slotted DS/SSMA Packet Systems with Random Signature Sequences", IEEE Trans. Commun., Vol.37, No.10, October 1989.

[39] M. B. Pursley, "Performance Evaluation for Phase-Coded Spread-Spectrum Multiple-Access Communication–Part I: System Analysis", IEEE Trans. Comun., Vol.25, No.8, August 1977.

[40] M. B. Pursley and D. V. Sarwate, "Performance Evaluation for Phase-Coded Spread-Spectrum Multiple-Access Communication-Part II: Code Sequence Analysis", IEEE Trans. Commun., Vol.25, No.8, August 1977.

[41] K. Yao, "Error Probability of Asynchronous Spread Spectrum Multiple Access Communication Systems", IEEE Trans. Commun., Vol.25, No.8, August 1977.

[42] L. R. Welch, "Lower Bounds on the Maximum Cross Correlation of Signals", IEEE Trans. Inform. Theory, Vol.IT-29, No.3, May 1974.

[43] L. F. Chang, "Performance of Convolutional Codes with Interleaving in the Interference Limited Rayleigh Fading Channel", IEEE Proc. of ICC'91.

[44] P. Ho and D. Fung, "Error Performance of Interleaved Trellis-Coded PSK Modulations in Correlated Rayleigh Fading Channel", IEEE Trans. Commun., Vol.40, December 1992.

[45] L. F. Chang and N. Sollenberger, "Comparison of Two Interleaving Techniques for CDMA Radio Communications Systems", IEEE Proc. of VTC'92.

[46] M. Schwartz, W. R. Bennett and S. Stein, "Communication Systems and Techniques", McGraw-Hill, 1966.

[47] W. C. Lee, "Mobile Communications Engineering", McGraw-Hill 1982.